ONE- AND TWO-PHOTON PUMPED ORGANIC SEMICONDUCTOR LASERS

Georgios Tsiminis

A Thesis Submitted for the Degree of PhD
at the
University of St. Andrews

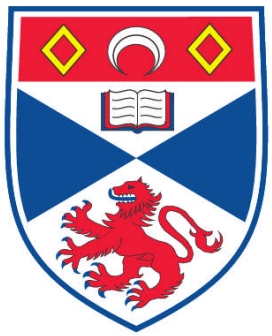

2010

ONE- AND TWO-PHOTON PUMPED ORGANIC SEMICONDUCTOR LASERS

Georgios Tsiminis

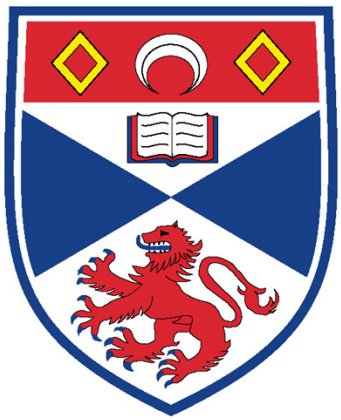

University
of
St Andrews

April 2009

A thesis submitted to the School of Physics and Astronomy, at the University of St Andrews, for the degree of Doctor of Philosophy

Declarations

I, Georgios Tsiminis, hereby certify that this thesis, which is approximately 35000 words in length, has been written by me, that it is the record of the work carried out by me and that is has not been submitted in any previous application for a higher degree.

Georgios Tsiminis April 2009

I was admitted as a research student in October 2005 and as a candidate for the degree of Doctor in Philosophy in October 2005; the higher study for which this is a record was carried out in the University of St. Andrews between 2005 and 2009.

Georgios Tsiminis April 2009

I hereby certify that the candidate has fulfilled the conditions of the Resolution and Regulations appropriate for the degree of Doctor in Philosophy in the University of St. Andrews and that the candidate is qualified to submit this thesis in application for that degree.

Graham A. Turnbull April 2009

Copyright Declaration

In submitting this thesis to the University of St. Andrews I understand that I am giving permission for it to be made available for use in accordance with the regulations of the University Library for the time being in force, subject to any copyright vested in the work not being affected thereby. I also understand that the title and abstract will be published, and that a copy of the work may be made and supplied to any *bona fide* library or research worker, that my thesis will be electronically accessible for personal, or research use, and that the library has the right to migrate my thesis into new electronic forms as required to ensure continued access to the thesis. I have obtained any third-party copyright permissions that may be required in order to allow such access and migration.

Georgios Tsiminis April 2009

Acknowledgments

Doing a PhD is never a solitary affair, except perhaps from the actual writing of the thesis. There are a lot of people that I feel I need to thank for their help along the way, so here goes.

First of all I must thank my supervisors, Dr Graham Turnbull and Prof Ifor Samuel. I could not have wished for better academic supervisors to guide me along the long journey through the semi- or completely unchartered lands of scientific research. I am grateful to them for all their help, their useful suggestions, motivation and encouragement and for the occasional pat on the back whenever things did work.

The Organic Semiconductor Optoelectronics group in the University of St Andrews consists of some of the nicest people I've come to know. I have had the pleasure of working closely with some of them, so thanks go out to Dr Arvydas Ruseckas, whose "You don't have to be Greek to make good organic lasers, but it helps" line nearly made it as a subtitle of this thesis. Also thanks to Ying Yang that always seems to know things I don't (but should), to Yue Wang that keeps on trying long after I've given up, to Paul Shaw for teaching me ellipsometry (at least twice) and for being a really nice guy, and to Gordon Hedley for his willingness to help with both scientific and other challenges and to listen to my views and comments on the world.

Past members of the group have also contributed greatly, so thanks goes out to Dr Andreas Vasdekis who helped me start my PhD smoothly and was a true friend and to Dr Jean-Charles Ribierre for teaching me the most efficient way of doing research, even if I don't always abide by it. And to everyone else in the Physics department, especially the secretaries and the technical staff, thank you for making all this work possible.

And of course to Joanna. Your continuing faith in me, your love and support inspire everything I do. Thank you.

Abstract

This thesis describes a number of studies on organic semiconductors focused around using them as gain media for lasers. The photophysical properties of organic semiconductors are studied using a wide range of experimental techniques, allowing the evaluation of new materials and novel excitation schemes for use in organic semiconductor lasers.

Polyfluorene is a well-established conjugated polymer laser gain medium and in this thesis its excellent lasing properties are combined with its two photon absorption properties to demonstrate a tunable two-photon pumped solid-state laser based on a commercially available organic semiconductor.

A family of bisfluorene dendrimers was studied using a number of photophysical techniques to evaluate their potential as laser materials. Distributed feedback lasers based on one of the dendrimers are demonstrated with lasing thresholds comparable to polyfluorene. The same materials were found to have enhanced two-photon absorption properties in comparison to polyfluorene, leading to the fabrication of tunable two-photon pumped dendrimer lasers.

A member of a novel family of star-shaped oligofluorene truxenes was evaluated as a laser gain material and the distributed feedback lasers made from them show some of the lowest lasing thresholds reported for organic semiconductors, partly as a consequence of exceptionally low waveguide losses in comparison to other single-material thin films.

Finally, an organic laser dye is blended with a conjugated polymer, where the dye molecules harvest the excitation light of a GaN laser diode and transfer its energy to the polymer molecules. This is the first time such a scheme is used in an organic laser and in combination with a novel surface-emitting distributed Bragg reflector resonator allows the demonstration of a diode-pumped organic laser, a significant step towards simplifying organic lasers.

To my parents,

Stefano and Aphrodite

Table of contents

1. Introduction

Plastic materials have long played an important role in various technological applications mainly due to their ease of processing and flexibility of synthesis. The ability to produce and process them cheaply and in large amounts has made plastics perhaps the most successful and widespread category of man-made materials in existence today, with applications ranging from household items to industrial components and from disposable tools to unique equipment used in scientific endeavours.

One of the properties thought to be common amongst plastics is the lack of electrical conductivity, leading to some of the most common applications of plastic materials being as electrical insulators. It was only in 1963 that the first reports on electrical conductivity in the polymer polypyrrole emerged [1], followed by the better known reports of electrical conductivity in polyacetylene in 1977.[2, 3] The world of science acknowledged the importance of this new category of materials by awarding a Nobel price in Chemistry for the discovery of conductive polymers in 2000 [4, 5] and the properties of these materials have been the object of intense research ever since.

Light-emitting organic semiconductors are an even more recent discovery, as it was only in 1987 that electroluminescence was first observed in small molecules [6] and not until 1990 that the same effect was observed in conjugated polymers [7], leading to the first organic light-emitting diodes (OLEDs). Today these devices show very high efficiencies [8-10] and long operating times while the first commercial applications using OLED displays have appeared in the market and are taking the first step towards becoming an established and reliable displays technology [11, 12], while the idea of using white OLED lighting to replace the standard incandescent and fluorescent lighting tubes is increasing in popularity. [13]

The first suggestion of the possibility of lasing under microwave excitation in organic materials came in 1961 [14] opening up a vast field of research over the

next years in organic laser gain media.[15] In 1992 the first demonstration of lasing in a conjugated polymer [16] highlighted materials suitable for lasing and in 1996 the first solid-state conjugated polymer lasers were reported [17], a development that sparked a renewed interest in organic semiconductor lasers. Some of the key lasing properties of organic semiconductor lasers are compared against other well-established solid-state laser gain media in Table 1.a.

Gain medium	Optical gain (cm^{-1})	Gain bandwidth (nm)
Ruby [18]	0.2	<1
Nd:YAG [18]	0.05	<1
ND:Glass [18]	0.03	28
Ti:Sapphire [18]	0.2	180
GaN semiconductors [19]	50 - 200	50
AlGaAs semiconductors [20]	100 – 800	20
Organic semiconductors [21-23]	10 - 80	10 - 120

Table 1.a Optical gain and gain bandwidth at room temperature for some of the key gain media used in solid-state lasers.

The key advantage of organic semiconductor lasers comes from the combination of reasonably high values of optical gain with the excellent gain spectral bandwidth in materials that demonstrate ease of processing. This gives rise to a large family of organic semiconductor lasers that combine compact dimensions with output wavelength tunability that spans the visible spectrum.[21]

The excitation of these lasers however is almost exclusively done optically due to the low charge mobilities of organic semiconductors [21], a fact that ultimately limits their minimum size.[24] The efforts of the scientific community have therefore lately concentrated on miniaturising the optical pump sources needed for organic lasers, leading to the use of an inorganic light-emitting diode as the pump source for a laser based on a highly-efficient conjugated polymer.[25] Very recently there has been a report of an electrically-pumped organic semiconductor laser in the literature [26] that could move some organic lasers away from optical excitation and would allow for devices directly comparable in terms of size and integration to their inorganic counterparts but the need for further improvement remains.

The key aspect in down-sizing the pump sources of organic semiconductor lasers is lowering the threshold of laser emission, as lower pump intensities are then required to achieve lasing, allowing the use of more compact pump sources. The two key parameters in achieving such improvements are the design of better optical resonators that enhance the feedback of the material's emission and thus lower the lasing threshold and improving the gain medium itself by creating molecules that have improved optical properties, are more efficient at light emission and can reduce the additional losses that can sometimes inhibit the operation of organic lasers.

At the beginning of this PhD project, the smallest organic semiconductor laser systems were pumped by microchip Nd:YAG lasers.[27] These laser sources are matchbox-sized and have replaced the much bulkier gas lasers and optical amplifiers that preceded them.[21] The lasing wavelength of Neodymium crystals however is 1064 nm that is far too long for optically exciting materials that emit in the visible part of the spectrum. Microchip lasers therefore have to include nonlinear crystals that convert the infrared light to green (532 nm) through second-harmonic generation and ultraviolet light (355 nm) through third-harmonic generation, increasing the complexity and price of these systems.

This thesis focuses on photophysical studies of organic semiconductors with the scope of using them as laser gain media and demonstrates how improvements can be made in the optical pumping of organic semiconductor lasers. The material properties required for lasing are investigated in both commercially-available materials as well as custom-synthesised molecules that were designed with efficient light-emission in mind. Additional nonlinear optical properties of organic semiconductors are studied, leading to the demonstration of lasers that utilise two-photon absorption for their optical pumping. This technique can be used to remove the nonlinear wavelength conversion from the pump source and into the gain material itself, leading to further simplification and downsizing of organic laser systems.

An introduction to organic semiconductors and their electronic, photophysical and optical properties is given in Chapter 2, where the various aspects of organic semiconductor lasers are also discussed. The different types of organic lasers are examined, with emphasis on distributed-feedback laser resonators.[28] This chapter also discusses some of the photophysical processes that were encountered in some of the experiments, such as two-photon absorption. Chapter 3 describes the experimental techniques and methods that were used to obtain the data in the rest of this thesis, from simple absorption measurements to femtosecond optical excitation of organic lasers. The fabrication and characterisation of organic semiconductor lasers are also discussed here, focusing on distributed-feedback (DFB) lasers.

Chapter 4 focuses on the nonlinear optical properties of polyfluorene, one of the best-established conjugated polymers used for lasing.[29] The two-photon absorption properties of polyfluorene are investigated in two different time regimes providing a comprehensive study of the phenomena associated with nonlinear absorption and subsequent light emission. The information collected is then used to demonstrate a two-photon pumped solid-state polyfluorene laser using a distributed-feedback resonator structure, providing an alternative optical pumping scheme for a UV-absorbing organic laser material.[30] This is the first example of a two-photon pumped polyfluorene laser and one of only two demonstrations of two-photon induced lasing in conjugated polymers.

A family of bisfluorene-cored dendrimers are the subject of chapter 5. Dendrimers are a novel category of organic semiconductors that consist of a light-emitting core onto which different arms called dendrons are attached that control different properties of the molecule such as the intermolecular interactions and solubility.[10] The dendrimers studied here are based on a blue-emitting core and have previously been known to exhibit optical gain.[31] A study of their photophysical properties is performed and the most efficient member of the family is used to make distributed-feedback lasers with low lasing threshold and wide tunability. [32]

The two-photon absorption properties of these dendrimers are also investigated across two different time domains and two-photon pumped lasers operating with both nanosecond and femtosecond pump pulses are fabricated. The lasing performance of the two-photon pumped dendrimer lasers is evaluated and compared to the one-photon pumped lasers from the same material, allowing for conclusions to be extracted on the efficiency of this alternative pumping scheme for organic semiconductor lasers.[33]

A member of a new category of organic semiconductors, star-shaped oligofluorene truxenes, is studied in chapter 6 as a gain medium for organic lasers. These molecules have advantages that stem from their well-defined structure and make them particularly attractive for optoelectronics applications.[34] In this chapter, the combination of good film quality with high photoluminescence quantum yield and low optical losses allow the demonstration of an organic laser with very low lasing threshold and excellent tunability in the blue part of the spectrum.[35] The DFB lasers made from the truxene material are compared against polyfluorene lasers in a number of key areas that include device lifetime, one of the most important aspects for a practical laser system and prove to be an improvement on the already very good performance of polyfluorene.

Organic semiconductor lasers have a number of advantages in comparison to their inorganic counterparts, but one of the areas where they currently lag behind is the requirement for optical excitation as the electrical properties are still not as good. A great amount of effort has been put in trying to downsize the optical pump source for organic lasers, from large regenerative optical amplifiers to more compact systems. Chapter 7 focuses on using an inorganic laser diode as the pump source for an organic semiconductor laser that uses energy transfer from a laser dye to a conjugated polymer to achieve lasing.[36] This is one of the few examples of a laser-diode organic laser in the literature and, in combination with the other publications on this field, has paved the way for the recent development of a LED-pumped polymer laser. [25]

As research continues on organic semiconductors lasers, a broad spectrum of potential benefits and unique applications begins to emerge. New materials continue to be synthesised in groups around the world that receive feedback from studies like this on material properties and there is very little doubt that organic lasers will move from the research stage to becoming an established technology for certain application areas such as optical spectroscopy, chemical [37] and bio sensing [38] and point-of-care medical diagnostics. The basic work outlined in this thesis should provide a guideline for studies on the optimization of the materials used as gain media in organic lasers in terms of the photophysical properties that affect optical gain and lasing and hopefully has contributed towards the further development of this exciting area of research.

1.1. References

[1] B. Bolto, R. McNeill, D. Weiss, *Australian Journal of Chemistry* **1963**, *16*, 1090.

[2] H. Shirakawa, E. J. Louis, A. G. Macdiarmid, C. K. Chiang, A. J. Heeger, *J. Chem. Soc.-Chem. Commun.* **1977**, 578.

[3] C. K. Chiang, C. R. Fincher, Y. W. Park, A. J. Heeger, H. Shirakawa, E. J. Louis, S. C. Gau, A. G. Macdiarmid, *Physical Review Letters* **1977**, *39*, 1098.

[4] http://nobelprize.org/nobel_prizes/chemistry/laureates/2000/public.html

[5] A. J. Heeger, *Reviews of Modern Physics* **2001**, *73*, 681.

[6] C. W. Tang, S. A. Vanslyke, *Applied Physics Letters* **1987**, *51*, 913.

[7] J. H. Burroughes, D. D. C. Bradley, A. R. Brown, R. N. Marks, K. Mackay, R. H. Friend, P. L. Burns, A. B. Holmes, *Nature* **1990**, *347*, 539.

[8] M. A. Baldo, D. F. O'Brien, Y. You, A. Shoustikov, S. Sibley, M. E. Thompson, S. R. Forrest, *Nature* **1998**, *395*, 151.

[9] M. A. Baldo, M. E. Thompson, S. R. Forrest, *Nature* **2000**, *403*, 750.

[10] P. L. Burn, S. C. Lo, I. D. W. Samuel, *Advanced Materials* **2007**, *19*, 1675.

[11] http://www.oled-display.net/pictures-of-the-world-largest-oled-television-from-samsung-40-inch-with-1920x1080-pixel

[12] http://www.sony.co.uk/product/tvp-oled-tv/xel-1

[13] http://www.oled100.eu/homepage.asp

[14] E. G. Brock, P. Csavinszky, E. Hormats, H. C. Nedderman, D. Stirpe, F. Unterleitner, *The Journal of Chemical Physics* **1961**, *35*, 759.

[15] N. Tessler, *Advanced Materials* **1999**, *11*, 363.

[16] D. Moses, *Applied Physics Letters* **1992**, *60*, 3215.

[17] F. Hide, M. A. DiazGarcia, B. J. Schwartz, M. R. Andersson, Q. B. Pei, A. J. Heeger, *Science* **1996**, *273*, 1833.

[18] W. T. Silfvast, *Laser fundamentals*, Cambridge University Press, Cambridge **2004**.

[19] A. Ishibashi, I. Kidoguchi, A. Tsujimura, H. Yoshiaki, Y. Ban, T. Ohata, M. Watanabe, T. Hayashi, *Journal of Luminescence* **2000**, *87-89*, 1271.

[20] M. V. Kisin, V. B. Gorfinkel, M. A. Stroscio, G. Belenky, S. Luryi, *Journal of Applied Physics* **1997**, *82*, 2031.

[21] I. D. W. Samuel, G. A. Turnbull, *Chem. Rev.* **2007**, *107*, 1272.

[22] M. Punke, T. Woggon, M. Stroisch, B. Ebenhoch, U. Geyer, C. Karnutsch, M. Gerken, U. Lemmer, "Organic semiconductor lasers as integrated light sources for optical sensor systems - art. no. 665909", presented at *Conference on Organic-based Chemical and Biological Sensors*, San Diego, CA, Aug 28, **2007**.

[23] T. Yamao, K. Yamamoto, S. Hotta, *J. Nanosci. Nanotechnol.* **2009**, *9*, 2582.

[24] M. D. McGehee, A. J. Heeger, *Advanced Materials* **2000**, *12*, 1655.

[25] Y. Yang, G. A. Turnbull, I. D. W. Samuel, *Applied Physics Letters* **2008**, *92*, 163306.

[26] X. Liu, H. Li, C. Song, Y. Liao, M. Tian, *Opt. Lett.* **2009**, *34*, 503.

[27] C. J. Norrie, B. D. Sinclair, N. Gallaher, M. H. Dunn, W. Sibbett, *Electron. Lett.* **1989**, *25*, 1115.

[28] M. D. McGehee, M. A. Diaz-Garcia, F. Hide, R. Gupta, E. K. Miller, D. Moses, A. J. Heeger, *Applied Physics Letters* **1998**, *72*, 1536.

[29] R. D. Xia, G. Heliotis, D. D. C. Bradley, *Applied Physics Letters* **2003**, *82*, 3599.

[30] G. Tsiminis, A. Ruseckas, I. D. W. Samuel, G. A. Turnbull, *Applied Physics Letters* **2009**, *94*, 3.

[31] J. R. Lawrence, G. A. Turnbull, I. D. W. Samuel, G. J. Richards, P. L. Burn, *Optics Letters* **2004**, *29*, 869.

[32] J. C. Ribierre, G. Tsiminis, S. Richardson, G. A. Turnbull, I. D. W. Samuel, *Applied Physics Letters* **2007**, *91*.

[33] G. Tsiminis, J. C. Ribierre, A. Ruseckas, H. S. Barcena, G. J. Richards, G. A. Turnbull, P. L. Burn, I. D. W. Samuel, *Advanced Materials* **2008**, *20*, 1940.

[34] X. H. Zhou, J. C. Yan, J. Pei, *Org. Lett.* **2003**, *5*, 3543.

[35] G. Tsiminis, Y. Wang, P. E. Shaw, A. L. Kanibolotsky, I. F. Perepichka, M. D. Dawson, P. J. Skabara, G. A. Turnbull, I. D. W. Samuel, *Applied Physics Letters* **2009**, *94*, 3.

[36] A. E. Vasdekis, G. Tsiminis, J. C. Ribierre, L. O'Faolain, T. F. Krauss, G. A. Turnbull, I. D. W. Samuel, *Optics Express* **2006**, *14*, 9211.

[37] A. Rose, Z. Zhu, C. F. Madigan, T. M. Swager, V. Bulovic, *Nature* **2005**, *434*, 876.

[38] D. Schneider, T. Rabe, T. Riedl, T. Dobbertin, M. Kroger, E. Becker, H. H. Johannes, W. Kowalsky, T. Weimann, J. Wang, P. Hinze, A. Gerhard, P. Stossel, H. Vestweber, *Advanced Materials* **2005**, *17*, 31.

2. Theory of organic semiconductor lasers

The word “Laser” is an acronym that stands for “Light Amplification by Stimulated Emission of Radiation” and contains both the cause (stimulated emission) and the effect (light amplification) of these devices.[1] Every laser consists of three parts: a medium that can produce optical gain and hence light amplification, a resonator that allows multiple passes of the amplified light through the gain medium to increase the overall amplification and a pump source that provides the energy to the gain medium. Some organic semiconductors have shown the required properties of stimulated emission and light amplification, leading to the development of organic semiconductor lasers.[2]

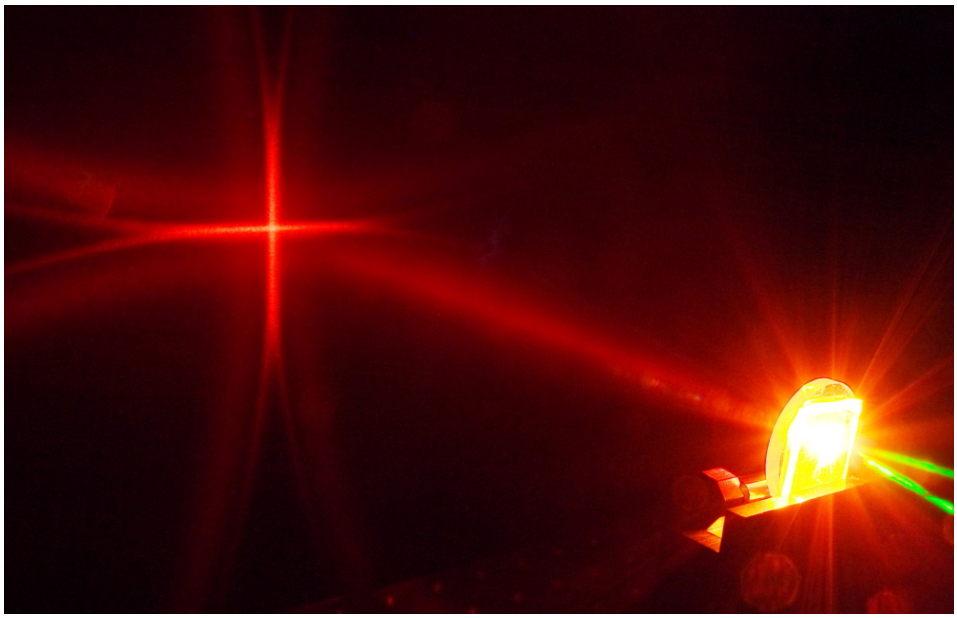

Figure 2.1 Lasing beam and far-field emission pattern from a two-dimensional distributed feedback laser based on the conjugated polymer MEH-PPV.

This chapter reports on the background theory of organic semiconductors, giving an overview of their electronic and optical properties that make them attractive for use as laser gain media. A review of organic semiconductor lasers is also presented, with emphasis placed on the types of lasers studied later on in this thesis.

2.1. Introduction

Organic semiconductors differ from other organic materials due to the nature of the bonds that connect adjacent carbon atoms. It is this special electronic structure that gives rise to their interesting properties such as electrical conductivity and light emission. It makes sense then to start by describing the electronic properties of organic semiconductors before proceeding to their photophysical properties.

2.2. Electronic properties

The basis of organic semiconductors is the conjugated nature of the carbon bonds that form their backbone. The alternation of single and double carbon bonds in organic semiconductor molecules gives rise to properties that are not found in other organic materials, such as electrical conductivity and light emission. To better understand the conjugation effect, it is helpful to look into how carbon atoms bond together and under which conditions conjugations appear.

2.2.1. Electron delocalisation in carbon double bonds

Carbon has six electrons and these are arranged in a number of different orbital surrounding the nucleus. The first two electrons occupy the 1s state that has a spherical symmetry around the nucleus, while the other four are split between the 2s state (2 electrons) and the 2p state (2 electrons), giving a total electronic configuration of $1s^2\ 2s^2\ 2p^2$. The symmetries of these states can be seen in Figure 2.2.

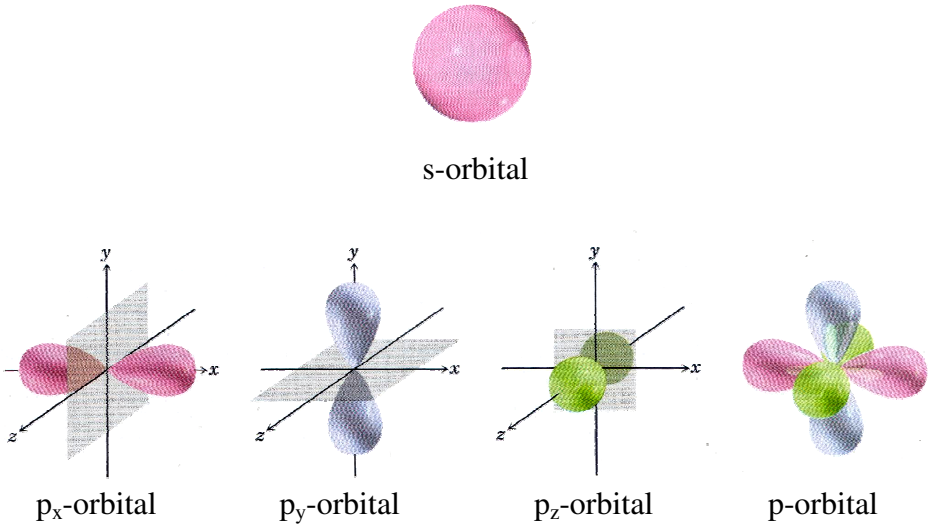

Figure 2.2 s and p electron orbitals (adapted from [3])

Hybrid orbitals are also possible, as is the case for ethylene (C_2H_4) where the two carbon atoms are connected by a double bond. Each carbon atom has three of its four valence electrons in sp^2 hybridized orbitals, two of which are bound to the 1s orbitals of two hydrogen atoms and the other connects to the other carbon atom, leading to the formation of σ-bonds between all atoms involved. To minimise the electrostatic forces between the atoms, these sp^2 hybrid orbitals dictate a 120^o angle of the σ-bonds. The fourth valence electron in each carbon atom remains in a p-orbital and these two p-orbital electrons form a π-bond between the carbon atoms, as seen in Figure 2.3.

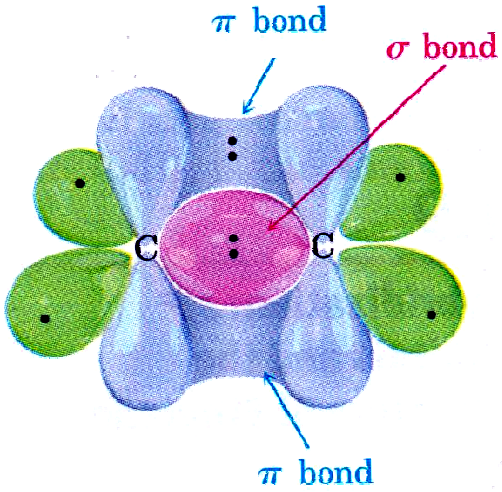

Figure 2.3 Molecular bonding in an ethylene molecule showing the σ and π bonds forming the double bond between neighbouring carbon atoms (adapted from [3]).

The π-bond is much weaker than the σ-bond, a fact that makes the π-electrons less strongly bound to the molecule, causing electron delocalisation across the molecule. This electronic delocalisation gives semiconducting properties to these so-called conjugated molecules, where the π-electrons are able to move along the conjugated bonds. In larger molecules, where many carbon atoms are connected through alternating single and double bonds, the delocalisation of the π-electrons can extend along the entire length of the molecule.

2.2.2. Types of organic semiconductors

There are several different types of organic semiconductors and they can be categorised based on their chemical structure and processing properties. The first category to be studied was crystals grown from organic molecules such as anthracene[4] (Figure 2.4a), but the difficulty in synthesis and handling of these materials meant that other materials became more widespread. Small molecule organic semiconductors were the next step, where deposition of thin films was done via evaporation. A typical example of a small molecule organic semiconductor used in light-emitting applications is aluminum tris(quinolate) (Alq3) [5] and is shown in Figure 2.4b.

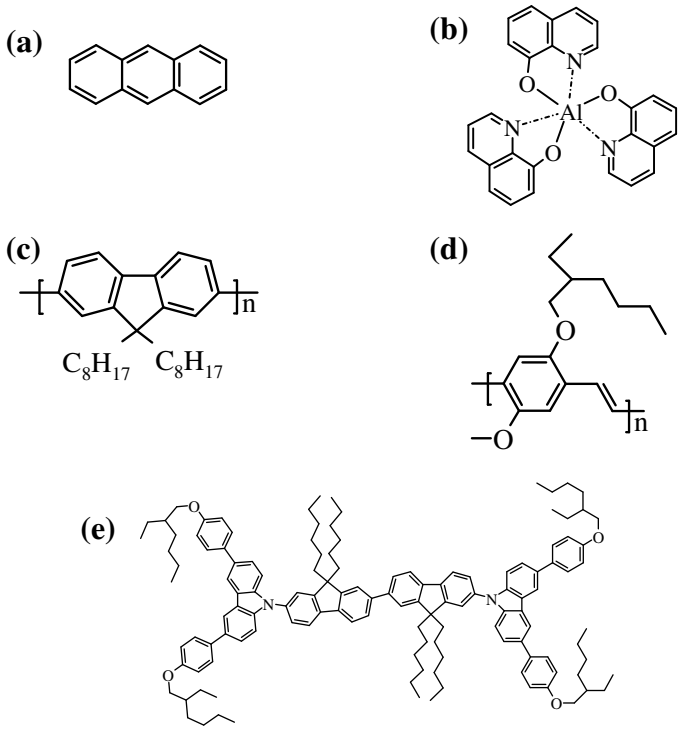

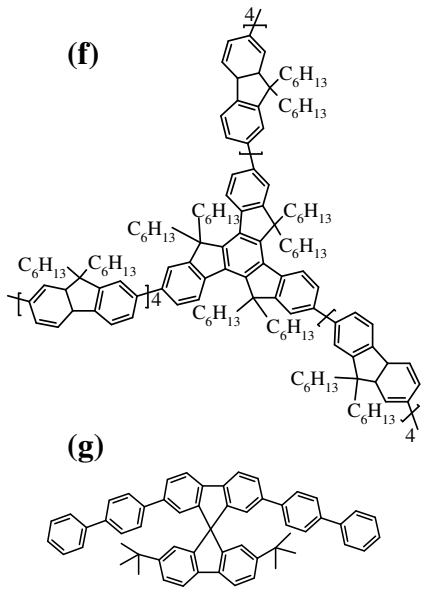

Figure 2.4 Molecular structures of some typical organic semiconductors. (a) Anthracene (b) Alq3 (c) polyfluorene (d) MEH-PPV (e) bisfluorene-cored dendrimer (f) star-shaped oligomer (g) spiro-linked oligomer.

Polymerisation techniques allowed the synthesis of conjugated polymers, where the electron delocalisation extends along the length of the molecule. Notable examples of conjugated polymers are the polyfluorenes[6] and the poly(phenylene vinylene)s,[7] examples of which are shown in Figure 2.4 (c) and (d) respectively . Conjugated polymers are solution processable, making it possible to process them using techniques such as spin-coating or inkjet printing, a great aid in simplifying device fabrication.

Another category of organic semiconductors is conjugated dendrimers,[8] where a light-emitting core has conjugated arms known as dendrons attached to it with surface group at their ends, leading to highly branched architectures. The core defines the photophysical properties of the molecules while the dendrons control the intermolecular interactions by spacing the molecules apart and the surface groups control solubility. A conjugated denrdimer based on a bisfluorene core is shown in Figure 2.4e. Oligomers form another category of organic semiconductors, placing themselves between small molecules and conjugated polymers. These materials have a wide variety of geometries ranging from linear chains to star-shaped molecules (Figure 2.4f)[9], while a

particular type of molecule where two oligomers are linked by a spiro linkage[10] has proven very successful in lasers (Figure 2.4g).

2.2.3. Energy levels and energy band gap

The p-electrons that connect the two carbon atoms can interfere in different ways depending on the sign of their wavefunctions. The interference can be either constructive, resulting in a bonding π orbital that adds stability to the molecule, or destructive, leading to the formation of an anti-bonding π* orbital that destabilises the molecular bond. The presence of π and π* orbitals creates two energy levels in each double bond that are separated by an energy gap. These energy levels can be estimated using the Hückel approximation, whereby the number of p-electrons is equal to the number of energy levels, as seen in for ethylene.

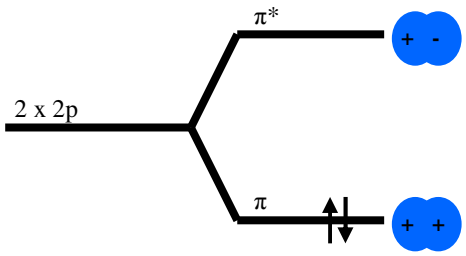

Figure 2.5 Molecular orbital energy levels for the p-bond in ethylene (adapted from [11]).

In conjugated molecules that have a larger number of double bonds, the number of π and π* orbitals is greatly increased, leading to a more complicated energy level structure where the π and π* energy levels become wider energy bands. Sublevels of these energy levels also appear due to the vibrational degrees of freedom of each molecule, creating even more levels within the bands. Under thermal equilibrium, the highest π orbital is occupied by two electrons and is referred to as the highest occupied molecular orbital (HOMO), while the low-energy π* orbital is called the lowest unoccupied molecular orbital (LUMO) of the molecule. The energy band gap can then be defined as

$$E_g = E_{LUMO} - E_{HOMO} \qquad \textbf{2-I}$$

Since two electrons can occupy each π or π* energy level, the spin of the electrons involved becomes important, leading to the appearance of two well-defined spin states called singlet and triplet. We can imagine the different spin combinations at each energy level to be

$$\uparrow\uparrow,\uparrow\downarrow,\downarrow\uparrow,\downarrow\downarrow \qquad \textbf{2-II}$$

The singlet state is anti-symmetric and therefore has a total angular momentum of zero, while the triplet is symmetric with a total angular momentum of one. These states can be represented using the Clebsch-Gordan coefficients as follows

$$|0,0\rangle = \frac{1}{\sqrt{2}}(\uparrow\downarrow - \downarrow\uparrow) \quad \textbf{(singlet state)} \qquad \textbf{2-III}$$

$$\left(\begin{array}{l} |1,1\rangle = \uparrow\uparrow \\ |1,0\rangle = \frac{1}{\sqrt{2}}(\uparrow\downarrow + \downarrow\uparrow) \\ |1,-1\rangle = \downarrow\downarrow \end{array}\right) \quad \textbf{(triplet states)} \qquad \textbf{2-IV}$$

The spin-conservation principle dictates that transitions are only allowed between same-spin states, i.e. singlet-singlet or triplet-triplet, while single-triplet transitions are forbidden.

2.3. Optical properties

The optical properties of conjugated molecules have their origin in the transitions of the p-electrons between the π and π* energy levels as determined by their electronic structure and number of double bonds, as the energy gap is given by the energy difference between the LUMO and HOMO energy levels. Formal calculations of energy levels require density function theory models on supercomputers. To a first approximation, the length of a molecule determines the extent of the electron delocalisation. In analogy to electrons in an infinite potential well, longer conjugated molecules have lower energy gaps. The energy gap strongly depends on the specific molecular structure and can be tuned by means of synthetic chemistry, for example by changing the

conjugation length. It is therefore possible to make organic semiconductors that emit across the entire visible spectrum, as seen in Figure 2.6. The conservation of spin also plays an important role, particularly in the light emission of organic semiconductors as will be discussed later on in this chapter.

Figure 2.6 Various organic semiconductors emitting across the visible spectrum under UV illumination.

2.3.1. Absorption and emission

When light is incident upon a conjugated molecule, absorption is caused by the π-π* transition of the p-electrons when the energy of the photons is equal to the energy gap between the π and π* levels. As the electrons move into the higher energy level they leave behind them a net positive charge know as an electron hole. The hole is bound to the electron by a Coulomb force forming an exciton,[12] so all the optical transitions are of excitonic nature in organic semiconductors.

Absorption and emission in conjugated molecules is best explained by using a Franck-Condon diagram [13] as seen in Figure 2.7. The main optical transitions occur between the singlet states, shown below as S_0 and S_1.

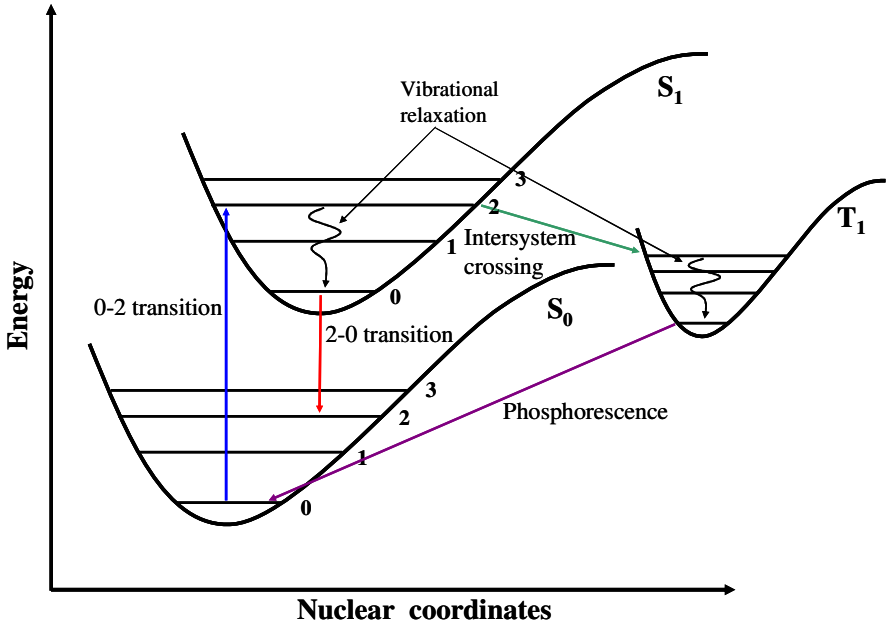

Figure 2.7 A Frank-Condon diagram showing the key electronic transitions for light absorption and emission in conjugated molecules.

Light is absorbed from the lowest vibrational level of S_0 into one of the higher vibrational levels of S_1. This can be explained using the Frank-Condon principle that states that "the intensity of a vibronic transition is proportional to the square of the overlap integral between the between the vibrational wavefunctions of the two states involved in the transition". [13, 14] Since the electronic transitions are very fast (~10^{-15} s) compared to the movements of the nuclei (~10^{-13} s), transitions between vibrational levels are favoured when the wavefunction overlap occurs for a minimal change in the nuclear coordinates [15], a condition satisfied between the lowest vibronic of the ground state and a higher vibronic level of the first excited state as signified by the straight transition lines in the previous figure.

The intensity of the incident light as it passes through a length z of material is determined by the Beer Lambert law, expressed as

$$I = I_0 e^{-\alpha z} \qquad \textbf{2-V}$$

where I_0 is the initial intensity and α is the absorption coefficient of the material that is a function of the energy of the incident light and the type of molecule.

When the molecules are in the S_1 state they very quickly relax to its lowest vibrational level. Light emission occurs when the molecules relax from the S_1 state back to a higher vibrational level of S_0 due again to the Frank-Condon principle. This type of emission is called fluorescence and is the strongest light emission mechanism in conjugated molecules as it is spin-allowed. The emission of conjugated molecules is red-shifted from their absorption due to the Stokes' shift that occurs due to the change of nuclei positions following excitation, as the potential across the molecule changes in comparison to the ground state resulting in a rearrangement of the molecule's morphology. This separation between absorption and emission can be further enhanced under the influence of the environment of the molecule, for example in the presence of a solvent.

An alternative relaxation path is for molecules in the S_1 state to convert their spin and thus move from a singlet to a triplet state, a process known as intersystem crossing. Light emission can then occur in the form of phosphorescence as the molecules relax from the T_1 triplet state back to S_0, but as this is a spin-forbidden transition it is less probable than fluorescence and so the relaxation times are much longer (milliseconds to seconds as compared to nanoseconds for fluorescence). In practice, in organic molecules nonradiative relaxation of the triplets is much faster than phosphorescence and so few triplet excitons emit a photon.

Conjugated molecules show strong absorption and emission bands as a direct consequence of their electronic structure consisting of alternating single and double carbon bonds. In addition, the presence of additional vibronic states allows for separation between absorption and emission, a fact that enhances fluorescence by reducing self-absorption and also has consequences on achieving light amplification as discussed in a following section.

2.3.2. Two-photon absorption

The energy required to bridge the band gap of a material usually comes from one photon of appropriate energy, hence the resulting absorption as also known as linear absorption (one photon per molecular transition). It is however possible for two photons that have half the energy of the band gap each to be absorbed simultaneously by the material in a nonlinear absorption process known as two-photon absorption, although at a much lower probability than linear absorption, resulting in orders of magnitude reduced strength for two-photon absorption.[16, 17]

Two-photon absorption follows different absorption transitions due to different symmetries that make the normal S_0 to S_1 absorption transition forbidden. The ground state energy level is double occupied (two electrons) and therefore has an A_g symmetry, meaning that the orbital at this energy level is symmetric.[18] The next energy level has an opposite symmetry denoted as B_u, after which the energy levels alternate again between the two spin symmetries. One-photon transitions are only allowed between states of opposite symmetries due to the need to conserve the angular momentum of the system, making $A_g \rightarrow B_u$ the transition for linear absorption. In contrast, the excited A_g states are accessible for two-photon being simultaneously absorbed, as shown in Figure 2.8.

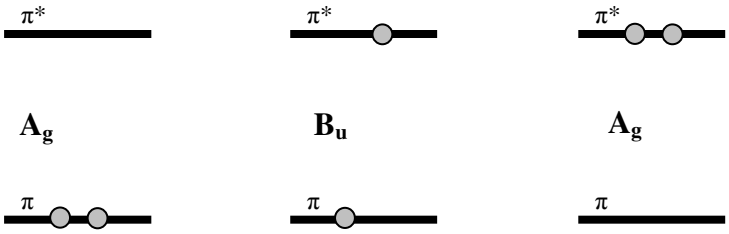

Figure 2.8 Different symmetry configurations in π-π* energy levels.

The A_g energy levels sit higher in energy than the one-photon accessible B_u energy level system as shown in Figure 2.9.

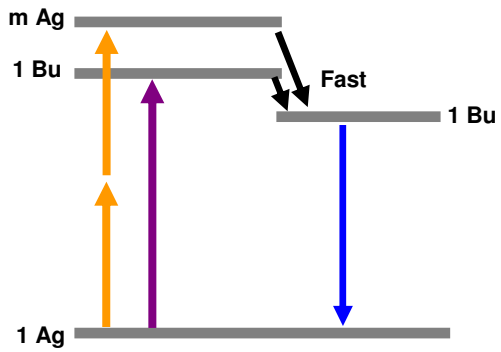

Figure 2.9 Linear (purple arrow) and two-photon (orange arrows) absorption processes in a simple energy level diagram.

As a consequence, the photon energy for maximum two-photon absorption is higher than the value for the same material under one-photon excitation.[19] From the two-photon excited state the excitons relax very quickly back to the lowest vibronic of the B_u state ($S_{1\text{-}0}$) so any further electronic transitions such as fluorescence are the same as for one-photon excitation.

Theoretical predictions on the efficiency of the two-photon absorption process are extremely difficult and rely on complicated quantum chemistry calculations that run on dedicated mainframe computers. An indication of the two-photon absorption efficiency however is the percentage of photons absorbed through a given length of material in comparison to the same measurement for linear absorption. As an example, a film of a semiconducting polymer such as polyfluorene will absorb just over 1% of the incident two-photon excitation for a thickness of 600 nm, indicating the reduced probablitiy of the two-photon absorption process. In the case of linear absorption, practically all of the incident photons are absorbed in a film thickness of only 200 nm, an absorption strength that is over 300 times higher the=an the two-photon absorption.

2.3.3. Stimulated emission

Stimulated emission is the process behind the optical gain of a laser material and is one of the possible outcomes of a photon interacting with a material.

A simple two-level energy system is a good starting point in studying light-induced electronic transitions in a material, and the general analysis presented

here can be adapted to fit what is observed in organic semiconductors as well. This model system consists of a collection of molecules, each with two energy levels, E_0 and E_1, with E_0 having the lowest energy. When the system is at thermal equilibrium, the molecules are distributed between the two levels E_0 and E_1 that have populations N_0 and N_1 respectively with $N_1>N_0$, as shown in Figure 2.10.

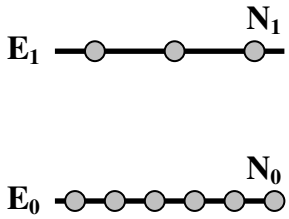

Figure 2.10 A simple two-level system used to describe light-matter introductions.

If photons of energy $hv=E_1-E_0$ are incident on the material, there are three possible interactions that can occur.

The material can absorb the energy of the photon, whereby some of the molecules will be excited from E_0 to E_1. Molecules in excited states stay there for a brief period of time known as the lifetime τ of the excited state before returning to the ground state. The rate at which the population of E_1 changes as a result of absorbing the photon energy is given by

$$\frac{dN_1}{dt} = B_{10}\rho(v)N_0 \qquad \textbf{2-VI}$$

where B_{10} is the Einstein coefficient of the transition and $\rho(v)$ is the photon density.

After staying in this excited state for a time period of τ, the molecules may spontaneously relax back to the ground state, resulting in fluorescence. The rate of change for the N_1 population is then given by

$$\frac{dN_1}{dt} = -A_{01}N_1 \qquad \textbf{2-VII}$$

where A_{01} is the Einstein coefficient for spontaneous light emission, defined as the inverse of the excited state's lifetime.

Alternatively, the presence of an incoming photon may cause a molecule from the excited state to relax to the ground state, emitting an additional photon of the same energy and phase, resulting in a pair of coherent photons. The rate of change in the N_1 population can be written as

$$\frac{dN_1}{dt} = -B_{10}\rho(v)N_1 \qquad \textbf{2-VIII}$$

where B_{10} is the Einstein coefficient for the E_1 to E_0 transition and is equal to B_{01} for absorption. Since this emission was stimulated by the presence of an external photon, it is called stimulated emission.[20, 21]

In the case of stimulated emission, amplification of the input light occurs since for each input photon two photons are emitted. At low excitation energies however spontaneous emission is a much more likely transition path since $N_0>N_1$ as most of the molecules reside in the lower energy level with only a small proportion in the excited state due to a combination of external stimulation and temperature effects. To increase the probability of stimulated emission, the population of the excited state must be greatly increased, requiring therefore high excitation densities. At these higher excitation densities the coefficients for absorption and stimulated emission are the same (and are both higher than the spontaneous emission coefficient) and we can define three separate regimes.

If $N_1<N_0$ then the absorption of light is stronger than the stimulated emission and no amplification can be observed. If $N_1=N_0$ then the rate of absorption becomes equal to the rate of stimulated emission, leading to a state of transparency for the incident photons. When $N_1>N_0$, stimulated emission becomes the dominating photophysical process. This condition is called population inversion and is responsible for the appearance of optical gain that leads to light amplification.

It can be shown that, for a system in thermal equilibrium, the population of the two energy states are given by Boltzmann statistics

$$\frac{N_1}{N_0} = \frac{g_1}{g_0}\exp(-\Delta E / kT) \qquad \textbf{2-IX}$$

where g_1 and g_0 are the degeneracies of levels E_1 and E_0 respectively and $\Delta E=E_1-E_0$.

In a two-level system however the ground state has a much larger number of molecules. When the population of the excited state becomes comparable to that of the ground state, a photon interacting with the material has an equal probability to be absorbed as it has to cause stimulated emission (since the Einstein coefficients for these two processes are the same). As a consequence, the best attainable result in a two-level system is transparency but population inversion is impossible.

The presence of additional vibronic energy levels in organic semiconductors means that they can be viewed as a 4-level energy system.[22] Figure 2.11 shows the 4 energy levels in an organic semiconductor that can lead to stimulated emission and population inversion.

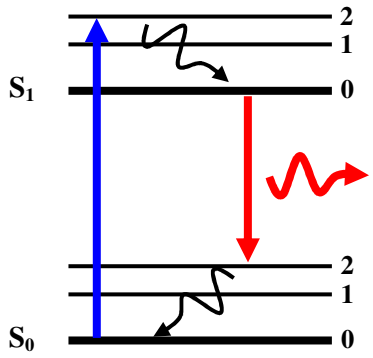

Figure 2.11 The 4-level system of electronic transitions in organic semiconductors that makes population inversion possible.

In the above scenario, absorption of light occurs between the lowest vibronic level $S_{0\text{-}0}$ of the ground state and the highest vibronic level $S_{1\text{-}2}$ of the excited state. The molecules than quickly relax through vibrational transitions to the lowest vibronic of the excited state $S_{1\text{-}0}$. Population inversion then is possible between this level and the highest vibrational level of the ground state $S_{0\text{-}2}$ where fluorescence occurs, giving rise to strong amplification of light, as shown in Figure 2.12. The key to this process is the fast vibrational relaxation in the ground and excited states that deplete the highest vibrational levels of population and thus make stimulated emission and population inversion much easier to attain.

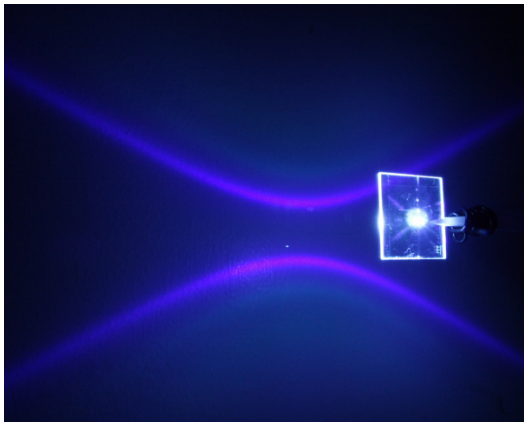

Figure 2.12 Amplified spontaneous emission from a thin film of an oligofluorene truxene. The emission pattern is caused by the corrugated substrate.

The population of the excited state can however be depleted by a number of additional processes. The presence of chemical defects within the material offers alternative paths for the excitons to relax, thus removing them from the $S_{1\text{-}0}$ energy state.[23] In addition, the large number of excitons under high pump photon densities can lead to exciton-exciton annihilation, where excitons travelling along the backbone of a conjugated collide with one another and the energy they carry does not contribute to fluorescence.[24]

Apart from the losses mentioned previously, the change in the intensity of light as it passes through a length l of material showing optical gain can be expressed using the following equation for intensity

$$I = I_0 \exp[(g - \alpha)l] \qquad \textbf{2-X}$$

where I_0 is the initial intensity of the light, g is the gain coefficient (per unit length) and α is the optical loss coefficient (per unit length) of the material.

The gain coefficient per unit length g can be expressed in terms of the populations of the excited state N_1 and the ground state N_0 as

$$g = \sigma(N_1 - N_0) \qquad \textbf{2-XI}$$

where σ is the stimulated emission cross-section, measured in m^2.

The optical loss comes from a number of factors such as ground-state absorption and photoinduced absorption. The ground-state absorption comes

from the fact that there is a small overlap between the absorption and emission bands of conjugated molecules, although the Stokes' shift alleviates this problem to a great extent. One of the ways to work around this type of loss is to split absorption and emission onto different materials using a nonradiative energy transfer mechanism known as Forster energy transfer.[25] This greatly reduces ground state absorption and allows for stronger light amplification that reduces the threshold for amplified spontaneous emission and lasing.[26, 27]

Photoinduced absorption originates from two different sources, excited-state absorption and polaron absorption. Excited state absorption occurs when singlet excitons are re-excited into a higher singlet state, therefore reducing the number of excitons that contribute to fluorescence.[28] Polarons are formed when an unpaired electron in an excited state interacts with the surrounding molecule changing the polarisation around the charge carrier [29] creating a virtual particle called a polaron between the electron and the polarisation change in the medium around it. This virtual particle has its own absorption bands that are based on the first excited state of the molecule and can thus reduce the population of the excited state.[30]

When all these loss mechanisms are taken into consideration, the optical gain per unit length available from organic semiconductors is still very high, with stimulated emission cross-sections up to 10^{-16} cm^2.[7] The combination of high optical gain with low concentration quenching [31] allows for solid-state thin films that show strong light amplification within a few hundred nanometres of the material.[7]

2.4. Organic semiconductor lasers

A laser consists of an optical gain medium combined with a feedback mechanism that allows for multiple passes through the gain medium and therefore higher amplification of the light. The simplest example of a laser device is shown in Figure 2.13, where a slab of gain material is placed between two mirrors that form a Fabry-Perot cavity.[32]

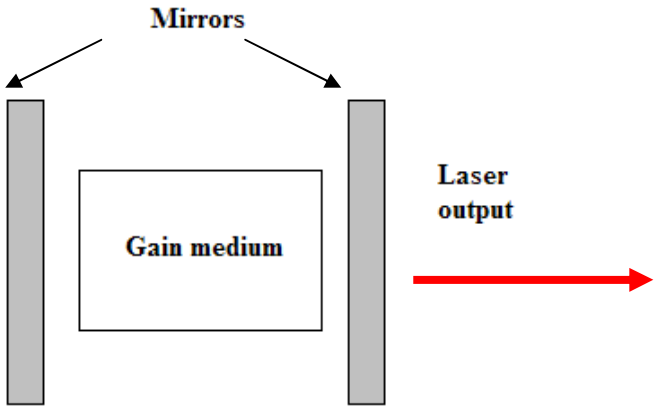

Figure 2.13 A simple laser structure based on a Fabry-Perot resonator cavity

The presence of a resonator cavity also has the effect that it imposes certain selection rules to the wavelengths that can be amplified within it. The two mirrors cause the field to form standing waves between them under the condition that an integer number of half wavelengths must fit into the cavity

$$m\frac{\lambda}{2} = nL \qquad \textbf{2-XII}$$

where nL is the optical length of the cavity given by its physical length L multiplied by the refractive index n of the medium. This leads to the appearance of a multitude of longitudinal modes that are separated by

$$\delta\lambda = \frac{\lambda^2}{2nL} \qquad \textbf{2-XIII}$$

2.4.1. Microcavity lasers

The first organic semiconductor lasers were based on Fabry-Perot microcavities to provide optical feedback, with the organic medium being either in solution[33] or in the solid state in thin films.[34, 35] The novel element in the case of organic semiconductors in the solid state was that due to the high values of optical gain available within the material, layers of only 100 nm thickness were required to achieve population inversion and lasing. A photo of such a laser in operation is shown in Figure 2.14, where the gain medium is the red-emitting polymer MEH-PPV pumped by a frequency-doubled ND:YAG microchip laser. Two dichroic mirrors form the Fabry-Perot microcavity that has a length equal to the thickness of the polymer layer (~200 nm).

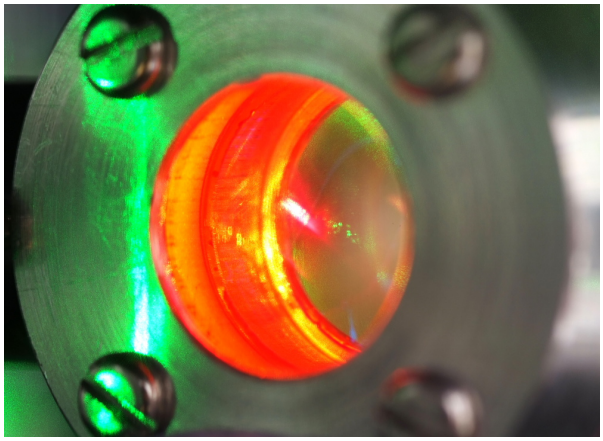

Figure 2.14 A Fabry-Perot microcavity MEH-PPV laser.

The ease of processing of organic semiconductors has since allowed a range of unusual resonator geometries to be developed, moving away from traditional flat cavities. Novel microcavity geometries include microrings,[36] microdisks[37] and microspheres[38] as shown in Figure 2.15, all of which are based on total internal reflection and whispering gallery modes to provide optical feedback.

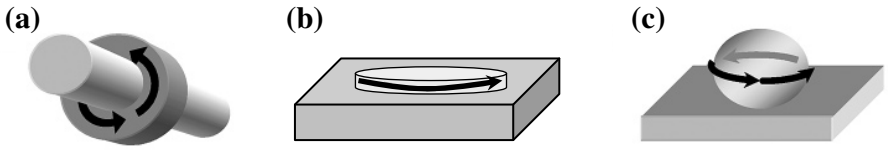

Figure 2.15 Whispering gallery-based organic microcavity lasers, (a) microring, (b) microdisk and (c) microsphere (adapted from [2]).

As these resonators were not used in this work, a detailed review of their properties is not included. Their key property though is the large number of lasing modes they support, as seen in Figure 2.16 but the quality of the lasing beam they emit is usually not very good as light is emitted in all directions around the cavity.

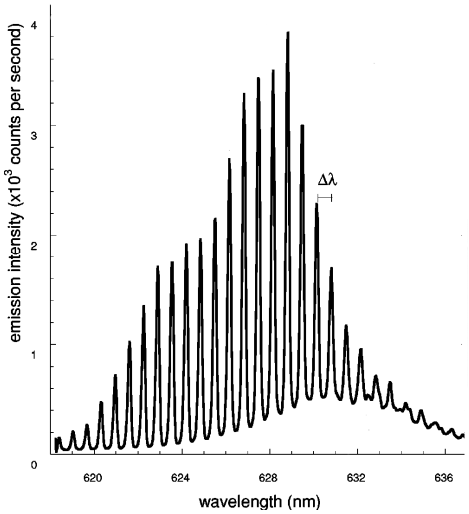

Figure 2.16 Emission spectrum from a microring laser based on DOOPPV (adapted from [39])

2.4.2. Distributed feedback lasers

One of the best-studied categories of organic lasers is distributed feedback (DFB) lasers. The resonators in this case are microscopic with dimensions from 100 μm to a few millimetres and make use of a periodic change in refractive index to provide optical feedback. A typical structure of a distributed feedback laser is seen in Figure 2.17.

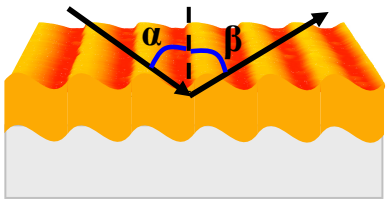

Figure 2.17 A thin-film one-dimensional distributed feedback organic laser (adapted from [2]).

A thin organic semiconductor film is spin-coated on top of a corrugated fused silica substrate. The fluorescence from the material is waveguided in the higher refractive index organic film and gets scattered by the periodic corrugations. If the period of the corrugations is suitable, the scattered light from each corrugation can combine through constructive interference to create a "Bragg-scattered" wave that also propagates within the film but in a different direction. This effect also depends on the angle of propagation, with different angles resulting in different Bragg-scattering conditions.

There is a case where a wave propagating in one direction through the plane of the film gets back-reflected due to Bragg scattering. This occurs if the wavelength λ of the light satisfies the Bragg equation

$$m\lambda_{Bragg} = 2n_{eff}\Lambda \qquad \textbf{2-XIV}$$

where Λ is the period of the corrugation, n_{eff} is the effective refractive index of the combined structure and m is an integer that corresponds to the order of the diffraction. In addition, the periodic structure acts as a diffraction grating [40] for a wave incident at an angle α that is diffracted at a new angle β when the wavelength is given by

$$n_{eff}\Lambda(\sin\alpha + \sin\beta) = m'\lambda_{Diff} \qquad \textbf{2-XV}$$

For a wave resonating in the plane of the film ($\alpha = 90^o$) due to Bragg scattering it is possible to extract light perpendicularly to the surface of the film ($\beta = 90^o$) through diffraction if the two wavelengths are the same, i.e. $\lambda_{Bragg} = \lambda_{Diff}$ that results in $m = 2m'$. In the simplest case $m = 2$ *and* $m' = 1$, so the feedback is provided in the plane of the film through second-order Bragg reflection and vertical output coupling results from first-order diffraction. This combination of properties makes DFB structures very attractive as it is generally difficult to fabricate a clean edge to the organic semiconductor waveguide, meaning that light that reaches the edges of a film is highly scattered in different directions. When combined with highly efficient materials, DFB resonators display some of the lowest lasing thresholds recorded in organic lasers as the light interacts with the gain medium over long distances (typically a few hundred micrometers or a few millimetres) in the plane of the waveguide.[41-45]

The periodic corrugation is usually fabricated on the silica substrate, in which case the pattern is firstly defined by holography in a photoresist layer spin-coated on the silica substrate. Chemical development of the resist followed by reactive-ion etching makes the corrugations permanent on the surface of the substrate.[46] Alternatively, a pattern from a master structure can be transferred onto the free surface of an organic film using techniques like nanoimprint lithography (NIL),[47] or solvent-assisted micro moulding (SAMiM).[48] Nanoimprint lithography consists of transferring the pattern from a master structure onto the surface of a softened organic film, a process that requires

pressure, UV light and/or heat that can have a great effect in the emission properties of the material.[49] The SAMiM technique on the other hand uses a small amount of solvent to ink an elastomeric mould, leading to the organic material being redissolved when in contact with the mould. The top surface of the film is then free to reshape itself following the corrugations of the mould that can be removed once the film is dry.

Distributed feedback gratings can be one-dimensional or two-dimensional, as shown in Figure 2.18. This two-dimensional grating can be considered as the superposition of two one-dimensional gratings rotated by 90^{o} and therefore provide optical feedback in two directions in the plane of the film. This allows for stronger light amplification from the same optically excited area, leading to lower lasing thresholds.[50]

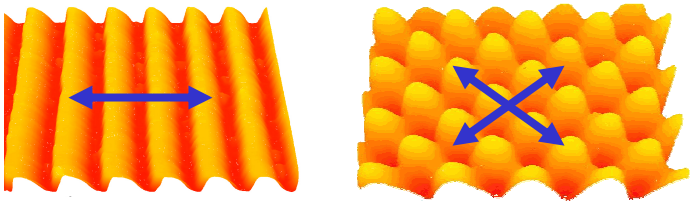

Figure 2.18 One- (left) and two-dimensional (right) distributed feedback gratings, showing the direction of light. Images are taken using an atomic-force microscope (AFM).

The quality of the output beam from distributed feedback lasers is an area where they have an advantage over the whispering gallery resonators. Below are two examples of emission from one-and two-dimensional DFB lasers.[51]

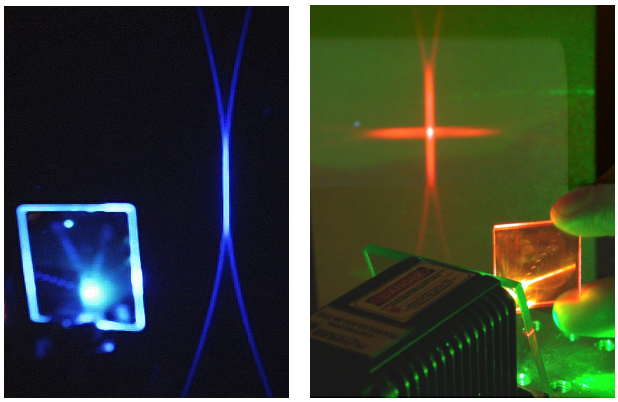

Figure 2.19 Emission patterns of the output beam for a one-dimensional (left) and a two-dimensional organic DFB laser.

The emission pattern from a 1D DFB laser is made up by two arcs of light that are identical but in the opposite directions, while the 2D DFB emission consists of two such sets of arcs rotated by 90°. The 1D case is the simplest one to study and can provide insight into the scattering mechanism that causes light emission in DFB lasers [51], but similar arguments can be used for a 2D grating.[46]

A one-dimensional distributed feedback grating is shown in Figure 2.20. We can define two directions of interest, one that runs perpendicular to the corrugation and one that is vertical to the surface of the film and therefore two angles, θ and φ that come away from them.

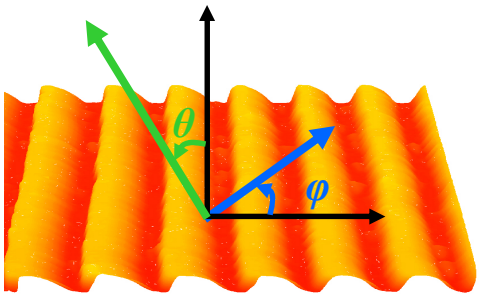

Figure 2.20 A one-dimensional distributed feedback grating where the angles that play an important role in Bragg scattering are noted. φ lies in the plane of the film while θ moves away from the perpendicular to the surface of the film.

For angles φ that are perpendicular to the in-plane axis, light travelling within the film does not experience a periodic change of refractive index and therefore no Bragg scattering occurs. Bragg scattering is strongest when φ is zero and so it makes sense to examine this condition to understand light emission for DFB gratings. The following discussion will therefore assume that $\varphi=0^o$. Within the plane guide a critical angle θ_c can be defined, beyond which any light becomes trapped in the waveguide due to total internal reflection and is either coupled into a new mode or interferes destructively with it, resulting in either case to no out-of-plane emission. For this paradigm then it is also assumed that $\theta<\theta_c$.

As described before, for surface emitting DFB gratings two different orders of Bragg scattering occur simultaneously, with the first order being responsible for coupling light out of (and into) the plane of the grating and the second order causing the optical feedback by forcing the waveguided light to be coupled into a counter-propagating optical mode. If light of a specific wavelength λ is

already travelling within a waveguided mode, it interacts with the grating and is coupled into a new mode. The momentum of the system needs to be conserved before and after this interaction and the momentum conservation is easier expressed using wavenumbers

$$k_{after} = k_{before} = \mp k_{mode} \pm mk_{grating} \quad \textbf{2-XVI}$$

where the ± symbols account for the different directions of propagation within the plane of the film and the in-plane wavevectors are defined as follows

$$k_{after} = \frac{2\pi}{\lambda}\sin(\theta),\ k_{mode} = \frac{2\pi n_{eff}}{\lambda},\ k_{grating} = \frac{2\pi}{\Lambda} \quad \textbf{2-XVII}$$

where Λ is the period of the corrugation and n_{eff} is the effective refractive index for the mode travelling in the waveguide.

The momentum conservation equation can then be written as

$$\frac{2\pi}{\lambda}\sin(\theta) = \mp\frac{2\pi n_{eff}}{\lambda} \pm m\frac{2\pi}{\Lambda} \quad \textbf{2-XVIII}$$

Solving this equation for light travelling in each direction separately, we can calculate that for a given grating period and scattering angle two different wavelengths will be scattered out of the plane of the waveguide, with wavelength given by

$$\lambda_{\pm} = \frac{n_{eff} \pm \sin(\theta)}{m}\Lambda \quad \textbf{2-XIX}$$

The previous equation can be used to plot the transmission of light through the gating as a function of both wavelength and the angle θ, as seen in Figure 2.21 for a second order ($m = 2$) grating.

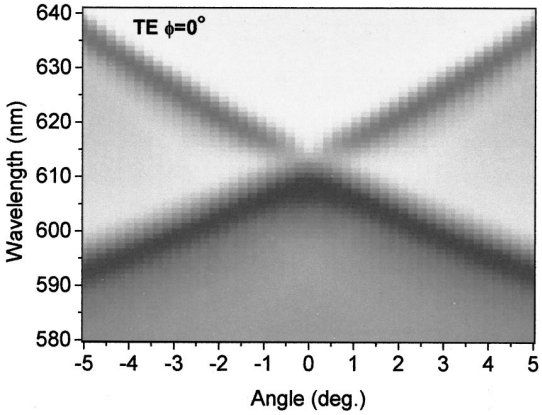

Figure 2.21 Wavelength coupled out of the surface of a thin waveguide as a function of the angle to the surface vector (adapted from [51]). The dark regions correspond to areas of low transmission.

When looking at angles close to normal incidence (θ~0^o), the counter-propagating modes due to second-order Bragg scattering are the same as the out-coupled modes of the first order. These two modes then interfere to produce a standing wave that has a periodicity equal to $\Lambda/2$. Based on symmetry arguments,[52] it has been shown that two such modes are supported that have nodes at either at the maxima or the minima of the fundamental spatial component of the grating wave-vector $\Lambda/2$. This means that the two standing waves that are supported for $\theta=0^o$ have different energies, leading to the appearance of an energy gap between them as any modes with energy between the two standing waves cannot propagate within the waveguide. This means that any light with wavelength near the band gap wavelength cannot propagate in the plane of the waveguide and therefore has to exit the waveguide at an angle to the surface. This occurs around 610 nm in the example shown in Figure 2.21. Lasing will occur near the edge of the band gap in the top quarter of the graph in Figure 2.21. This is demonstrated in Figure 2.22 where an actual emission pattern is shown for a one-dimensional DFB laser based on MEH-PPV.

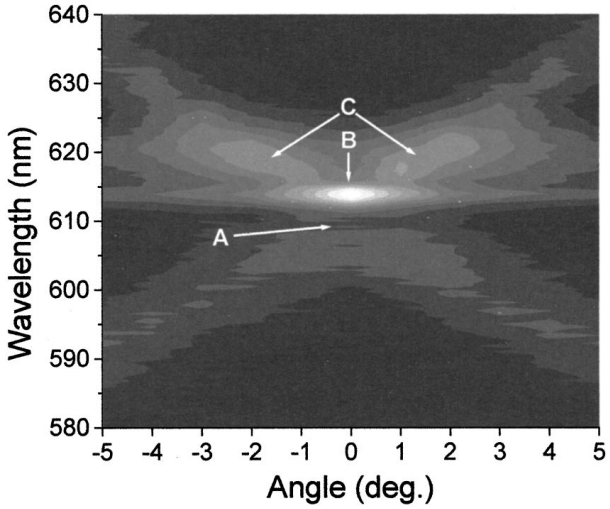

Figure 2.22 Angle-dependent emission from a one-dimensional DFB laser operating above lasing threshold. A denotes the photonic bandgap, B is the lasing emission and C is the Bragg-scattered ASE (adapted from [51]).

The same approach can account for higher order transverse modes within the waveguide, and also for cases where the wavelength of the mode does not exactly match the conditions for Bragg scattering at $\varphi=0^o$. These conditions give rise to emission patterns that are similar in shape as the ones shown above but their centres are offset from normal incidence as shown in Figure 2.23,

where a longer grating period moves the arcs across the stop band on either side and a shorter period further separates them.

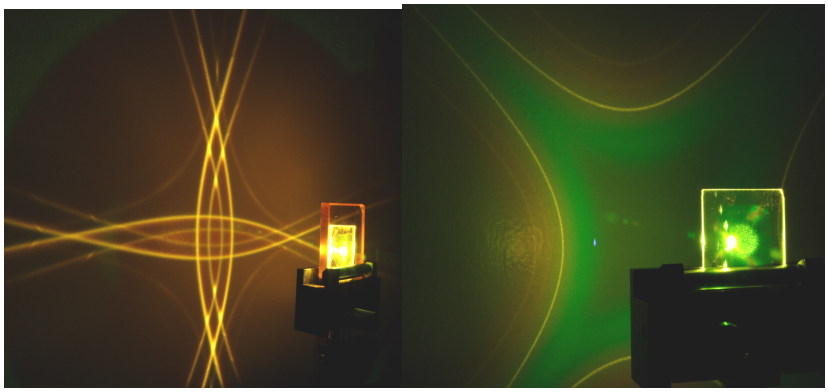

Figure 2.23 Bragg-scattered amplified spontaneous emission from a laser dye matched to a 2D grating with a longer-than-ideal grating period (left) and from a green-emitting polymer with a shorter-than-ideal 2D DFB grating.

2.4.3. Distributed Bragg reflector lasers

This category of organic semiconductor lasers can be considered a variation of the distributed feedback resonators described previously. A distributed Bragg reflector (DBR) cavity consists of a one-dimensional distributed feedback grating that has a defect region in the middle, an area without corrugations. The presence of this defect creates additional modes that can resonate between the two corrugated areas, resembling to some extent a classic Fabry-Perot cavity where the two corrugated areas acts as Bragg mirrors and the flat region is the optical cavity in which the standing waves of the different modes oscillate. This configuration gives rise to multiple longitudinal lasing modes supported within the cavity as seen in Figure 2.24.

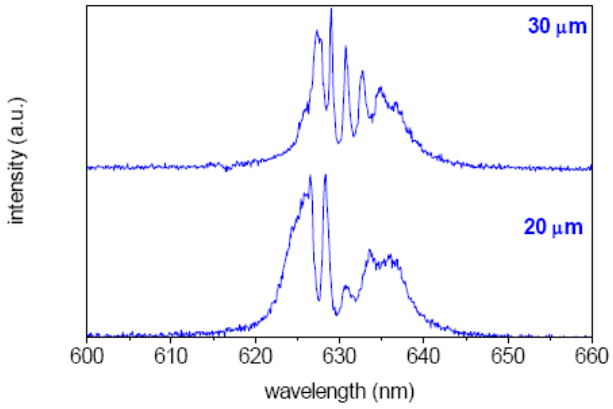

Figure 2.24 Cavity modes from a distributed Bragg reflector cavity using MEH-PPV as the gain medium. [44]

Usually DBRs are edge-emitting cavities, but in this thesis a surface-emitting DBR laser was used to circumvent the problem of poor edge-forming in organic waveguides. Its structure can be seen in Figure 2.25 where the amplification area is excited by a pump laser and laser emission is out-coupled by the Bragg mirrors on either end.

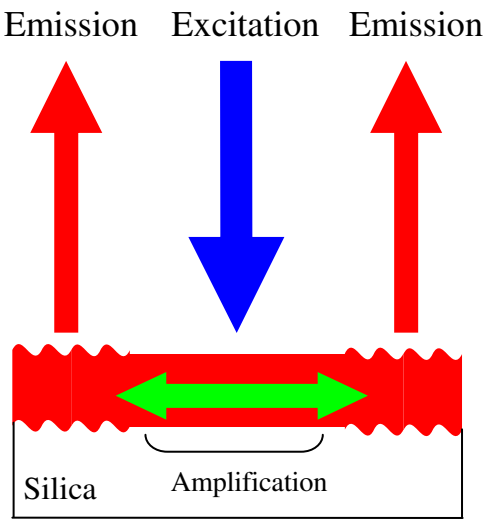

Figure 2.25 A distributed Bragg reflector organic laser.

The main advantage of DBR lasers is the separation of the optically pumped region from the Bragg grating that can introduce losses due to the fact that a thin film spin-coated on top of the corrugations can have increased surface roughness that reduces the quality of the waveguide. Separating the two regions can therefore reduce the waveguide losses and by doing that allow for lower lasing threshold in these structures.[53] More information on the spectral and spatial output of this resonator can be found in reference [44].

2.5. References

[1] T. H. Maiman, *Nature* **1960**, *187*, 493.

[2] I. D. W. Samuel, G. A. Turnbull, *Chem. Rev.* **2007**, *107*, 1272.

[3] J. McMurry, *Organic chemistry*, Brooks/Cole - Thomson Learning, Belmont **2004**.

[4] O. S. Avanesjan, V. A. Benderskii, V. K. Brikenstein, V. L. Broude, L. I. Korshunov, A. G. Lavrushko, Tartakovskii, II, *Molecular Crystals and Liquid Crystals* **1974**, *29*, 165.

[5] C. W. Tang, S. A. Vanslyke, *Applied Physics Letters* **1987**, *51*, 913.

[6] G. Heliotis, R. Xia, D. D. C. Bradley, G. A. Turnbull, I. D. W. Samuel, P. Andrew, W. L. Barnes, *Applied Physics Letters* **2003**, *83*, 2118.

[7] N. Tessler, G. J. Denton, R. H. Friend, *Nature* **1996**, *382*, 695.

[8] J. R. Lawrence, G. A. Turnbull, I. D. W. Samuel, G. J. Richards, P. L. Burn, *Optics Letters* **2004**, *29*, 869.

[9] A. L. Kanibolotsky, R. Berridge, P. J. Skabara, I. F. Perepichka, D. D. C. Bradley, M. Koeberg, *Journal of the American Chemical Society* **2004**, *126*, 13695.

[10] T. Spehr, A. Siebert, T. Fuhrmann-Lieker, J. Salbeck, T. Rabe, T. Riedl, H. H. Johannes, W. Kowalsky, J. Wang, T. Weimann, P. Hinze, *Applied Physics Letters* **2005**, *87*, 3.

[11] P. W. Atkins, *Physical Chemistry*, **1986**.

[12] W. Y. Liang, *Physics Education* **1970**, *5*, 226.

[13] J. Franck, *Transactions of the Faraday Society* **1926**, *21*, 536.

[14] E. Condon, *Physical Review* **1926**, *28*, 1182.

[15] IUPAC, **1997**.

[16] M. Göppert-Mayer, *Ann. Phys.* **1931**, *9*, 273.

[17] W. Kaiser, C. G. B. Garrett, *Physical Review Letters* **1961**, *7*, 229.

[18] H. Kuhn, J. Robillard, *Nonlinear Optical Materials*, CRC Press, Florida **1991**.

[19] G. Y. Zhou, W. Dong, X. M. Wang, Z. S. Shao, M. H. Jiang, *Optics Communications* **2004**, *241*, 215.

[20] A. Einstein, *Physikalische Zeitschrift* **1917**, *18*.

[21] R. C. Tolman, *Reviews of Modern Physics* **1924**, *23*, 693.

[22] B. Schweitzer, G. Wegmann, H. Giessen, D. Hertel, H. Bassler, R. F. Mahrt, U. Scherf, K. Mullen, *Applied Physics Letters* **1998**, *72*, 2933.

[23] G. J. Denton, N. Tessler, N. T. Harrison, R. H. Friend, *Physical Review Letters* **1997**, *78*, 733.

[24] R. H. Friend, D. D. C. Bradley, P. D. Townsend, *Journal of Physics D-Applied Physics* **1987**, *20*, 1367.

[25] T. Förster, *Annalen der Physik* **1948**, *437*, 55.

[26] R. Gupta, M. Stevenson, A. Dogariu, M. D. McGehee, J. Y. Park, V. Srdanov, A. J. Heeger, H. Wang, *Applied Physics Letters* **1998**, *73*, 3492.

[27] A. K. Sheridan, A. R. Buckley, A. M. Fox, A. Bacher, D. D. C. Bradley, I. D. W. Samuel, *Journal of Applied Physics* **2002**, *92*, 6367.

[28] K. D. Belfield, M. V. Bondar, I. Cohanoschi, F. E. Hernandez, O. D. Kachkovsky, O. V. Przhonska, S. Yao, *Applied Optics* **2005**, *44*, 7232.

[29] L. D. Landau, *Phys. Z. Sowjetunion* **1933**, *3*, 644.

[30] M. D. McGehee, A. J. Heeger, *Advanced Materials* **2000**, *12*, 1655.

[31] G. A. Turnbull, (Ed: B. D. Guenther), Elsevier, Oxford **2005**, 485.

[32] O. Svelto, *Principles of Lasers*, Plenum Press, New York **1982**.

[33] D. Moses, *Applied Physics Letters* **1992**, *60*, 3215.

[34] F. Hide, M. A. DiazGarcia, B. J. Schwartz, M. R. Andersson, Q. B. Pei, A. J. Heeger, *Science* **1996**, *273*, 1833.

[35] N. Tessler, *Advanced Materials* **1999**, *11*, 363.

[36] A. Schulzgen, C. Spiegelberg, M. M. Morrell, S. B. Mendes, P. M. Allemand, Y. Kawabe, M. Kuwata-Gonokami, S. Honkanen, M. Fallahi, B. Kippelen, N. Peyghambarian, *Opt. Eng.* **1998**, *37*, 1149.

[37] M. Berggren, A. Dodabalapur, R. E. Slusher, Z. Bao, "Organic lasers based on Forster transfer", presented at *International Conference on Electroluminescence of Molecular Materials and Related Phenomena*, Fukuoka, Japan, May 21-24, **1997**.

[38] M. Berggren, A. Dodabalapur, Z. N. Bao, R. E. Slusher, *Advanced Materials* **1997**, *9*, 968.

[39] R. C. Polson, G. Levina, Z. V. Vardeny, *Applied Physics Letters* **2000**, *76*, 3858.

[40] E. Hecht, *Optics*, Addison Wesley, San Francisco **2002**.

[41] C. Rothe, F. Galbrecht, U. Scherf, A. Monkman, *Advanced Materials* **2006**, *18*, 2137.

[42] G. Heliotis, S. A. Choulis, G. Itskos, R. Xia, R. Murray, P. N. Stavrinou, D. D. C. Bradley, *Applied Physics Letters* **2006**, *88*.

[43] C. Karnutsch, C. Pflumm, G. Heliotis, J. C. Demello, D. D. C. Bradley, J. Wang, T. Weimann, V. Haug, C. Gartner, U. Lemmer, *Applied Physics Letters* **2007**, *90*.

[44] A. E. Vasdekis, *PhD Thesis, University of St Andrews* **2007**.

[45] W. Y. Lai, R. D. Xia, Q. Y. He, P. A. Levermore, W. Huang, D. D. C. Bradley, *Advanced Materials* **2009**, *21*, 355.

[46] G. A. Turnbull, P. Andrew, W. L. Barnes, I. D. W. Samuel, *Physical Review B* **2003**, *67*, 165107.

[47] D. Pisignano, L. Persano, E. Mele, P. Visconti, M. Anni, G. Gigli, R. Cingolani, L. Favaretto, G. Barbarella, "First-order imprinted organic distributed feedback lasers", presented at *International Conference on Science and Technology of Synthetic Metals*, Wollongong, AUSTRALIA, Jun 28-Jul 02, **2004**.

[48] J. R. Lawrence, G. A. Turnbull, I. D. W. Samuel, *Applied Physics Letters* **2003**, *82*, 4023.

[49] D. Pisignano, E. Mele, L. Persano, G. Paladini, R. Cingolani, *Applied Physics Letters* **2005**, *86*, 3.

[50] G. Heliotis, R. D. Xia, G. A. Turnbull, P. Andrew, W. L. Barnes, I. D. W. Samuel, D. D. C. Bradley, *Advanced Functional Materials* **2004**, *14*, 91.

[51] G. A. Turnbull, P. Andrew, M. J. Jory, W. L. Barnes, I. D. W. Samuel, *Physical Review B* **2001**, *64*, 125122.

[52] W. L. Barnes, T. W. Preist, S. C. Kitson, J. R. Sambles, *Physical Review B* **1996**, *54*, 6227.

[53] A. E. Vasdekis, G. Tsiminis, J. C. Ribierre, L. O'Faolain, T. F. Krauss, G. A. Turnbull, I. D. W. Samuel, *Optics Express* **2006**, *14*, 9211.

3. Experimental methods

3.1. Introduction

This chapter gives an overview of the various experimental techniques and instruments that were used throughout this thesis. Several experimental setups were used for the preparation and characterization of the organic materials studied in this work and a number of laser devices were fabricated and evaluated in numerous ways.

Any laser consists of three basic components: the gain medium, the feedback resonator and the pump source that provides energy to the gain medium. This thesis focuses mostly on the gain medium of organic semiconductor lasers and therefore the techniques used were aimed towards the photophysical and optical characterization of organic semiconductors.

All the materials used in this thesis are solution-processable, so all of the samples studied here begin their life as solution in various organic solvents. Initial measurements are usually performed in solution before proceeding to measuring thin films, but the techniques used are the same.

3.2. Sample preparation

The first step in any characterization is preparing a suitable sample. All the materials used in this thesis are obtained in powder form and are added to a suitable solvent to prepare solutions. Once the exact amount of material is weighed and placed in a dark yellow vial to reduce UV light exposure, an appropriate amount of solvent is added and a magnetic stirrer is placed in the vial to help dissolve the material as the solution is placed on a stirrer plate. Different organic molecules are soluble to different degrees and therefore the time required can vary from near-instant to 24 hours, while some materials require heating at moderate temperatures (~60 ^{0}C) for brief periods of time to

dissolve properly. The concentrations prepared in this way vary between 1 and 30 mg/ml depending on the solubility and the size of each molecule, with typical concentrations of 30 mg/ml for fluorene-based materials and 5 mg/ml for MEH-PPV.

3.2.1. Thin film preparation

Films of organic semiconductors can be prepared from solution using different techniques such as spin-coating, dip-coating or doctor-blade.[1] The method used in this work is spin-coating as it is better suited to the thin films required for lasing and allows for a more accurate control of the film thickness. This method also results in films of high optical quality (flat top surface of the films) that is required for efficient waveguiding within the film.

The substrate on which the thin film will be deposited (usually glass or quartz) is cleaned by rinsing it in acetone and isopropanol inside an ultrasonic bath and is then placed on the holder of a spinner. The substrate is held there by a vacuum and a few drops of the solution are placed in its centre before it is spun at speeds ranging from 500 to 2000 rpm. The solution then spreads outwards under the influence of the centrifuge force, forming thin films of good optical quality that have a uniform thickness across most of their surface. The thickness of the spin-coated films is determined by the solution concentration, the spin speed and time as well as the solvent used and is measured using a surface profile meter. Usual film thicknesses for lasers are between 80 and 300 nm, although devices with film thickness up to a micron have been made.

3.3. Optical characterisation

3.3.1. Variable angle spectroscopic ellipsometry

Variable angle spectroscopic ellipsometry (VASE) is a powerful technique for characterising the dielectric properties of thin films. These properties include the complex refractive index $\underline{n}$ of the material as defined by

$$\underline{n} = n + ik \qquad \textbf{3-I}$$

where n is the refractive index of the material and k is the extinction coefficient that indicates the amount of absorption of an electromagnetic wave as it travels through the material.

Ellipsometric measurements record the change in the polarisation of light that is reflected from a flat sample as a function of wavelength and angle of incidence for p (parallel) or s (senkrecht) polarised light.[2] Ellipsometry then determines the change in the coefficient Ψ and Δ that are related to the reflection and transmission coefficients by

$$\frac{\hat{R}_p}{\hat{R}_s} = \tan\Psi_r \exp(i\Delta_r) \qquad \textbf{3-II}$$

$$\frac{\hat{T}_p}{\hat{T}_s} = \tan\Psi_t \exp(i\Delta_r) \qquad \textbf{3-III}$$

where $\hat{R}_p$, $\hat{T}_p$, $\hat{R}_s$ and $\hat{T}_s$ are the complex amplitude reflection ($\hat{R}$) and transmission ($\hat{T}$) coefficients for p and s polarized light. A sketch of a typical ellipsometry setup can be seen in Figure 3.1.

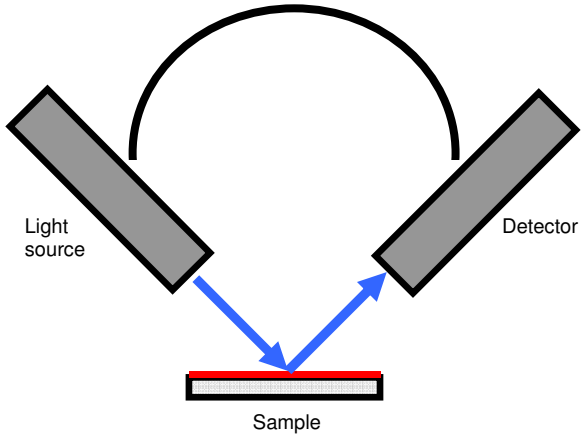

Figure 3.1 A typical variable angle spectroscopic ellipsometry setup showing the relative orientation of the light source and photodetector arms of the instrument.

The measured values of Ψ and Δ do not directly relate to the optical constants of refractive index n and extinction coefficient k, so an optical model using iterative fitting is required to extract these coefficients. Fitting parameters include the optical constants, the oscillator model that best describes each molecule, the plane-parallel interfaces between layers, reflections of the beam through the material and the thickness of the film. Some organic molecules show a degree of preferential orientation within a thin film and therefore show some optical anisotropy that leads to birefringence, therefore producing a set of ordinary and extra-ordinary refractive indexes and extinction coefficients while others are randomly orientated leading to isotropic films. A typical ellipsometry measurement showing values for both Ψ and Δ can be seen in Figure 3.2 for the range between 300 and 800 nm, the usual area of interest for organic light-emitting molecules. Differrrent angles of incidence display different degrees of change in the values of Ψ and Δ depending on the thickness of the film measured and the orientation of the molecules.

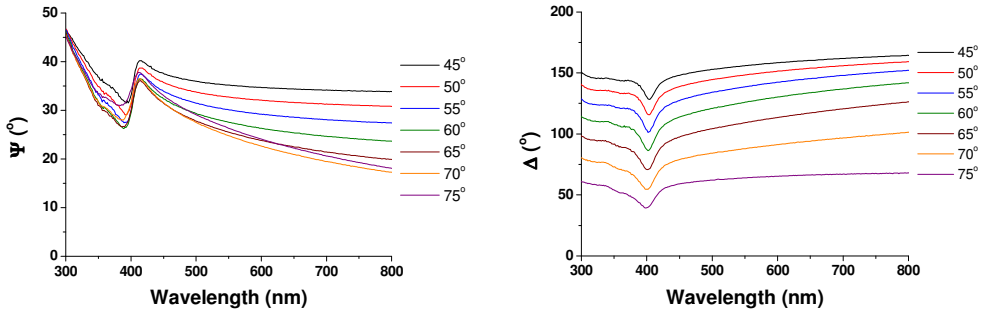

Figure 3.2 Ellipsometry data for Ψ (top) and Δ (bottom) collected between 300 and 800 nm for a range of different angles. These measurements were performed on oligofluorene truxene thin films.

The corresponding optical constants n and k that are extracted from the above parameters using the software's fitting module for the same range can be seen below:

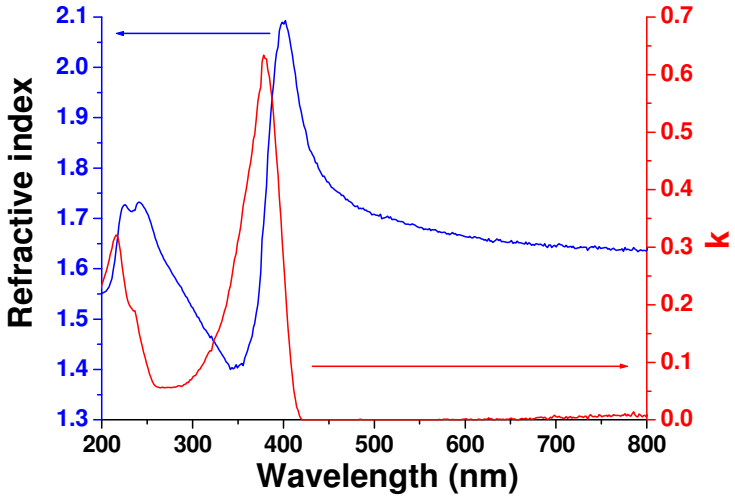

Figure 3.3 Refractive index and extinction coefficients of a thin film of an oligofluorene truxene as calculated through ellipsometry measurements.

The ellipsometric measurements in this thesis were performed using a J.A.Woolam Co. Inc. M-2000DI ellipsometer over a spectroscopic range of 200 nm to 1700 nm for angles of 45° to 75° in steps of 5°. The fitting software, Wvase32, comes from the same company and uses a Levenberg-Marquardt algorithm to fit the experimental data.[3]

3.4. Photophysical characterisation

Once samples are prepared, their basic photophysical properties are characterised. These originate in the way the molecules of a material absorb light and the different paths they follow to relax back to their ground state and are the first step in evaluating any material for optoelectronics applications.

3.4.1. Absorption and photoluminescence

For all materials, absorption and photoluminescence measurements are performed. The absorption measurements are carried out on a Cary Varian 300 UV-Vis absorption spectrometer, both in films and in solutions. For this measurement the substrate is always quartz (or quartz cuvettes for solutions) as the losses in the UV are smaller than plain glass. The sample is placed on one

arm of the instrument and a blank substrate (or empty cuvette) is placed in the other, allowing for correction of the losses due to the substrate.

Photoluminescence measurements are performed using a Jobin Yvon Fluoromax 2 spectrometer. The desired excitation wavelength can be accurately selected across the emission spectrum of a xenon lamp using a monochromator, and the resulting photoluminescence is recorded through a second monochromator by a photomultiplier tube. The data is then processed using a calibration file that corrects the photomultiplier's response across different wavelengths.

A typical absorption and photoluminescence spectrum can be seen in Figure 3.4 for a thin film of polyfluorene (PFO).

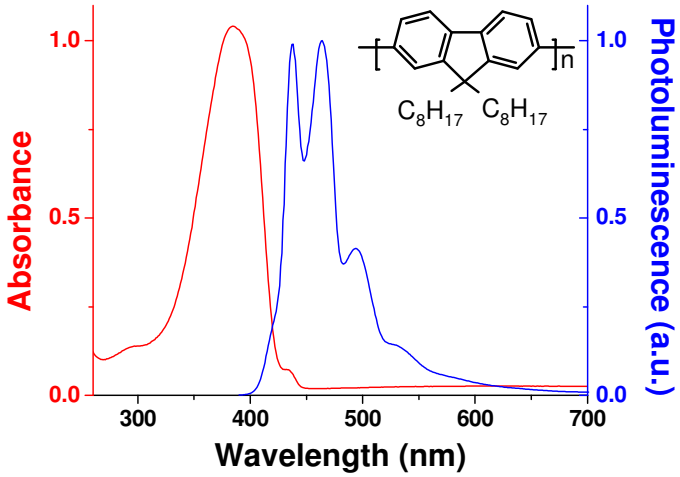

Figure 3.4 Absorption (red line) and emission (blue line) spectrum of polyfluorene for a thin film (thickness 100 nm). The inset shows the molecular structure of polyfluorene.

3.4.2. Photoluminescence quantum yield

The photoluminescence quantum yield (PLQY) of a material is the efficiency of its light emission. It is generally defined as the number of photons emitted by a sample of the material divided by the number of photons it absorbed.

Experimentally, a laser beam of a specific wavelength and known power is directed at a sample and the photoluminescence that the material produces is recorded using a calibrated photodiode.[4] In order to make sure that all of the emitted light is collected, the sample is placed within a hollow integrating sphere that is internally coated with a highly reflective layer. The integrating sphere has a number of openings, one for the pump beam to enter, another opening on the opposite side to allow for the transmitted excitation beam to be measured and one for the photodiode that includes a filter to cut off the excitation laser light, as seen in Figure 3.5.

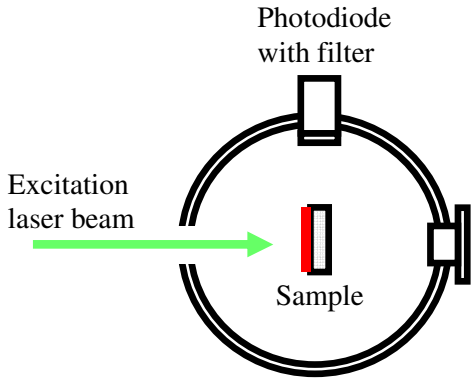

Figure 3.5 Typical setup for measurement of photoluminescence quantum yield in thin films of organic semiconductors.

The readings from the photodiode need to be corrected to take into account the reflections from the sample and the transmitted laser power, allowing for a calculation of the actual absorbed power. Neglecting the spectral response of the photodiode, the quantum efficiency x from such a measurement is given by equation 3-III

$$x = \frac{X_{sample} - (R+T)X_{sphere}}{(1-R-T)X_{laser}} \qquad \textbf{3-IV}$$

where R is the reflectance of the sample and T is the transmittance. The additional factors in the above equation account for a number of additional sources of light that are recorded by the photodiode besides the material's photoluminescence. X_{laser} is the signal that the photodiode measures as the laser light is hitting the walls of the integrating sphere without a sample in place in order to correct the measurement for scattered excitation light. X_{sphere} is the photodiode signal when the sample is illuminated indirectly by laser light that is

scattered from the sphere's interior and finally X_{sample} is the recorded signal for direct laser excitation of the film.

The spectral response of the photodiode across the material's emission spectrum also needs to be taken into account. If a white light source such as a tungsten lamp has an emission spectrum $S_{lamp}(\lambda)$, this is modified by the reflectance of the sphere and becomes $S_{sphere}(\lambda)$. The spectral response correction factor is then given by

$$y = \int \frac{S_{sphere}(\lambda)L(\lambda)G(\lambda)F(\lambda)}{S_{lamp}(\lambda)} d\lambda \times \left(\frac{S_{sphere}(\lambda_{exc})G(\lambda_{exc})}{S_{lamp}(\lambda_{exc})} \int L(\lambda)d\lambda \right)^{-1} \quad \textbf{3-V}$$

where $L(\lambda)$ is the emission spectrum from the material as recorded by a photoluminescence measurement, $G(\lambda)$ is the quantum efficiency of the photodiode across different wavelengths, $F(\lambda)$ is the transmission of the filter used and λ_{exc} is the excitation laser wavelength.

The absolute photoluminescence quantum yield of a material is then given by x/y and can be as high as 100% for some very efficient organic materials.[5]

3.5. Lasing studies

Lasing studies of organic semiconductors require high excitation densities to explore what the material's behaviour is under condition of population inversion when the material amplifies light. These studies include amplified spontaneous emission measurements to determine the threshold of amplified spontaneous emission, a precursor to lasing, and the values for optical gain and loss. In addition, the laser devices fabricated need to be characterised to determine their lasing threshold, slope efficiency and lifetime.

3.5.1. Excitation sources

Three different laser systems were used for the majority of the lasing studies, a nanosecond optical parametric oscillator, a femtosecond optical parametric amplifier system and a microchip laser.

3.5.1.1. Optical parametric oscillator

For most of the experiments described in this thesis an optical parametric oscillator (OPO) was used as a widely-tunable pump source. An OPO contains a non-linear crystal that, when illuminated with laser light of a specific energy (specific wavelength), produces a pair of photons with lower energies (longer wavelengths) than the original pump photon. The sum of the energies of the two photons (called signal and idler photons) must be equal to the energy of the initial photon in order for the energy to be preserved in the system. This can be written as

$$\nu_p = \nu_s + \nu_i \qquad \textbf{3-VI}$$

where ν_p is the frequency of the pump photon and ν_s, ν_i are the frequencies of the signal and idler photons respectively.

In addition, momentum must also be preserved for the photons participating in this interaction, as described in the following equation

$$\Delta k = k_p - k_s - k_i = 0 \qquad \textbf{3-VII}$$

where the corresponding wavevectors for the pump, signal and idler photons must result in a zero overall momentum difference. In order for that to happen within a non-linear crystal, a technique called phase matching is used, which utilises the different refractive index of the crystal material at different electric field polarisations to allow for a pair of signal and idler photons to be produced from a given pump photon. This pair of photons can be tuned across a wide spectrum by changing the phase-matching condition, always keeping in mind the energy conservation principle.

The OPO used in these experiments (Panther OPO, from Photonic Solutions) is pumped using the 3rd harmonic of an Nd:YAG laser (355 nm), which has an

energy of 100 mJ per pulse. The OPO produces a wide range of output wavelengths from 410 nm up to 2500 nm (expandable into the UV using double crystals that allow the extraction of wavelengths as low as 220 nm) at energies of up to 14 mJ per pulse, with a pulse duration of 4 ns at a repetition rate of 20 Hz. This OPO uses a BBO nonlinear crystal that is angle-tuned, meaning that the rotation of the crystal in relation to the path of the pump beam running through it changes the phase-matching condition to produce a different pair of signal and idler wavelengths. The BBO crystal is placed within a cavity that double passes the idler wavelengths (infra-red reflecting mirrors) to achieve self-seeding of the parametric process and increased conversion efficiency. A compensator crystal at the output of the cavity ensures that the wavelengths produced by angle-tuning of the nonlinear crystal exit the cavity in the same direction.

The OPO was incorporated in the setup seen in Figure 3.6, which allows for the energy of the OPO beam to be varied using a set of two cube polarisers (to maintain a constant polarisation of the beam hitting the sample) mounted on rotating base plates, and also provides enough space on the optical table to insert various elements such as focusing optics, vacuum chambers, neutral density filters and an observation screen to observe the emission patterns from organic lasers.

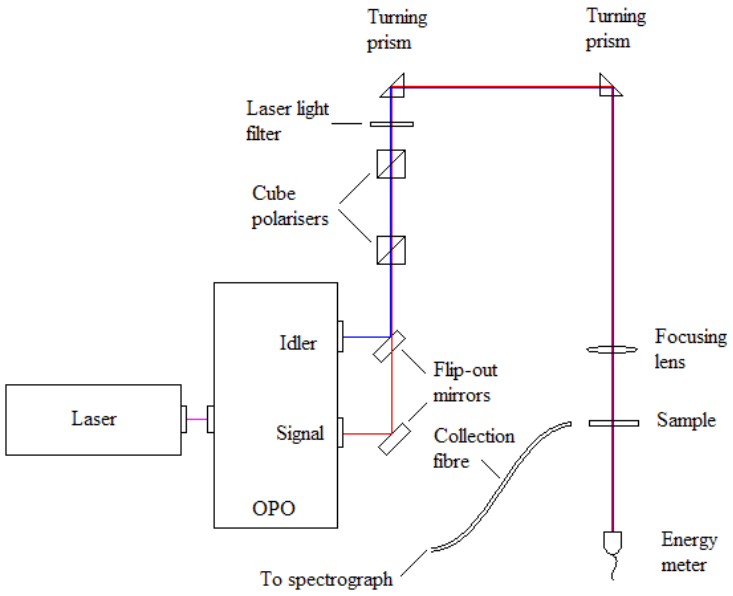

Figure 3.6 Photophysical measurements setup that uses the optical parametric oscillator for optical excitation of organic semiconductor samples.

The photoluminescence from the sample was recorded using a Jobin-Yvon Triax 180 spectrograph connected to a cooled CCD detector array that collected sample fluorescence through an optical fibre.

3.5.1.2. Optical parametric amplifier system

The pump light for the femtosecond experiments comes from a diode-pumped mode-locked Ti:Sapphire femtosecond laser emitting at 800 nm. This light is then passed through a Hurricane regenerative amplifier to increase the peak power of the beam. The amplified beam is then used as the pump source for an optical parametric amplifier (OPA) by Spectra Physics. Upon entering the OPA the beam is split into two parts, with the weakest part is tightly focused on a sapphire plate to generate a white-light continuum extending from 450 to 750 nm. The main part of the 800 nm beam is used to optically pump a Beta Barium Borate (BBO) nonlinear crystal that can be rotated to satisfy the phase-matching equation for a different pair of signal and idler photons, thus selecting what wavelength from the white-light continuum spectrum that is also incident on the BBO crystal will be amplified. Further nonlinear processes such as sum and difference frequency mixing are possible that, along with second and third-harmonic generation crystal can extend the tuning range of the system. The pump beam resulting from the above amplification stages has a pulse duration of 100 fs at a repetition rate of 5 kHz and can be tuned from 200 nm to 10 μm with energies in the range of tens of microjoules.

3.5.1.3. Microchip laser

At the beginning of this PhD, the microchip laser represents the most compact pump source for organic semiconductor lasers.[6, 7] Monolithic microchip lasers combine compact dimensions with high output efficiency, moderate output power and have been studied extensively, making them very robust and reliable.[8]

A typical microchip laser is based around a Neodymium-doped optical material, usually a crystal such as Yttrium Aluminium Garnet (Nd:YAG) or Yttrium Orthovanadate (Nd:YVO_4) that is optically excited by an infrared laser diode emitting at 808 nm. The gain medium is Neodymium and the host material acts as a spacer for the molecules, allowing for population inversion and lasing that occurs at 1064 nm. These lasers can be Q-switched to achieve nanosecond pulses at kHz repetition rates that lead to higher optical powers. They can also include frequency doubling and tripling nonlinear crystals to produce 532 nm and 355 nm respectively, allowing microchip lasers to be used as optical pumping sources for a wide range of organic semiconductors. Two such microchip lasers were used in this work to pump organic distributed feedback lasers with nanosecond pulses.

3.5.2. Amplified spontaneous emission measurements

As discussed in the introduction, amplified spontaneous emission (ASE) is an important factor in evaluating the suitability of organic materials for lasing. ASE appears just as the material reaches population inversion and is accompanied by a narrowing of the fluorescence spectrum down to 4-6 nm (determined by the spectral broadening of the material's optical gain). A low ASE threshold combined with a high-quality optical resonator results in low lasing thresholds. To investigate the appearance of ASE in a material and its properties, measurements in thin films are the most common approach.

A thin film is spin coated onto a glass substrate from a solution containing the organic semiconductor of interest and this sample is placed within a vacuum chamber (10^{-3} to 10^{-5}mbar pressure) to slow down photo oxidation. The pump beam from a laser source is focused to a thin stripe onto the surface of the film and the induced fluorescence that is waveguided through the film and is scattered out from the edges is recorded using a CCD spectrograph. The intensity and spectral width of the fluorescence is then recorded for increasing excitation powers using an optical fibre as seen in Figure 3.7.

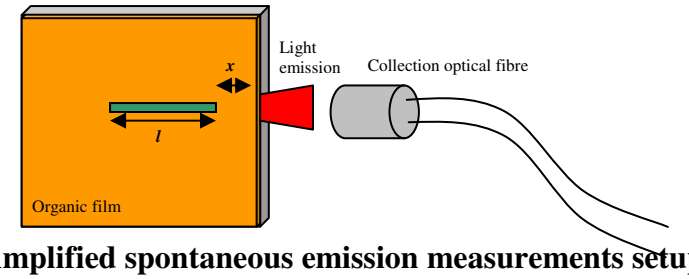

Figure 3.7 Amplified spontaneous emission measurements setup.

As the excitation power becomes progressively higher, the emission spectrum from the material begins to narrow from an original value of 40-50 nm to below 10 nm as a consequence of the optical gain profile of ASE. At the same time, the intensity of the fluorescence increases in a nonlinear way as light within the gain curve is amplified by the material. The pump power threshold for these two observations is the ASE threshold and can be seen in Figure 3.8.

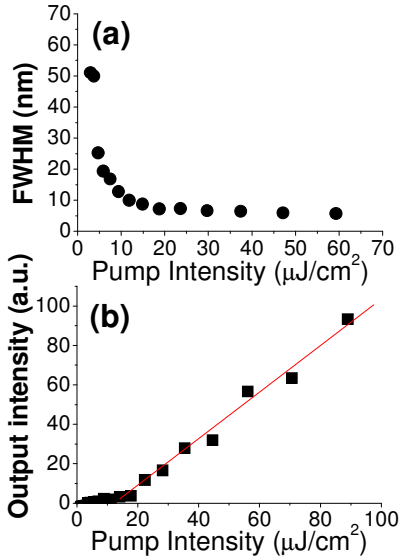

Figure 3.8 Emission (a) linewidth and (b) output intensity as a bisfluorene dendrimer crosses the amplified spontaneous emission threshold.

Amplified spontaneous emission is also very useful for determining the optical gain and loss of organic semiconductors by using the variable stripe technique.[9] The same setup is used as for measuring ASE threshold but the dimensions and positions of the stripe change and the ASE scattered from the edge of the film is recorded for different stripe lengths and positions.

When the material is above the ASE threshold and the length of the excitation stripe changes, the output intensity I_{out} from the edge of the film as a function of the stripe length is given by equation 3-VIII

$$I_{out} = \frac{A(\lambda)I_p}{g(\lambda)}(e^{g(\lambda)l} - 1) \qquad \textbf{3-VIII}$$

where $g(\lambda)$ is the optical gain, $A(\lambda)$ is a constant of the material related to the spontaneous emission cross-section, I_p is the pump intensity and l is the length of the stripe.

If instead of the length of the excitation stripe its distance x from the edge of the film is changed, the output ASE intensity is given by equation 3-IX

$$I_{out} = I_0 e^{-\alpha x} \qquad \textbf{3-IX}$$

where I_0 is the output intensity when the stripe is at the edge of the film and α is the waveguide loss coefficient of the film.

Based on the above method, the optical gain and loss coefficients of a thin film of organic semiconductor can be calculated by fitting the collected data with the corresponding equations. An example of such measurements and fittings is shown in Figure 3.9 for a bisfluorene dendrimer.

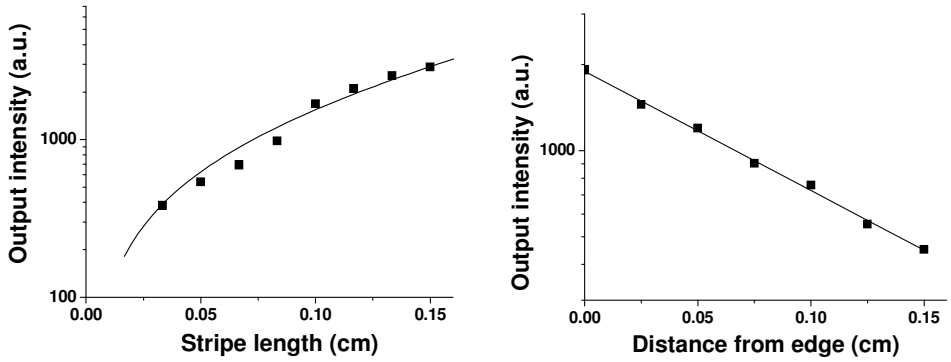

Figure 3.9 Optical gain (top) and loss (bottom) measurements and fitting lines from an ASE measurement in a bisfluorene dendrimer. The intensity axes are in logarithmic scale.

The optical gain and loss coefficients of a material can be used to evaluate its performance as a laser gain medium, with the combination of high gain and low losses being the markers for low-lasing thresholds when used with an appropriate resonator.

3.5.3. Lasing measurements

Once the material has been evaluated, a laser using it as a gain medium is made. In this thesis all lasers presented are distributed feedback lasers, fabricated by spin-coating from solution onto a corrugated silica substrate. The devices are then placed inside a vacuum chamber to reduce photo-degradation and are optically excited by one of the laser sources described in section 3.5.1. Since all DFB gratings used in this work were chosen for surface emission, the pump beam is incident at an angle onto the surface of the film so that the perpendicularly emitted organic laser beam does not spatially overlap with the excitation laser beam, making it easier to observe and detect and reducing the possibility of high-intensity pump laser light reaching the spectrograph's sensitive CCD. A schematic of the experimental setup used for measuring the performance of organic lasers can be seen in Figure 3.10.

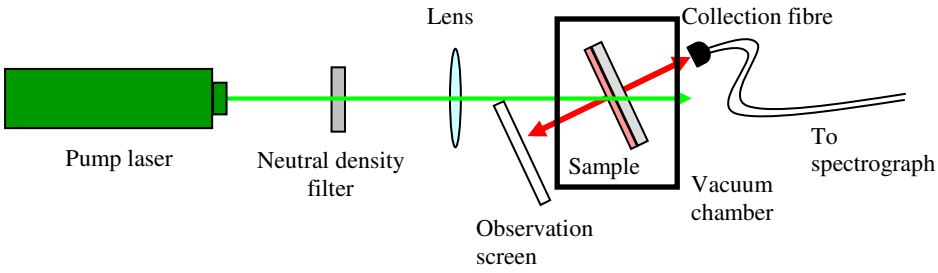

Figure 3.10 Experimental setup used for characterization of organic semiconductor lasers.

The incident pump energy on the sample is attenuated by using metallic neutral density filters and is focused using spherical or cylindrical lenses. When the pump energy is lower than the lasing threshold, ASE emission that is being modified by the grating is visible on the observation screen as a set of thick arches, as shown in Figure 3.11 for a one-dimensional DFB grating.

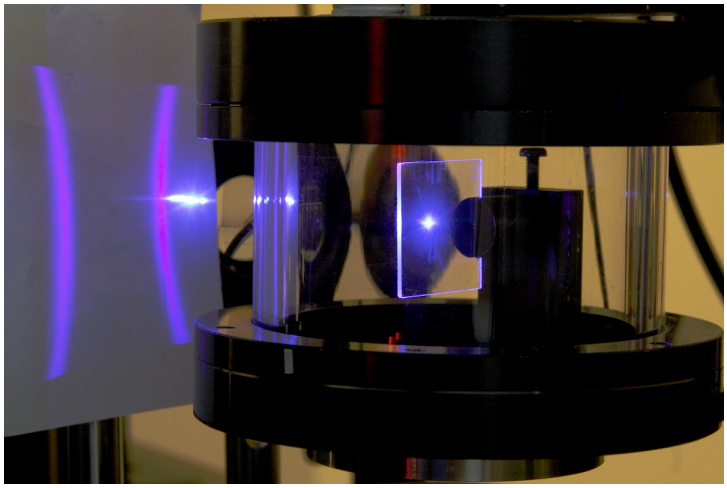

Figure 3.11 Bragg-scattered ASE from an oligofluorene truxene DFB laser operating below threshold. The vacuum chamber is also visible in this photo, along with the observation screen and the pump beam focusing lens.

The intensity of the emission is recorded using a CCD spectrograph that monitors both the spectral shape and the intensity of the fluorescence. As the pump energy is increased by changing to weaker neutral density filters, the organic laser comes above threshold and the slope of the emission changes due to stimulated emission. This results in a characteristic "kink" in the graph of input vs. output graph, as seen in Figure 3.12, from which the slope efficiency of the laser above threshold can be calculated.

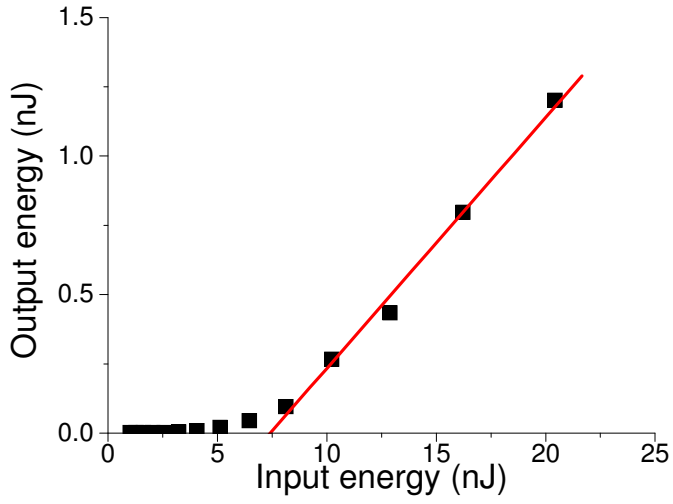

Figure 3.12 Output energy versus input energy for a bisfluorene dendrimer DFB laser. The slope efficiency in this example is 8.3%.[10]

3.6. Two-photon absorption techniques

Characterising the two-photon absorption of a material includes studying both the absorption of the excitation light as it passes through a volume of the material, as well as measuring the properties of the two-photon induced fluorescence. These two properties are measured simultaneously to allow for a direct correlation between them based on a modified version of the two-photon excited fluorescence technique.[11]

A solution is made from the material and is placed in a quartz cuvette. The cuvette is placed in the path of the pump beam that is made to pass near the edge of the cuvette to avoid re-absorption of the two-photon induced fluorescence. Because two-photon absorption is a nonlinear process, its magnitude is much smaller than that of the linear absorption and therefore an excitation source with high peak power is required. The optical parametric systems described previously were used for these measurements, where nanosecond pulses were provided by the OPO system and femtosecond from the OPA. The pump beam is gently focused within the solution and its power is measured before and after the cuvette to determine the two-photon absorption magnitude. The induced fluorescence is collected from the side of the cuvette using an optical fibre with collection optics connected to a CCD spectrograph that allows the monitoring of both intensity and spectrum of the material's fluorescence. The excitation wavelength is changed across the one-photon transparency region of the material to locate the wavelength for which absorption of the pump light and subsequent fluorescence are highest. The energy of the pump beam is also varied to examine the energy dependence of two-photon absorption and fluorescence, as it contains valuable clues about the nature of the observed photophysical processes.

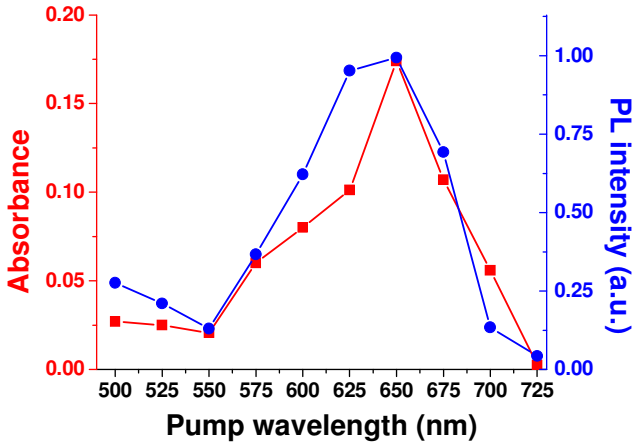

Figure 3.13 Two photon absorption (filled squares) and fluorescence (filled circles) measurements for a polyfluorene solution under two-photon excitation.

A picture of the setup used for the two-photon measurements can be seen in Figure 3.14, where the cuvette containing the sample is excited by 640 nm light from the nanosecond OPO. The power meter monitors the transmitted power of the pump beam and the collection fibre connects to a CCD spectrograph to monitor the material's two-photon induced fluorescence.

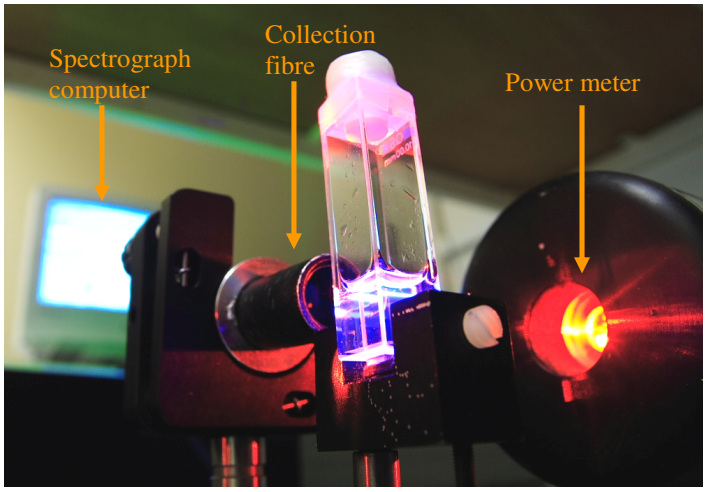

Figure 3.14 Experimental setup of the two-photon absorption and fluorescence measurements. The cuvette contains a polyfluorene solution excited at 640 nm.

The absorption of the pump beam was measured in two different ways. In the case of nanosecond excitation, where the two-photon absorption coefficient was large, the amount of light absorbed was in the region of 40-70%, which meant that measuring the absorption of the pump beam was done by measuring the power of the pump beam before and after the cuvette. Under femtosecond

excitation though, the amount of light absorbed was much lower, as little as 2-5% for the thin film measurements. Small fluctuations in the power of the pump laser were of the same order, making reliable measurements difficult. In order to perform a more accurate measurement, two identical photodiodes were used to pick off a small percent of the pump beam before and after the sample. The two photodiodes were connected to two lock-in amplifiers and the ratio of their outputs was recorded over a period of time to allow for averaging of the measured absorption, thus reducing the effect of small fluctuations of the pump beam intensity.

In both cases the quartz cuvette was filled with the solvent used for the solution and was placed in the path of the beam prior to the actual measurement. This helped determine any contribution coming either from the walls of the cuvette and the reflections they cause or from the solvent itself, as at such high excitation densities certain solvent display two photon absorption of their own that can interfere with the values measured for a material in solution. The baseline recorded this way was then subtracted from the two-photon absorption measurements, allowing for the net absorption of the organic material to be calculated in the final data sets.

Two-photon pumped laser measurements were done using the same experimental setup as for one-photon lasers (described in section 3.5.3), with the only difference being that the excitation wavelength is changed to match the peak of the two-photon absorption intensity as determined be the above measurement technique.

3.7. References

[1] I. M. Arabatzis, S. Antonaraki, T. Stergiopoulos, A. Hiskia, E. Papaconstantinou, M. C. Bernard, P. Falaras, *Journal of Photochemistry and Photobiology A: Chemistry* **2002**, *149*, 237.

[2] C. M. Ramsdale, N. C. Greenham, *Journal of Physics D-Applied Physics* **2003**, *36*, L29.

[3] H. Tompkins, E. Irene, E. A. Haber, *Handbook Of Ellipsometry*, William Andrew Publishing, New York, **2005**.

[4] N. C. Greenham, I. D. W. Samuel, G. R. Hayes, R. T. Phillips, Y. Kessener, S. C. Moratti, A. B. Holmes, R. H. Friend, *Chemical Physics Letters* **1995**, *241*, 89.

[5] W. Y. Lai, R. D. Xia, Q. Y. He, P. A. Levermore, W. Huang, D. D. C. Bradley, *Advanced Materials* **2009**, *21*, 355.

[6] T. Voss, D. Scheel, W. Schade, *Applied Physics B-Lasers and Optics* **2001**, *73*, 105.

[7] G. A. Turnbull, P. Andrew, W. L. Barnes, I. D. W. Samuel, *Applied Physics Letters* **2003**, *82*, 313.

[8] J. J. Zayhowski, A. Mooradian, *Optics Letters* **1989**, *14*, 24.

[9] M. D. McGehee, A. J. Heeger, *Advanced Materials* **2000**, *12*, 1655.

[10] J. C. Ribierre, G. Tsiminis, S. Richardson, G. A. Turnbull, I. D. W. Samuel, *Applied Physics Letters* **2007**, *91*.

[11] C. Xu, W. W. Webb, *Journal of the Optical Society of America B-Optical Physics* **1996**, *13*, 481.

4. Two-photon absorption and lasing in polyfluorene

In this chapter a two-photon pumped polyfluorene laser is demonstrated for the first time. The two-photon absorption properties of polyfluorene are studied across two different time domains in solution and in film. The combination of two-photon absorption and high photoluminescence quantum efficiency leads to a tunable distributed feedback laser based on a commercially available conjugated polymer.

4.1. Introduction

Amongst the different light-emitting polymers, poly(9,9-dioctylfluorene) (polyfluorene, PFO) and its variations is one of the most thoroughly studied.[1] The simple, well-defined backbone structure of fluorene units (see top structure in Figure 4.1) allows for both good conducting properties and efficient light emission, while variations in the synthesis to create copolymers have allowed polyfluorenes to span the entire visible spectrum. Polyfluorenes have been used to fabricate efficient light-emitting diodes with results amongst the best for organic materials. [2, 3] Different types of polyfluorene have been developed by copolymerisation with other molecules to extend the photophysical properties, leading to materials such as poly[(9,9-dioctylfluorene)-co-(9,9-di(4-methoxy)phenylfluorene)] (F8DP) and poly[(9,9-dioctylfluorene)-co-(benzothiadiazole)] (F8BT) (Figure 4.1) that have shown excellent performance in optoelectronic devices such as solar cells, light-emitting diodes and lasers.

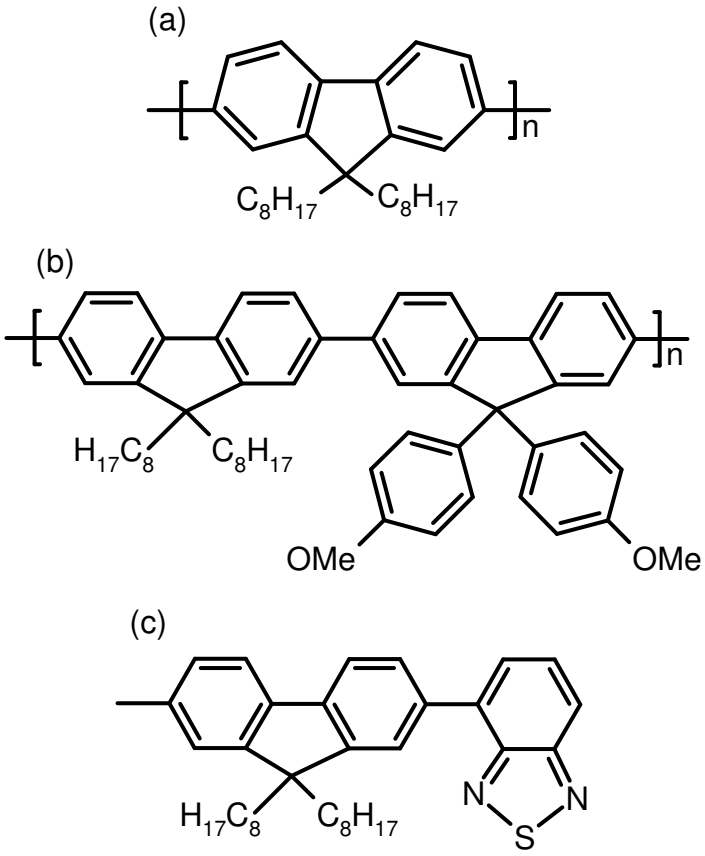

Figure 4.1 Chemical structures of some fluorene-based conjugated polymers. From top to bottom: (a) PFO, (b) F8DP and (c) F8BT.

Lasing in particular is one of the areas where polyfluorenes have excelled. Their strong optical transitions give both high absorption coefficients and large stimulated emission cross-sections, while the photoluminescence quantum yields of PFO in thin films can be as high as 73% (as mentioned later in this chapter), with F8DP and F8BT having PLQY values between 50 and 60%.[4] Fluorene-based conjugated polymers also combine high optical gain with low waveguide losses, leading to some of the lowest lasing thresholds amongst all organic semiconductors.[5-8] In addition, the blue emission of PFO also makes it very attractive for accessing the blue part of the spectrum, where compact and tunable laser sources are less abundant. The morphology of the polymer chains in films can vary as PFO is a liquid crystalline material at high temperatures. The polymer chains can assume different conformations depending on the solvent environment they are exposed to, leading to different phases that change the photophysics of the polymer. [9-11] Some of the lowest lasing thresholds for organic semiconductors have been reported in polyfluorene distributed

feedback lasers where the β-phase of polyfluorene is used as the gain medium in a film consisting mostly of normal PFO.[12] The best PFO laser reported shows a lasing threshold energy of 0.8 nJ/pulse (3.2 μJ/cm^2, or 3.2 kW/cm^2), a very high slope efficiency of 7.8% from one side of the grating and tunability across ~40 nm, as seen in Figure 4.2.[8]

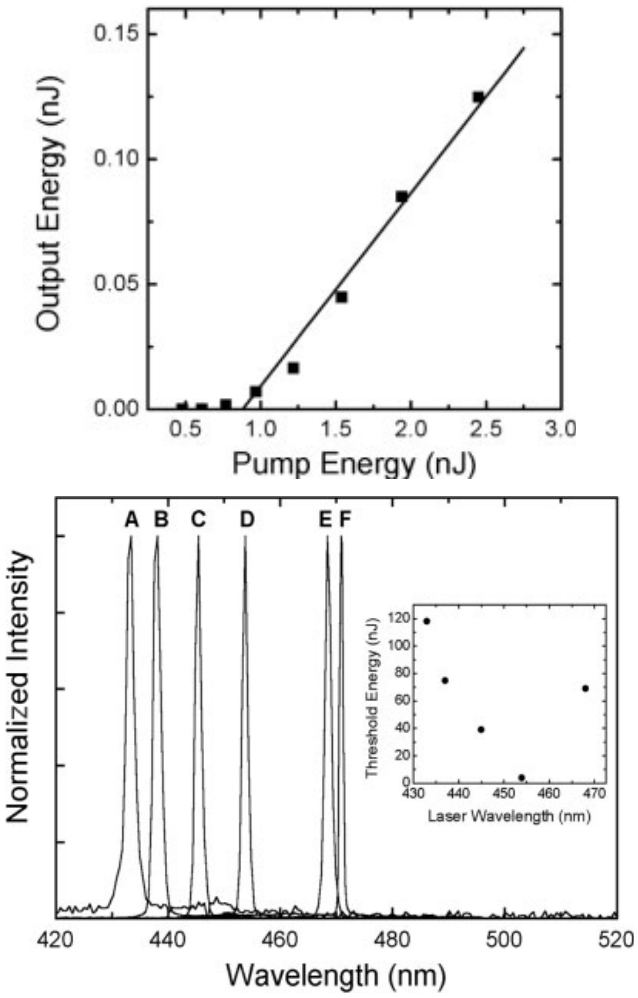

Figure 4.2 Lasing threshold (top) and tuning range (bottom) of the best reported polyfluorene laser. The inset of the bottom figure shows the dependence of the lasing threshold on the emission wavelength (adapted from [8]).

The structure and symmetries of organic semiconductors also give rise to non-linear absorption phenomena such as two-photon absorption.[13, 14] Several studies of this process have been performed in the past on polyfluorene and its derivatives [15-19], highlighting their suitability for use in applications that benefit from the nonlinear nature of absorption such as optical limiting, optical data storage, two-photon microscopy. [16, 20, 21] These reports however all cover different aspects of the two-photon absorption properties of PFO, leading

to a somewhat confusing picture of the material's behaviour under different excitation conditions where the energy and wavelength of the pump pulses changes across a wide range of values. The effect of the excitation pulse duration in particular is one of the key areas where comparisons are scarce as the pump sources required to perform such studies are not usually combined within the same research group. As of the writing of this thesis there is no single report that extends across different time domains for the excitation pulses or makes any comparisons between solution and thin film measurements in polyfluorene.

Of particular interest is the combination of the strong optical transitions of organic semiconductors with two-photon absorption giving the possibility to make two-photon pumped lasers, whereby the pump wavelength is shifted to approximately twice the wavelength of the material's linear absorption. This approach could allow novel optical pumping schemes where the excitation wavelength is longer than the emission wavelength, thus shifting the required pump wavelength to more easily accessible parts of the spectrum where photo-oxidation of organic semiconductors is reduced. Two-photon induced lasing has been previously studied in organic laser dyes, some of which are synthesised specifically for enhanced two-photon absorption and lasing. [22-26] Prior to the work in this thesis however there has only been a single example of a two-photon pumped laser based on organic semiconductors using the green-emitting ladder-type polymer MeLPPP [27], while despite the two-photon absorption studies of PFO there are no published examples of a two-photon pumped polyfluorene laser.

In this chapter the two-photon absorption and fluorescence of polyfluorene are studied as a function of both pump wavelength and energy density in the nanosecond and femtosecond time domains, making this a very thorough investigation of the two-photon properties of polyfluorene. The nonlinear optical properties of PFO are discussed and comparisons are made between measurements to understand the nonlinear optical properties of the material. In addition, the combination of the two-photon absorption properties of polyfluorene with its good lasing performance allows us to demonstrate the

world's first tunable two-photon pumped polymer laser due to a combination of improved material synthesis and better understanding of the optimal excitation conditions that reduce additional losses. These results highlight both the excellent lasing properties of polyfluorene as well as the novel options available in organic semiconductor lasers based on their unique optical properties and provide an alternative pumping scheme for polymer lasers.

4.2. Two-photon absorption measurements

The first step towards examining the two-photon absorption properties of polyfluorene is determining the strength of the nonlinear absorption of a high intensity beam. In general it is expected that the wavelength for maximum two-photon absorption will be blue-shifted by some amount in comparison to the peak of the material's linear absorption. [28] This is due to the different spin-allowed transitions for a nonlinear absorption process, making a detailed examination of the two-photon absorption essential, to obtain a detailed mapping of the transitions involved in two-photon absorption. To this end, solutions of PFO (10 mg/ml in toluene) were illuminated by a pump beam from a tunable laser source and the transmission of the pump beam through the material along with the induced fluorescence was recorded. Two pump sources were used, a 4-nanosecond pulse optical parametric oscillator (OPO) tuned in the region between 500 and 725 nm and a femtosecond optical parametric amplifier (OPA) system delivering 100 fs long pulses in the region between 580 and 700 nm. The asymmetric pump beams were focused using a cylindrical lens for the nanosecond pulses to a spot of 4000 x 170 μm and a spherical lens for the femtosecond experiments leading to a spot size of 80 x 30 μm. The excited volume was assumed to be the spot size multiplied by the length of the cuvette due to the weak focusing of the excitation beam.

The recorded two-photon absorption spectrum can be seen in Figure 4.3 where absorbance, defined as $-\log_{10}$(transmission), is plotted as a function of the pump wavelength for both nanosecond and femtosecond excitation pulses at the peak

excitation densities available from both systems (83 GW/cm^2 for the nanosecond excitation and 167 GW/cm^2 for the femtosecond excitation).

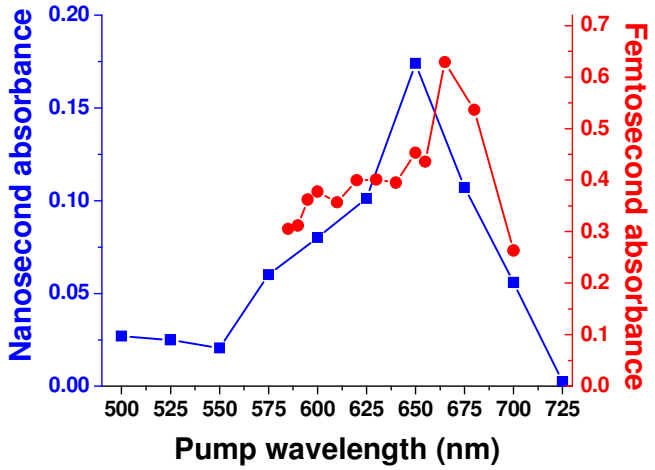

Figure 4.3 Two-photon absorbance as a function of the pump wavelength for a polyfluorene solution.

The spectral dependence of two-photon absorption is very similar in the two time domains, with the maximum absorption occurring around 650 nm for both nanosecond and femtosecond pump pulses. When compared to twice the wavelength of the maximum for linear absorption at 760 nm (2x380 nm), the resulting peak is blue-shifted by approximately 100 nm, in good agreement with similar differences noted in the literature for two-photon absorption in other organic semiconductors.[28] There is a small redshift in the peak wavelength for the femtosecond case which could be due to a combination of factors. Firstly, the femtosecond beam is much broader spectrally (~10 nm) than the nanosecond excitation beam (< 1 nm), leading to some uncertainties as to the exact excitation wavelength. Secondly, the much faster femtosecond pulses induce less excited-state absorption in the material than the nanosecond pulses do which could account for a slightly different absorption spectrum as excited-state absorption peaks at different wavelengths than two-photon absorption, leading to the absorption spectrum being a composite of two underlying spectra from the two absorption processes. [29]

Other reports in the literature place the two-photon absorption peak of polyfluorene at 625 nm for nanosecond pump pulses [15] and at 670 nm for

femtosecond pulses [18], in good agreement with what is observed here. I should be noted though that this is the first time that these measurements are in direct comparison to each other for the same batch of material, creating a more complete picture of the two-photon absorption behaviour of polyfluorene.

4.2.1. Energy dependence of two-photon absorption

By studying the energy dependence of absorption at each wavelength, the two-photon absorption coefficients of the material can be calculated. In the case of two-photon absorption the change in the intensity of the pump beam with propagation length is given by

$$\frac{dI}{dz} = -\sigma_2 (N_g - N_e) I^2 - \sigma_{ESA} N_e I \qquad \textbf{4-I}$$

where I is the pump beam intensity, σ_2 is the two-photon absorption cross-section, N_g is the ground state population, N_e the first excited state population and σ_{ESA} is the excited-state cross-section. For low pump intensities we can assume that the population of the excited state N_e is negligible (and therefore also $N_e << N_g$), making the above equation

$$\frac{dI}{dz} = -\alpha_2^0 I^2 \qquad \textbf{4-II}$$

where the absorption coefficient is defined as $\alpha_2{}^0 = \sigma_2 N_g$. Assuming that the absorption coefficient is independent of the pump energy and by integrating the previous equation, we get

$$\frac{1}{T} = 1 + \alpha_2 z I_{pump} \qquad \textbf{4-III}$$

where T is the transmission of the pump beam through the sample, α_2 is the two-photon absorption coefficient (intensity-independent) and z is the thickness of the sample.

The resulting plot should be a straight line going through transmission of one for zero pump intensity. Such a plot for the polyfluorene data can be seen in Figure 4.4.

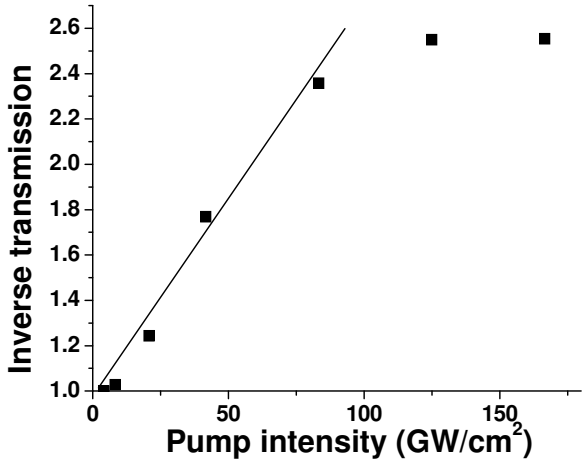

Figure 4.4 Inverse transmission as a function of pump intensity for a polyfluorene solution under two-photon excitation with femtosecond pulses. The solid line corresponds to a linear fit based on equation

The above graph shows good compliance with what is expected for two-photon absorption up to a certain pumping level. Above that, saturation of two-photon absorption becomes apparent as a roll-off in the inverse transmission data, as the large number of pump photons removing a significant number of the ground state electrons causing a change in the two-photon absorption coefficient.[17] The values for the two-photon absorption coefficient can still be calculated for the linear part of the above graph, as seen in Figure 4.5.

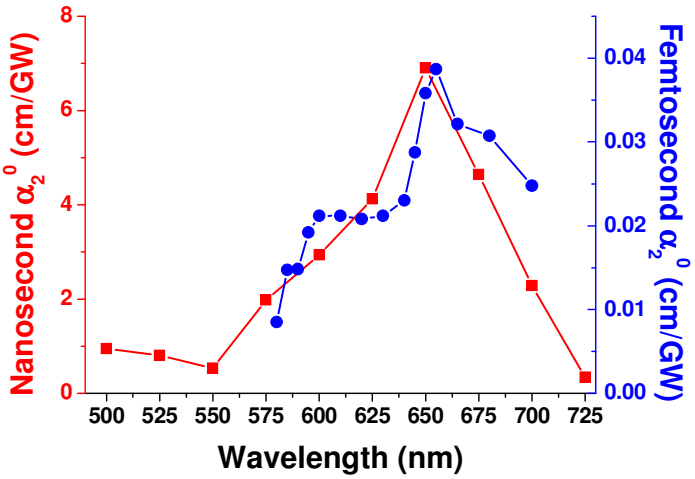

Figure 4.5 Two-photon absorption coefficients for different excitation wavelengths under nanosecond and femtosecond illumination in a polyfluorene solution.

Note here that the excitation wavelength difference in the peak of absorption between nanosecond and femtosecond data has been reduced. This means that the energy dependence of two-photon absorption is very similar in the two different time domains studied.

The two-photon absorption cross-section can be calculated using the equation

$$\delta = \frac{hv\alpha_2(M_w)}{N_A \rho} \qquad \textbf{4-IV}$$

where hv is the energy of the pumping photon, M_w is the molecular weight of the molecule, N_A is the Avogadro number and ρ is the density of the system investigated. The unit for two-photon absorption cross-sections is 1 GM (named after its discoverer, Nobel laureate Maria Göppert-Mayer, who first predicted two-photon absorption) and is defined as

$$1\ GM = 10^{-50} cm^4 \cdot s \cdot photon^{-1} molecule^{-1}$$

In polymer measurements there is an uncertainty in calculating these cross-sections due to the difficulty in determining the relevant effective molecular weight of the chromophore. If the molecular weight of the polymer is used then the values calculated by the above formula are unrealistically high, while using the repetition unit's molecular weight does not account for the extent of the excitation along a polymer chain. Here it is assumed that each chromophore consists of approximately 7 fluorene units, as the emission spectrum from a 7-unit oligofluorene resembles very well the polymer fluorescence spectrum.[30] The resulting cross-section values for nanosecond and femtosecond pump pulses can be seen in Figure 4.6.

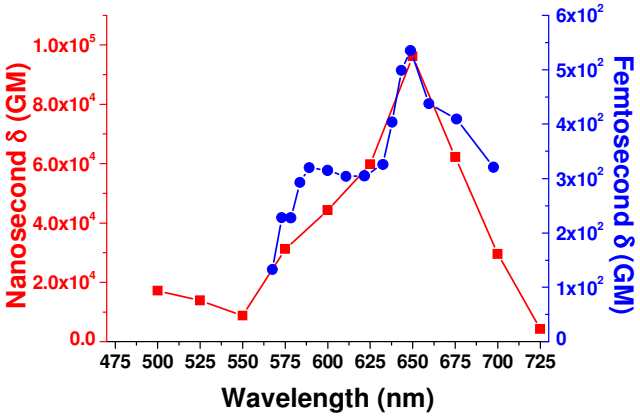

Figure 4.6 Two-photon absorption cross-sections at different excitation wavelengths for a polyfluorene solution.

The calculated two-photon absorption cross-section values presented here are amongst the highest recorded for conjugated polymers, making polyfluorene a good candidate for applications where strong two-photon absorption is required such as two-photon pumped lasing.

It is interesting to observe the difference between the values for the nanosecond and the femtosecond regime. This is attributed to the presence of excited state absorption. The magnitude of excited-state absorption depends on the population of the first excited state as it forms the ground level for this transition. For short excitation pulse lengths, the molecules that are initially excited in this first excited state have a very limited time in which to absorb more of the excitation pulse through excited-state absorption and the overall effect is relatively small. For long excitation pulses though, the molecules in the first excited state can interact with the pump pulse for the entire duration of the state's lifetime, meaning that there is a higher probability that some of them will absorb the excitation light again and move to a higher excited state through excited-state absorption. [31]

Separating the two phenomena is not easy as the excited state absorption also shows a square dependence on the pump intensity, since the first excited state's population is provided by two-photon absorption. This leads to higher apparent two-photon absorption coefficients, as in the transmission measurements there is no discrimination between different types of absorption. In addition, it has

previously been found that, for pulses much longer than the excited state lifetime of the material, the contribution of excited state absorption is proportional to the duration of the pulse until the point where the pulse duration becomes greater than the first excited state lifetime, therefore the contribution of excited state absorption is expected to be higher in the nanosecond case.[29] These measurements show that the values for nanosecond pulses are indeed approximately three orders of magnitude higher than those of the femtosecond experiments, in good agreement with what has been reported in the literature.[32]

4.2.2. Excited-state absorption

One of the processes that can compete with two-photon absorption is excited-state absorption. In this process the molecules that are being excited into the first excited energy state by the pump beam subsequently absorb another pump photon and are thus elevated a second excited state. This means that the overall absorption of the pump beam through the material appears to be enhanced in comparison to what is expected if excited-state absorption is not present.

In the case of two-photon absorption followed by excited-state absorption, this phenomenon can be more easily explained by using a simple energy diagram that includes the basic transitions and populations under consideration. We can consider a 4-level system for this study, as shown in Figure 4.7.

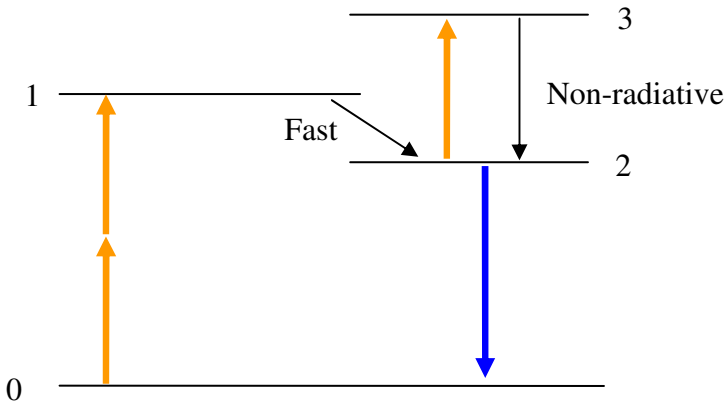

Figure 4.7 A 4-level energy diagram illustrating two-photon absorption followed by excited state absorption in a fluorescent material.

The first excited state is state number two, with excited-state absorption occurring between states 2 and 3. Let us consider the rate equations associated with the transitions mentioned above. If N_x is the population of the x-state, we can write

$$\frac{dN_1}{dt} = \frac{\sigma_{TPA} I^2}{2h\nu} N_0 - \frac{N_1}{\tau_1} \qquad \textbf{4-V}$$

$$\frac{dN_2}{dt} = \frac{N_1}{\tau_1} - \frac{N_2}{\tau_2} + \frac{N_3}{\tau_3} - \frac{\sigma_{ESA} I}{h\nu} N_2 \qquad \textbf{4-VI}$$

$$\frac{dN_3}{dt} = \frac{\sigma_{ESA} I}{h\nu} N_2 - \frac{N_3}{\tau_3} \qquad \textbf{4-VII}$$

where σ_{TPA} and σ_{ESA} are the two-photon absorption and excited-state absorption cross-sections respectively, I is the intensity of the pump beam, $h\nu$ is the pump photon energy and τ_x is the lifetime of the x-state.

Under steady-state conditions we get:

$$\frac{dN_1}{dt} = 0 \Rightarrow N_1 = \frac{\sigma_{TPA} N_0 I^2 \tau_1}{h\nu} \qquad \textbf{4-VIII}$$

$$\frac{dN_3}{dt} = 0 \Rightarrow N_3 = \frac{\sigma_{ESA} N_2 I \tau_3}{h\nu} \qquad \textbf{4-IX}$$

Substituting the last two equations into equation 5.XIII, the population of the first-excited state in the steady-state case is:

$$\frac{dN_2}{dt} = 0 \Rightarrow N_2 = \frac{\sigma_{TPA} N_0 I^2 \tau_2}{2h\nu} \qquad \textbf{4-X}$$

The base population for excited-state absorption in this case shows a square dependence on the pump intensity, making this transition indistinguishable from two-photon absorption in pump beam absorption measurements like the ones performed experimentally in this thesis.[31]

It has previously been shown that for pulses much longer than the excited state lifetime of the material, the contribution of excited state absorption is proportional to the duration of the pump pulse, until the point where the pulse duration becomes greater than the first excited state lifetime.[24] Therefore the

contribution of excited state absorption is expected to be higher in the nanosecond case and this difference can be up to 10 - 10^3 times depending on the strength of excited-state absorption.[29, 33] This explains why the values we measured experimentally show nanosecond absorption coefficients and cross-sections to be approximately 100 times higher than their femtosecond counterparts.

4.2.3. Film measurements

Two-photon absorption was also measured for a thin film of polyfluorene under femtosecond excitation to acquire a better insight into how the material would behave under conditions similar to those in future lasing experiments. Figure 4.8 shows the recorded data for the inverse transmission as a function of the pump energy for a pump wavelength of 640 nm. Note that the line does not give 100% transmission at zero pump power density due to additional absorption coming from the vacuum chamber in which the film was placed as well as not taking into account the reflectivity of the sample.

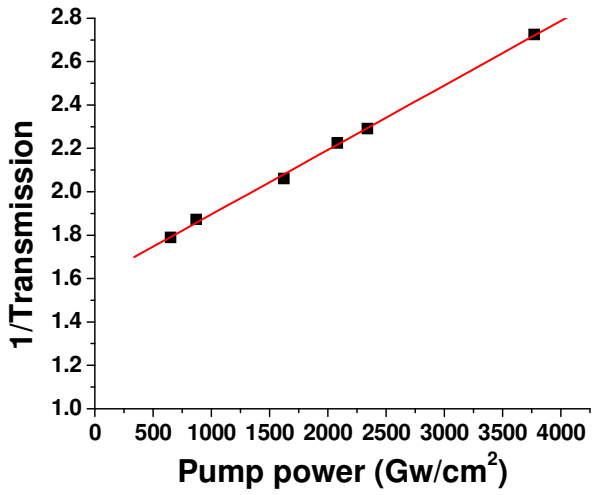

Figure 4.8 The inverse transmission of the pump beam as a function of different pump powers for a thin film of polyfluorene under femtosecond illumination. The red line corresponds to a linear fit.

The measured two-photon absorption coefficient was 2.3 cm/GW, while for the same pumping conditions a 10 mg/ml solution of polyfluorene has a two-photon

absorption coefficient of 0.023 cm/GW. This difference of 100 times in favour of the film corresponds to the difference in concentration (the film is assumed to have a 1 g/ml concentration). This indicates that the increase in concentration when moving from the solution to the solid state does not introduce significant additional losses to the system for two-photon absorption processes.

4.3. Two-photon photoluminescence excitation measurements

When the pump beam is incident on the cuvette containing the polyfluorene solution, light emission is clearly visible as seen in Figure 4.9. When the pump beam is at a wavelength suitable for one-photon absorption (410 nm), the high linear absorption coefficient means that most of the pump light absorption and therefore the material's luminescence occurs in the very first millimetre or so of the cuvette. In contrast, when two-photon excitation is occurring, the lower absorption coefficient means that the pump beam travels through most of the volume of the solution, leading to light emission throughout the cuvette along the path of the pump beam. The weak focusing of the pump beam leads to an almost uniform pencil-shaped excitation and consequent emission along the path of the pump beam.

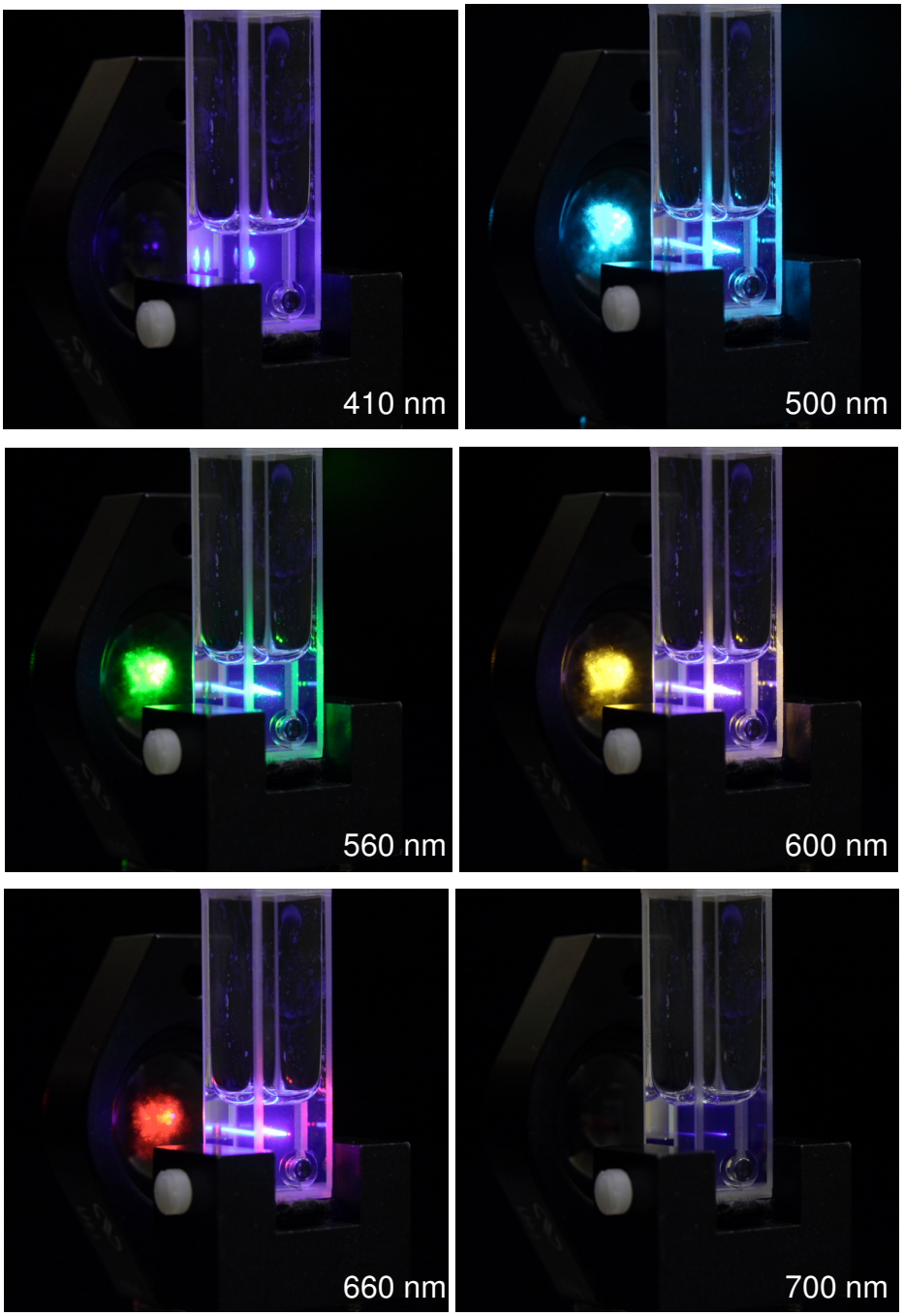

Figure 4.9 Polyfluorene fluorescence under one-photon (410 nm) and two photon (500 – 700 nm) excitation in a 10 mg/ml toluene solution.

The recorded two-photon induced photoluminescence excitation spectra for both nanosecond and femtosecond pump pulses can be seen in Figure 4.10 as a function of the excitation wavelength. Each data point corresponds to approximately 15,000 pump pulses, giving an average photoluminescence intensity with an error no larger than the fluctuations of the pump energy (typically around 5%).

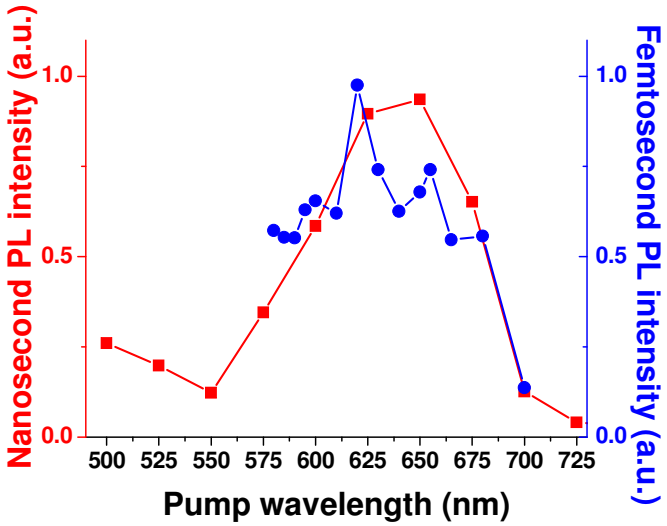

Figure 4.10 Nanosecond and femtosecond two-photon-induced luminescence intensity as a function of pump wavelength for polyfluorene.

As in the case of the two-photon absorbance, the spectra for the two time domains show a very good overlap, with a broad peak appearing around 650 nm. The femtosecond data shows some additional structure though it is not clear if that is due to the reduced contribution of excited-state absorption allowing for a better mapping of the two-photon absorption states or due to experimental uncertainties in the data collection.

4.3.1. Energy dependence of two-photon induced fluorescence

Changes in the fluorescence emission of the polymer with the pump power can give a useful insight into the nature of the underlying processes. For pure two-photon absorption, we expect the fluorescence to have a square dependence on the pump power.

A plot showing the intensity of the two-photon induced fluorescence integrated across all emission wavelengths for different excitation energies can be seen in Figure 4.11 as a function of the pump wavelength.

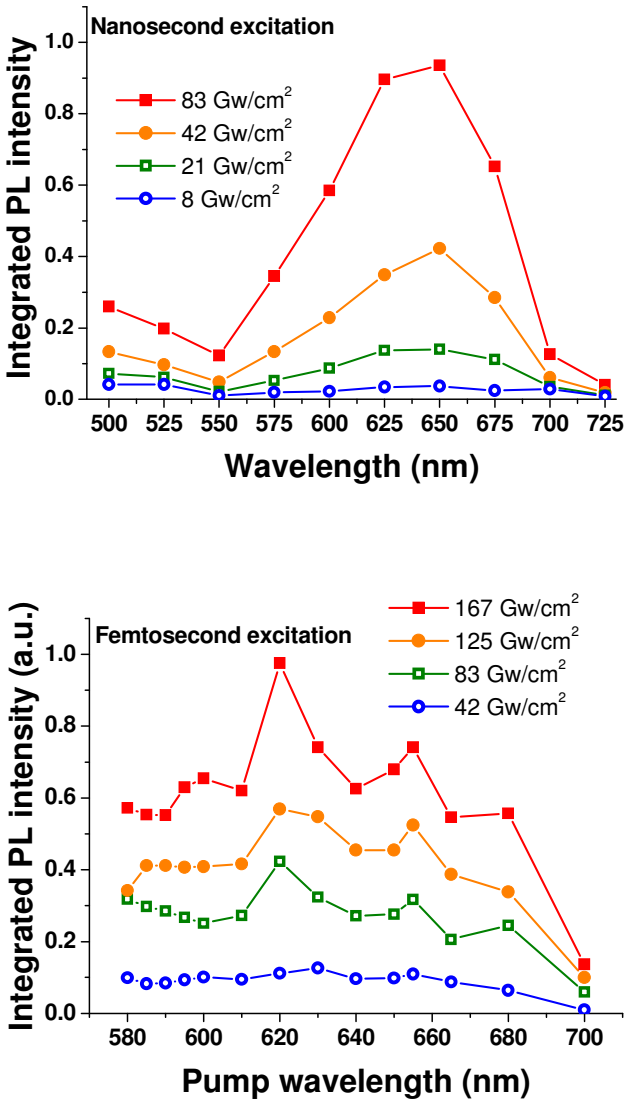

Figure 4.11 Two-photon induced fluorescence intensity plotted against pump wavelength for a range of different pump energies. Top graph: nanosecond data, bottom graph: femtosecond data.

When this data is plotted as a function of the excitation energy, a square dependence is expected. [17] in a double-log plot this should correspond to a linear graph with a slope of two, as seen in Figure 4.12, where a comparison between the calculated slopes for nanosecond and femtosecond excitation is also shown. The errors in these values come from the fitting software as well as the fluctuations in the excitation energy (typically 5%).

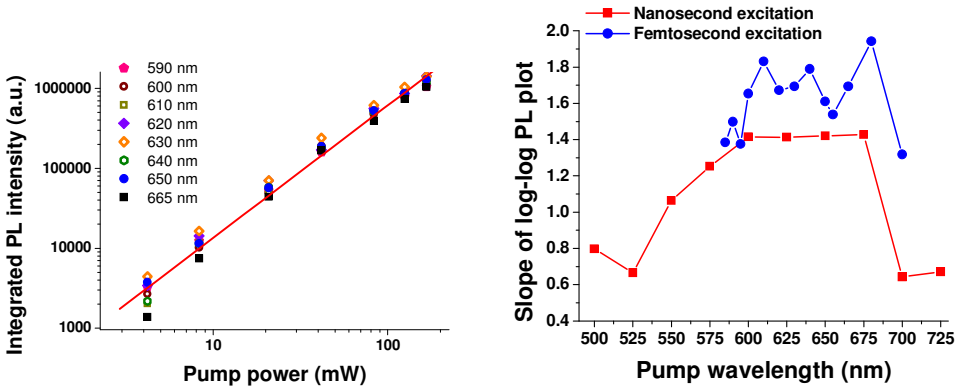

Figure 4.12 Left: Log-log plot of two-photon induced fluorescence intensity as a function of femtosecond incident pump power for a range of different excitation wavelengths. The solid line corresponds to square dependence. Right: The calculated best-fit slopes from the log-log plot showing the fluorescence intensity as a function of the pump energy across different wavelengths for both nanosecond and femtosecond excitation. The slope errors from the fittings are approximately 10% across all wavelengths.

Both set of values show similar trends, but the changes in the nanosecond regime are more pronounced. The nanosecond values tend to peak as the excitation wavelength is moved towards the maximum of the two-photon absorption but flatten out across an area of 75 nm around that peak. The femtosecond values are generally higher, but no clear peak can be seen where the two-photon absorption is maximised. This behaviour signifies that, at progressively higher excitation densities, some of the excitation photons absorbed by the material do not contribute to light emission, hence the slope of the graph becomes less than two. Possible processes that might deplete the light-emitting state include exciton - exciton annihilation and excited-state absorption. Both are expected to have a dependence on the pump pulse intensity and duration, but excited-state absorption is known to be practically indistinguishable from two-photon absorption in a transmission measurement under steady-state conditions like the ones described earlier in this chapter.[31] It seems reasonable then to attribute this deviation of the fluorescence behaviour to the presence of excited-state absorption, a process known to be strong in polyfluorene and can have a profound effect on the light emission efficiency of the material.[29, 34] Exciton-exciton annihilation can also have an effect in two-photon induced fluorescence as the excitons created by the pump beam are

lost in collisions with one another, reducing the overall luminescence efficiency. [35, 36]

From the above studies, it is clear that two-photon induced fluorescence is strongest in the region of 650 nm for both nanosecond and femtosecond time domains. It is also obvious that additional processes can deplete the light emitting state from excitations to a larger degree when nanosecond excitation pulses are used. For those reasons, a femtosecond pump beam at 640 nm was chosen as the source for two-photon pumped laser experiments in the next session, in an attempt to optimise the optical pumping of polyfluorene and minimise any additional losses that might affect the lasing threshold.

4.4. Two-photon pumped lasing experiments

Films were spin-coated from a toluene solution (20 mg/ml) onto square-array corrugated silica substrates. The period of the corrugation was 270 nm and was chosen to provide optical feedback at the peak of the material's amplified spontaneous emission. The films were spun at speeds of 700 – 1000 rpm (corresponding film thickness: 560 – 760 nm) in a protective Nitrogen atmosphere inside a glovebox to reduce the absorption of oxygen and water molecules. The samples were placed inside a vacuum chamber that was pumped down to 10^{-4} mbar in order to slow down photodegradation. The femtosecond pump beam was focused onto the surface of the film using a spherical lens and the pump spot size was measured to be 80 x 30 μm.

Upon increasing the pump energy, a narrow (<0.8 nm) peak appears in the emission of the material, as seen in Figure 4.13, signifying the onset of lasing.

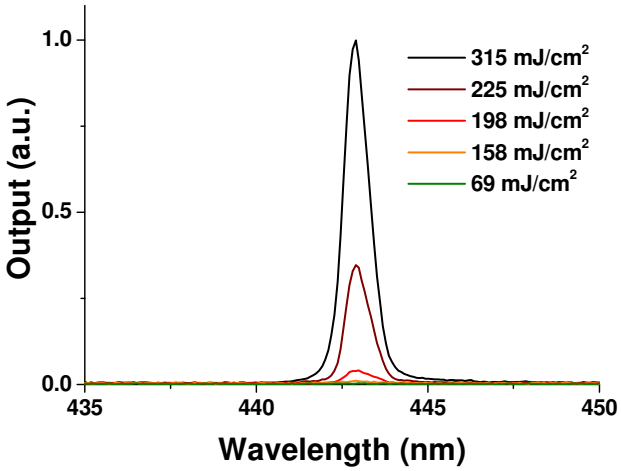

Figure 4.13 Emission spectrum from a two-photon pumped polyfluorene laser as a function of different pump energy densities under femtosecond excitation.

The input – output curve for a two-photon pumped polyfluorene laser is shown in Figure 4.14.

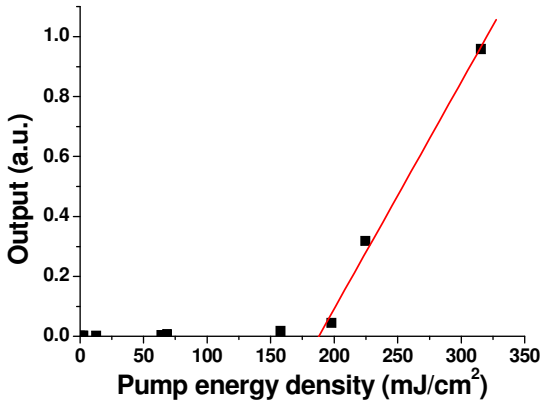

Figure 4.14 Output of a two-photon pumped polyfluorene laser as a function of the pump energy density under femtosecond excitation. The solid line corresponds to a linear fit.

The lowest recorded threshold was 42 mJ/cm^2 for a laser emitting at 443 nm, a value that is high in comparison to the one-photon pumped lasing threshold. Due to the fact that the material is being two-photon pumped though, the amount of pump energy absorbed is much lower. The absorbed energy density threshold can therefore be calculated by taking into account the amount of pump light that is actually absorbed. The fraction p of the light that is being absorbed by the film is given by

$$p = 1 - e^{-\alpha_2 z I} \qquad \textbf{4-XI}$$

where α_2 is the two-photon absorption coefficient for the film, z is the film thickness and I is the pump intensity.

The absorbed lasing threshold intensity can therefore be calculated as

$$I_{thr}^{abs} = pI_{thr} \qquad \textbf{4-XII}$$

Substituting the measured values for a polyfluorene film under femtosecond two-photon excitation, we can estimate the absorbed energy density lasing threshold to be 1.3 mJ/cm^2. This is a relatively high value when compared to the one-photon lasing threshold of 4μJ/cm^2, a difference that may be attributed to additional losses of excitations due to excited-state absorption.[34]

The two-photon pumped laser thresholds recorded here are relatively high in comparison to the other two examples of solid-state two-photon pumped organic semiconductor lasers. [19, 27] Of particular interest is the comparison to the two-photon pumped bisfluorene dendrimer laser reported in Chapter 5 of this thesis, as the light-emitting part of the dendrimer is the same as the basic repetition unit of polyfluorene. The absorbed energy density threshold for the bisfluorene dendrimer was 5.2 μJ/cm^2 and was directly comparable to the one-photon pumped lasing threshold of 4.5 μJ/cm^2. This large difference for polyfluorene shows just how different the polymer functions in comparison to the smaller dendrimer molecule, with additional loss mechanisms becoming more pronounced.

By using different combinations of grating periods and film thicknesses it was possible to tune the output wavelength of these lasers across 28 nm, as seen in Figure 4.15.

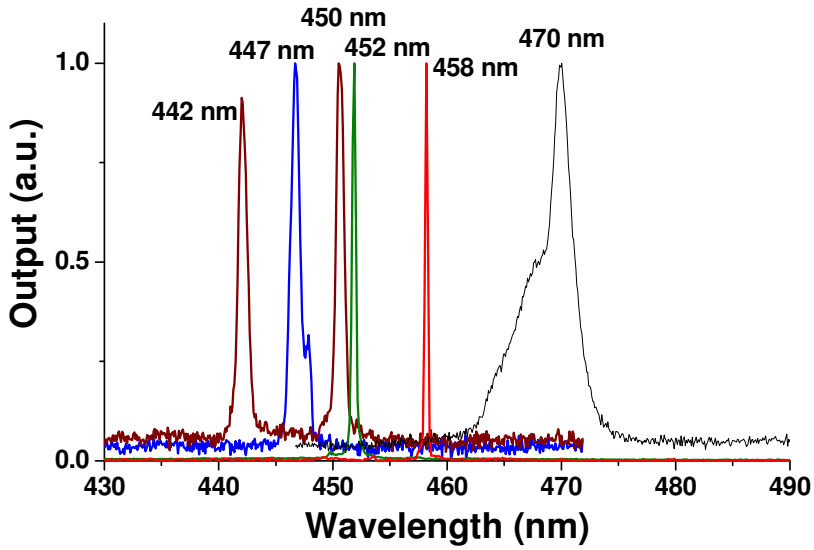

Figure 4.15 Output wavelength range of two-photon pumped polyfluorene lasers under femtosecond excitation obtained for different combinations of laser grating periods and film thicknesses.

As a result of the large thickness of the films fabricated, lasing in more than one transverse mode was observed, seen as two different lasing wavelengths in Figure 4.16.

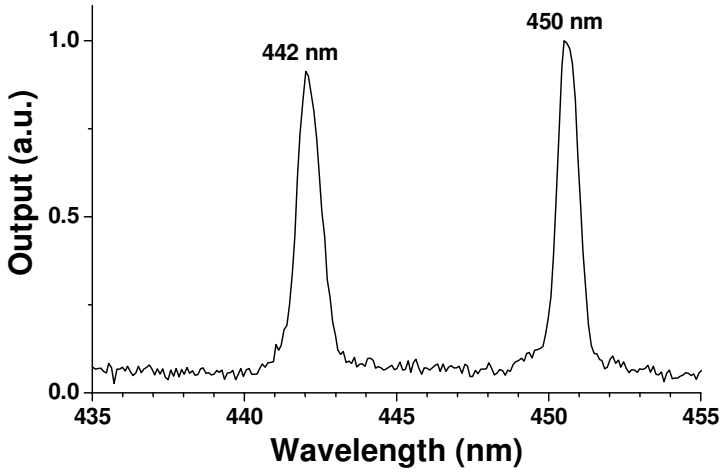

Figure 4.16 Dual-wavelength lasing emission from a two-photon pumped DFB polyfluorene laser under femtosecond illumination.

The multimode emission was also visible when imaging the output of the laser onto a white screen. The complicated pattern visible in Figure 4.17 is due to

laser light and some ASE being scattered out of the DFB grating in many modes, visible as extended criss-cross patterns on the observation screen.

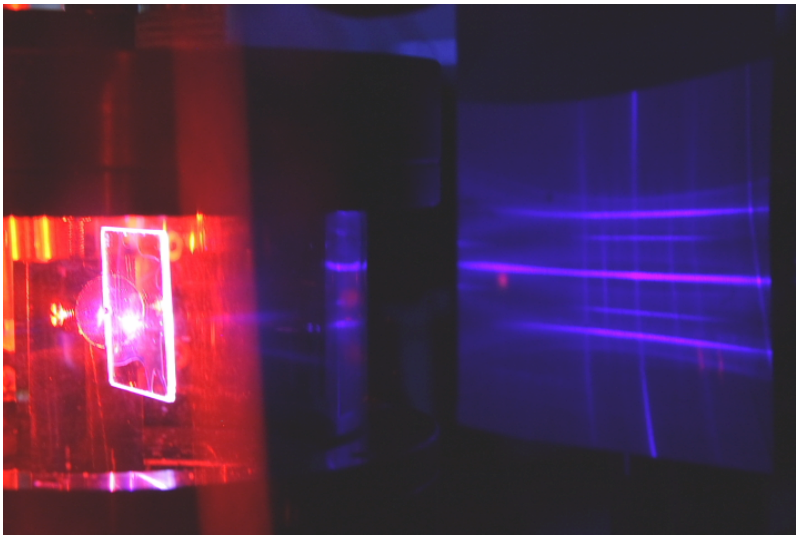

Figure 4.17 Multimode emission from a two-photon pumped polyfluorene laser under femtosecond excitation. The right-hand side of the image is covered by a blue filter that cuts out the scattered red pumping light.

4.5. Summary

Two photon absorption and induced luminescence studies have been performed on polyfluorene, one of the most popular conjugated polymers. The two-photon absorption spectrum of polyfluorene has been measured across a wide range of wavelengths and pump energies using both nanosecond and femtosecond excitation pulses. These measurements make it possible to determine the two-photon absorption coefficients and cross-sections of polyfluorene in both time domains, yielding results that are amongst the best recorded for conjugated polymers. The wavelength and pump energy dependence of two-photon induced luminescence was also studied using both nanosecond and femtosecond excitation pulses, making this one of the most complete two-photon absorption study of polyfluorene. The effects of pump pulse duration were discussed, highlighting the influence of additional transitions such as excited-state absorption on the two-photon behaviour of polyfluorene.

This information was used to determine the optimal conditions for optically pumping thin films of polyfluorene on distributed feedback gratings. This led to the demonstration of the world's first two-photon pumped solid-state polyfluorene laser. The output of this laser was tunable across 28 nm in the blue part of the visible spectrum, demonstrating the wide wavelength range of the available gain of polyfluorene even under nonlinear pumping conditions. The relatively high observed energy density threshold is a direct consequence of both the low absorption of the two-photon pump beam and additional excitation losses. This is only the second example of a two-photon pumped organic semiconductor laser and the only one based on a commercially available blue-emitting conjugated polymer.

4.6. References

[1] M. Leclerc, *J. Polym. Sci. Pol. Chem.* **2001**, *39*, 2867.

[2] H. N. Cho, J. K. Kim, D. Y. Kim, C. Y. Kim, N. W. Song, D. Kim, *Macromolecules* **1999**, *32*, 1476.

[3] A. Donat-Bouillud, I. Levesque, Y. Tao, M. D'Iorio, S. Beaupre, P. Blondin, M. Ranger, J. Bouchard, M. Leclerc, *Chemistry of Materials* **2000**, *12*, 1931.

[4] R. D. Xia, G. Heliotis, Y. B. Hou, D. D. C. Bradley, *Organic Electronics* **2003**, *4*, 165.

[5] G. Heliotis, D. D. C. Bradley, G. A. Turnbull, I. D. W. Samuel, *Applied Physics Letters* **2002**, *81*, 415.

[6] G. Heliotis, R. Xia, D. D. C. Bradley, G. A. Turnbull, I. D. W. Samuel, P. Andrew, W. L. Barnes, *Applied Physics Letters* **2003**, *83*, 2118.

[7] M. D. McGehee, A. J. Heeger, *Advanced Materials* **2000**, *12*, 1655.

[8] G. Heliotis, R. D. Xia, G. A. Turnbull, P. Andrew, W. L. Barnes, I. D. W. Samuel, D. D. C. Bradley, *Advanced Functional Materials* **2004**, *14*, 91.

[9] A. J. Cadby, P. A. Lane, H. Mellor, S. J. Martin, M. Grell, C. Giebeler, D. D. C. Bradley, M. Wohlgenannt, C. An, Z. V. Vardeny, *Physical Review B* **2000**, *62*, 15604.

[10] U. Scherf, E. J. W. List, *Advanced Materials* **2002**, *14*, 477.

[11] A. L. T. Khan, P. Sreearunothai, L. M. Herz, M. J. Banach, A. Kohler, *Physical Review B* **2004**, *69*.

[12] C. Rothe, F. Galbrecht, U. Scherf, A. Monkman, *Advanced Materials* **2006**, *18*, 2137.

[13] Y. Ren, Q. Xin, X. T. Tao, L. Wang, X. Q. Yu, J. X. Yang, M. H. Jiang, *Chemical Physics Letters* **2005**, *414*, 253.

[14] A. Bhaskar, R. Guda, M. M. Haley, T. Goodson, *Journal of the American Chemical Society* **2006**, *128*, 13972.

[15] P. Najechalski, Y. Morel, O. Stephan, P. L. Baldeck, *Chemical Physics Letters* **2001**, *343*, 44.

[16] Y. Morel, A. Irimia, P. Najechalski, Y. Kervella, O. Stephan, P. L. Baldeck, C. Andraud, *Journal of Chemical Physics* **2001**, *114*, 5391.

[17] R. Schroeder, B. Ullrich, W. Graupner, U. Scherf, *Journal of Physics-Condensed Matter* **2001**, *13*, L313.

[18] M. Tong, C. X. Sheng, Z. V. Vardeny, *Physical Review B* **2007**, *75*.

[19] G. Tsiminis, J. C. Ribierre, A. Ruseckas, H. S. Barcena, G. J. Richards, G. A. Turnbull, P. L. Burn, I. D. W. Samuel, *Advanced Materials* **2008**, *20*, 1940.

[20] G. Lemercier, J.-C. Mulatier, C. Martineau, R. Anemian, C. Andraud, I. Wang, O. Stephan, N. Amari, P. Baldeck, *Comptes Rendus Chimie Materiaux moleculaires* **2005**, *8*, 1308.

[21] H. E. Pudavar, M. P. Joshi, P. N. Prasad, B. A. Reinhardt, *Applied Physics Letters* **1999**, *74*, 1338.

[22] M. Albota, D. Beljonne, J. L. Bredas, J. E. Ehrlich, J. Y. Fu, A. A. Heikal, S. E. Hess, T. Kogej, M. D. Levin, S. R. Marder, D. McCord-Maughon, J. W. Perry, H. Rockel, M. Rumi, C. Subramaniam, W. W. Webb, X. L. Wu, C. Xu, *Science* **1998**, *281*, 1653.

[23] G. S. He, R. Signorini, P. N. Prasad, *Applied Optics* **1998**, *37*, 5720.

[24] M. Lal, S. Pakatchi, G. S. He, K. S. Kim, P. N. Prasad, *Chemistry of Materials* **1999**, *11*, 3012.

[25] D. Wang, G. Y. Zhou, Y. Ren, X. G. Xu, X. F. Cheng, Z. S. Shao, M. H. Jiang, *Chemical Physics Letters* **2002**, *354*, 423.

[26] G. Y. Zhou, W. Dong, X. M. Wang, Z. S. Shao, M. H. Jiang, *Optics Communications* **2004**, *241*, 215.

[27] C. Bauer, B. Schnabel, E. B. Kley, U. Scherf, H. Giessen, R. F. Mahrt, *Advanced Materials* **2002**, *14*, 673.

[28] J. D. Bhawalkar, G. S. He, P. N. Prasad, *Reports on Progress in Physics* **1996**, *59*, 1041.

[29] J. Swiatkiewicz, P. N. Prasad, B. A. Reinhardt, *Optics Communications* **1998**, *157*, 135.

[30] D. Wasserberg, S. P. Dudek, S. C. J. Meskers, R. A. J. Janssen, *Chemical Physics Letters* **2005**, *411*, 273.

[31] B. Lawrence, W. E. Torruellas, M. Cha, M. L. Sundheimer, G. I. Stegeman, J. Meth, S. Etemad, G. Baker, *Physical Review Letters* **1994**, *73*, 597.

[32] S. J. Chung, G. S. Maciel, H. E. Pudavar, T. C. Lin, G. S. He, J. Swiatkiewicz, P. N. Prasad, D. W. Lee, J. I. Jin, *Journal of Physical Chemistry A* **2002**, *106*, 7512.

[33] O. Varnavski, A. Leanov, L. Liu, J. Takacs, T. Goodson, *Journal of Physical Chemistry B* **2000**, *104*, 179.

[34] K. D. Belfield, M. V. Bondar, I. Cohanoschi, F. E. Hernandez, O. D. Kachkovsky, O. V. Przhonska, S. Yao, *Applied Optics* **2005**, *44*, 7232.

[35] M. A. Stevens, C. Silva, D. M. Russell, R. H. Friend, *Physical Review B* **2001**, *63*, 165213.

[36] I. B. Martini, A. D. Smith, B. J. Schwartz, *Physical Review B* **2004**, *69*, 035204.

5. One- and two-photon lasing in bisfluorene-cored dendrimers

In this chapter a family of bisfluorene-cored dendrimers is studied with the aim to use these materials as gain medium in solid-state organic lasers. Photophysical studies of these materials are performed and amplified spontaneous emission measurements help determine the most promising candidate for lasing. A tunable dendrimer laser is demonstrated that emits in the deep blue and performs similarly to the well-established polyfluorene lasers.

In addition, the two-photon absorption properties of these dendrimers are studied, as the bisfluorene core has been previously studied in this respect and the addition of conjugated dendrons is known to increase the nonlinear absorption. One of the dendrimers is used to demonstrate the first two-photon pumped dendrimer laser, showing an alternative optical pumping scheme for organic lasers and highlighting the versatility of organic semiconductors.

The author performed most of the photophysical measurements described in this chapter in collaboration with Dr. Jean-Charles Ribierre. Some of the steady-state spectra were collected by Scott Richardson, who also contributed to the lasing results.

5.1. Introduction

Organic semiconductor materials are of particular interest for making lasers that can access the violet and blue part of the optical spectrum between 400 and 500 nm. This is a wavelength regime where there is a relatively small number of available laser sources, constituting mainly from gas lasers, gas laser pumped dye lasers and nonlinear wavelength conversions of infrared lasers.[1] The main representatives for gas lasers are Argon-ion, Krypton and Helium-Cadmium lasers, while UV gas lasers such as Nitrogen lasers are used as pump sources for the dye lasers.[2] All these sources however are very bulky and expensive, require high operational voltages and at the same time offer limited tunability,

while the nonlinear conversions require expensive nonlinear crystals and have reduced efficiencies. Still, these systems have been very successful and dye lasers in particular are very widespread as they demonstrate great wavelength tunability and remain vital for accessing the visible spectrum below 500 nm with laser light.[3] Organic semiconductors that can access this part of the spectrum are therefore of great interest, as their solution processability, high optical gain and synthesis flexibility can lead to inexpensive, compact and tunable laser systems to access the violet and blue parts of the spectrum.[4]

Amongst the various organic semiconductors, the family of fluorene-based materials has emerged as the most important of the blue-emitting materials.[5, 6] Conjugated polymers such as polyfluorene and its numerous derivatives are based around the fluorene unit shown in Figure 5.1 and have demonstrated efficient light emission across the visible spectrum, leading to the manufacturing of organic light-emitting diodes with very attractive properties for applications such as displays. [7-9]

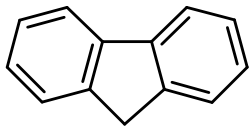

Figure 5.1 The basic fluorene unit, key component of many organic semiconductors

In addition, the lasing properties of fluorene-based conjugated polymers are amongst the best for any organic semiconductors, leading to solid-state organic lasers with exceptionally low lasing thresholds. [10-12] The polymer nature of these materials though can lead to unwanted variations in their properties as a result of the polydispersity of their chains, whereby each polymer molecule is made up of a different number of repetitions units leading to slightly different morphology, absorption and emission features.[13-15]

An alternative approach that attempts to circumvent these problems is the synthesis of smaller organic semiconductors that are based around fixed molecular structures rather than long polymer chains. The molecules produced

are typically larger than conventional laser dyes but are equally well-defined, allowing for accurate control of the material's photophysical properties.

5.2. Dendrimers

One such category of materials is dendrimers, in which a core unit, selected for its photophysical properties, is surrounded by additional units called dendrons (see Figure 5.2).[16] The dendrons act as spacers between the individual cores, controlling the intermolecular interactions that affect both the fluorescence and the charge transport. Surface groups are attached at the end of the dendrons to control the solubility of the molecules, making dendrimers soluble in a large range of organic solvents.

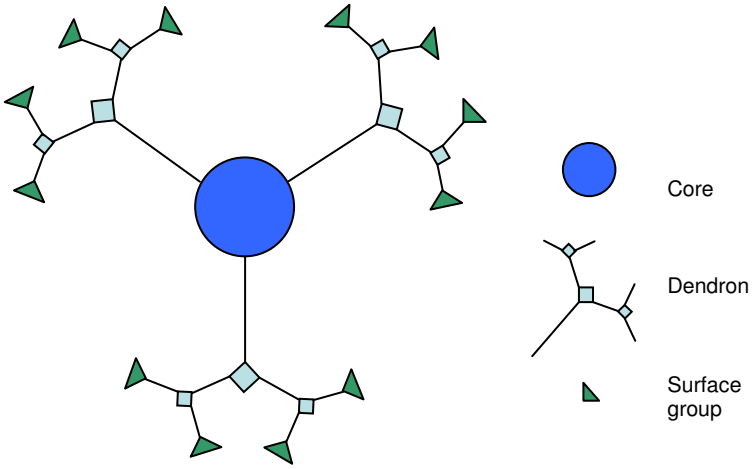

Figure 5.2 The basic dendrimer structure

The great advantage of the dendrimer design comes from the ability to tune the properties of each part of the molecule separately without affecting the rest of the properties. A different type of dendron could, for example, be combined with the same core and surface groups to give a material with the same fluorescence wavelength and solubility but greater separation between molecules.

Efficient light emission from dendrimer materials has been well documented in the literature, with organic light-emitting diodes reaching external quantum efficiencies up to 16 %,[17] though this is due to phosphorescence emission that

is unsuitable for lasing. Fluorescent cores have been used that demonstrate the potential for high available optical gain and good lasing properties, such as low lasing thresholds and high slope efficiencies.[18-20]

In this work the photophysical properties of a family of blue-emitting bisfluorene-cored dendrimers were investigated and the most suitable member of that family was used to fabricate distributed feedback organic semiconductor lasers. In addition, an alternative optical pumping scheme is explored by using two-photon absorption to pump a blue-emitting bisfluorene dendrimer laser at a wavelength much longer then the material's linear absorption and emission.

5.2.1. Bisfluorene dendrimers

The dendrimers studied as part of this work all share the same bisfluorene core onto which different dendrons are attached.[21] Figure 5.3 shows the molecular structure of the different dendrimers with biphenyl (BP), biphenyl-carbazol (BPCz) and E-stylbene (ES) dendrons attached to them.

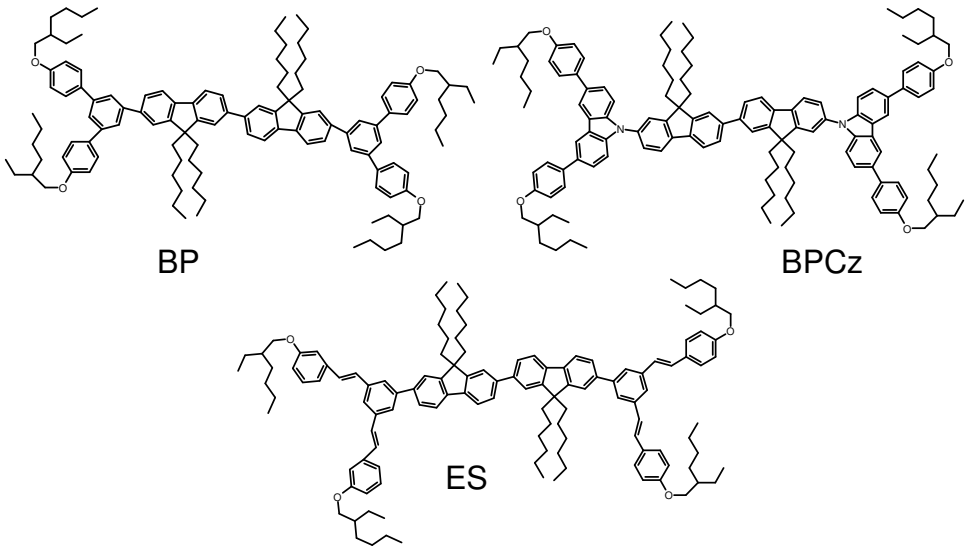

Figure 5.3 Chemical structures of bisfluorene dendrimers with different dendrons: biphenyl (BP), biphenyl-carbazol (BPCz) and E-stylbene(ES) dendrons.

5.3. Photophysical measurements

The absorption and fluorescence spectrum of the bisfluorene dendrimers can be seen in Figure 5.4. These materials all absorb in the UV and their emission spans the violet and blue parts of the spectrum. Dendrimers (BP) and (ES) have very similar emission spectra, while the (BPCz) dendrimer has a somewhat red-shifted emission spectrum. These measurements were performed by Jean-Charles Ribierre and Scott Richardson.

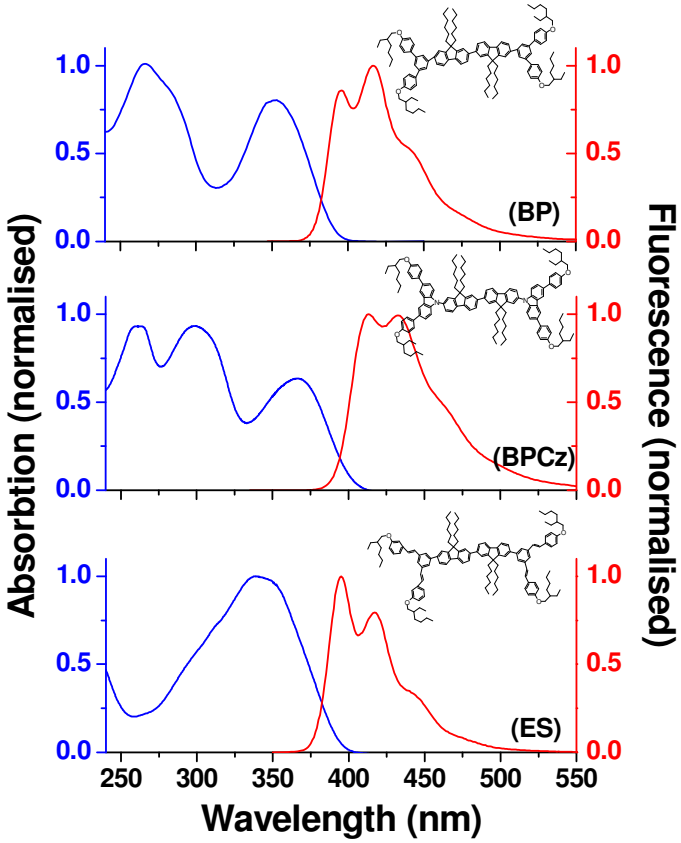

Figure 5.4 Absorption (red line) and fluorescence (blue line) spectra of the three bisfluorene-cored dendrimers.

5.3.1. Photoluminescence quantum yield

The photoluminescence quantum yield of each material was measured in film. The PLQY values are summarized in Table 5.a, where the dendrimer with BP dendrons presents an exceptionally high value of 92 %.

Dendron type	Film PLQY (%)
BP	92
BPCz	43
ES	52

Table 5.a PLQY values for the bisfluorene dendrimers studied.

5.3.2. Amplified spontaneous emission measurements

As a precursor to lasing, amplified spontaneous emission (ASE) measurements provide a benchmark for the lasing performance of materials independent of the resonator structures be used in the actual device. To observe ASE a thin film is spin coated from solution onto a glass substrate and the sample is placed in a vacuum chamber where it is excited by a pump beam focused to a narrow stripe. The resulting fluorescence is waveguided by the film and is scattered out at the edges of the film where it is collected using a fibre connected to a spectrograph. As the intensity of the pump beam is increased above a certain threshold level, the emission from the material becomes narrower in comparison to the steady-state fluorescence spectrum until it reaches a FWHM of approximately 5 nm, while the intensity of the output increases at a faster rate as the light is amplified as a result of ASE. This behaviour can be seen in Figure 5.5.

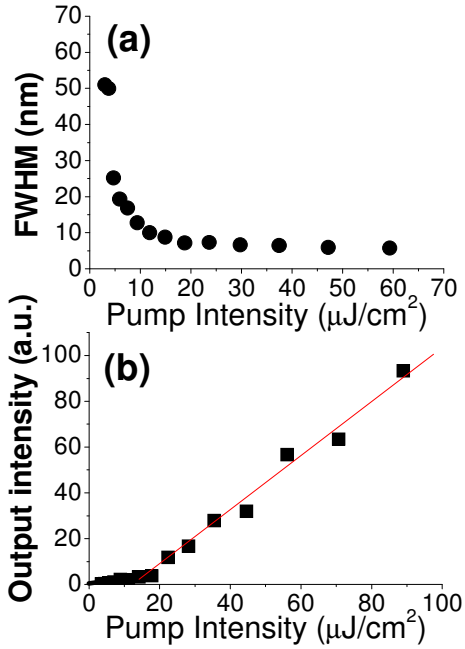

Figure 5.5 (a) Emission linewidth and (b) output intensity as the material crosses the amplified spontaneous emission threshold for a bisfluorene dendrimer.

The ASE spectrum of the three dendrimers can be seen in Figure 5.6.

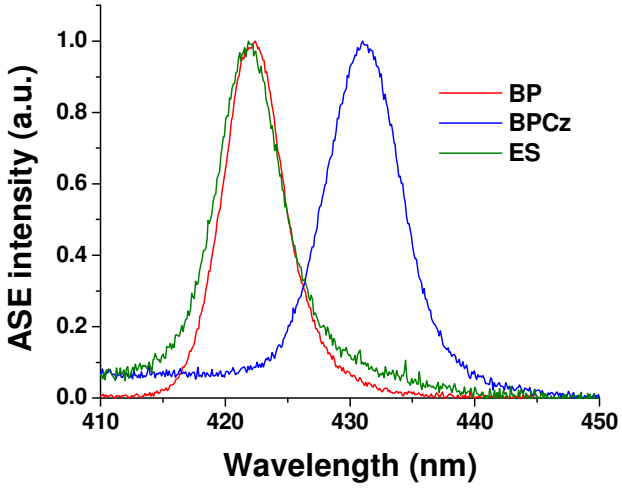

Figure 5.6 ASE spectra for the different bisfluorene dendrimers studied.

ASE threshold measurements were performed for each dendrimer and the results are summarized in Table 5.b, where the peak wavelength of the ASE emission is recorded along with the corresponding ASE threshold.

Dendron type	λ_{ASE} (nm)	ASE threshold ($\mu J/cm^2$)
BP	422.4	16
BPCz	431.0	50
ES	421.9	25

Table 5.b ASE wavelength and energy density threshold values for the bisfluorene dendrimers.

5.3.2.1. Optical gain and waveguide losses

It is important when characterizing a new type of material to determine some of the key properties that will ultimately affect its lasing performance. The most useful set of parameters consists of determining the optical gain available per unit length as well as the waveguide losses per unit length as the fluorescence is waveguided through the film. Using the variable stripe technique [22] we were able to perform these measurements for all three bisfluorene dendrimers.

Measuring the optical gain requires a thin film of the material excited by a pump beam focused to a thin stripe of varying length with a fibre placed near

the edge of the film to collect the intensity of the light scattered out. As described previously in Chapter 3, when the material is above the ASE threshold, the output intensity I_{out} from the edge of the film as a function of the stripe length is given by

$$I_{out} = \frac{A(\lambda)I_p}{g(\lambda)}(e^{(g(\lambda)l} - 1) \qquad \textbf{5-I}$$

where $g(\lambda)$ is the optical gain, $A(\lambda)$ is a constant of the material related to the spontaneous emission cross-section, I_p is the pump intensity and l is the length of the stripe. The data from the optical gain measurements can be seen in Figure 5.7 for all three bisfluorene dendrimers.

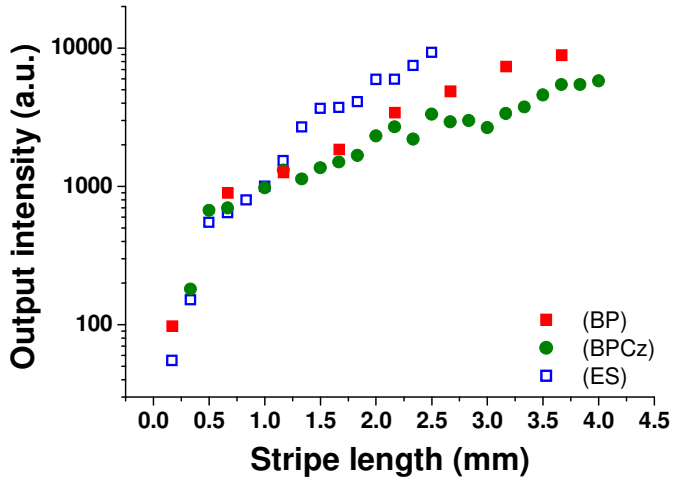

Figure 5.7 Amplified spontaneous emission intensity as a function of the excitation stripe length used to determine optical gain in bisfluorene dendrimers.

The waveguide loss coefficient can be calculated if the length of the excitation stripe is kept constant but the stripe is moved away from the edge of the film. This means that the generated ASE is waveguided to the edge of the film where it is scattered out and collected by the optical fibre; the longer this distance is, the higher the attenuation of the ASE becomes as the light experiences both scattering and re-absorption by the material. The waveguide loss coefficient α can then be calculated by $I=I_0exp(-\alpha x)$, where I_0 is the output intensity when the stripe is at the edge of the film. The data collected in this measurement for the bisfluorene dendrimers are shown in Figure 5.8.

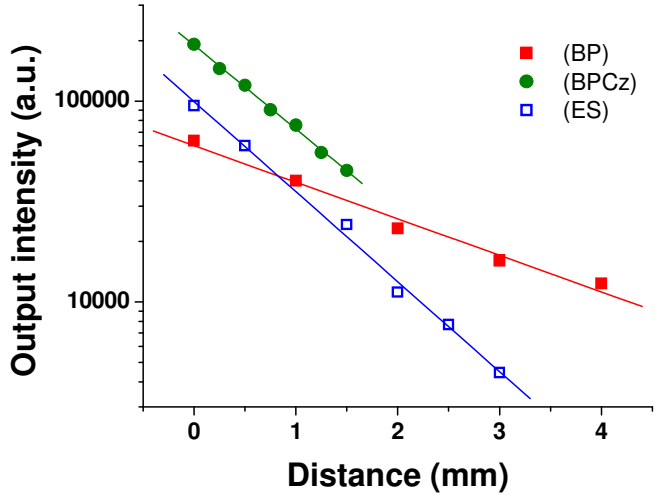

Figure 5.8 ASE output intensity as a function of changing distance from the edge of the film used to determine the waveguide loss coefficients of the bisfluorene dendrimers. The solid lines correspond to exponential decay fits.

The optical gain and waveguide loss data for the bisfluorene dendrimers are summarised in Table 5.c.

Dendron type	Gain (cm^{-1})	Losses (cm^{-1})
BP	51	4
BPCz	8	10
ES	21	10

Table 5.c Optical gain and waveguide losses of bisfluorene dendrimers.

5.3.2.2. Gain calculations

In order to understand the observed differences in the ASE performance of the bisfluorene dendrimers and to understand the effect that the key photophysical properties such as optical gain and loss have on the potential of a material as a gain medium for lasers, it is useful to look at how some of these properties are linked together. Under steady-state conditions, the net optical gain g of a material is given by

$$g = \sigma N \qquad \textbf{5-II}$$

where σ is the stimulated emission cross-section and N is the population of the first excited state. We can rewrite the above equation as

$$g = \sigma P \tau \quad \textbf{5-III}$$

where P is the pumping rate and τ is the lifetime of the first excited state.

The lifetime τ is a function of the radiative (k_R) and non-radiative (k_{NR}) decay rates of the material according to

$$\frac{1}{\tau} = k_R + k_{NR} \quad \textbf{5-IV}$$

The photoluminescence quantum yield Φ *can* also be expressed as a function of the two decay rates, as it represents the radiative percentage of the total decay rate

$$\Phi = \frac{k_R}{k_R + k_{NR}} \quad \textbf{5-V}$$

The lifetime of the first excited state can therefore be written as

$$\tau = \Phi / k_R \quad \textbf{5-VI}$$

leading to the following expression for the optical gain

$$g = \sigma \frac{P\Phi}{k_R} \quad \textbf{5-VII}$$

When considering that the amplified fluorescence also has to travel through a waveguide that presents a loss coefficient α, the net gain g_{net} observed by the variable stripe technique is

$$g_{net} = \sigma N - \alpha \quad \textbf{5-VIII}$$

It is therefore possible to theoretically calculate the optical gain available from the material based on the following expression:

$$g_{net} = \frac{\sigma P \Phi}{k_R} - \alpha \quad \textbf{5-IX}$$

where all the symbols are defined in the above set of equations.[21] Of these parameters, the pumping rate P can be calculated knowing the pump pulse duration (4 ns) and the ratio σ/k_R does not depend on the gain medium considered due to the proportionality of the Einstein A and B coefficients.

Additional measurements have shown that in dendrimer (BP), σ has been found to be 3.4×10^{-18} cm^2 and k_R has been measured to be 1.28×10^9 s^{-1}.[23] These values are expected to be very similar for all three bisfluorene dendrimers studied in this chapter.

Using this information, we can compare the gain coefficient values measured for the different dendrimers against the predictions from the above calculations. In Figure 5.9 the ASE threshold, waveguide losses and the measured and theoretical optical gain coefficients have been plotted as a function of the materials' PLQY values to allow for better overview of these key properties:

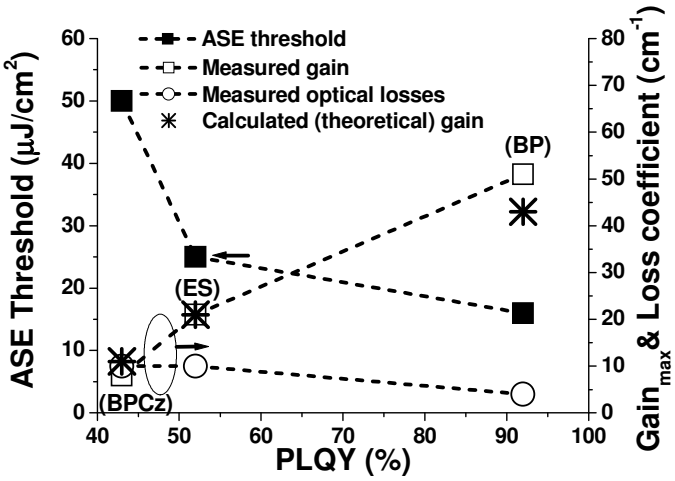

Figure 5.9 ASE threshold, waveguide losses, measured gain and theoretical gain (crosses) as a function of the PLQY of different bisfluorene dendrimers. The lines are guides for the eye.

Since the emitting core remains the same across all dendrimers, the family forms a good model system for such calculations, allowing for direct comparisons of the effect the different dendrons have on the performance of the materials.

From the ASE measurements it becomes obvious that the dendrimer with biphenyl dendrons (BP) combines very high film PLQY, high available optical gain and low ASE threshold, making it an ideal candidate for lasing. The lasing experiments therefore were performed using this dendrimer as the gain medium.

5.4. Lasing experiments

Distributed feedback lasers were fabricated by spin coating thin films from chloroform solution (25 mg/ml) of the BP dendrimer onto corrugated silica substrates. Both 1-D and 2-D DFB gratings were used and the grating period was varied between 270 and 290 nm. The laser structures were pumped using a nanosecond optical parametric oscillator with pulse duration 4 ns and repetition rate 20 Hz. The pump beam was incident at an angle to the film and was focused to a spot size of 270 x 270 μm.

A typical input-output measurement to determine the lasing threshold can be seen in Figure 5.10, where the lasing threshold is 16 μJ/cm^2.

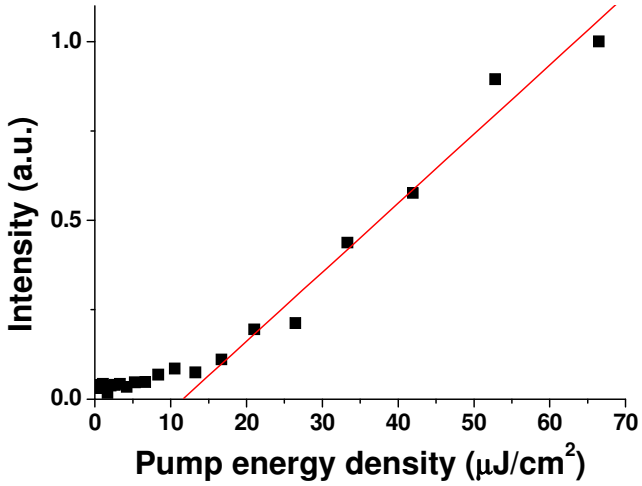

Figure 5.10 Output intensity as a function of the pump energy density for a DFB laser based on the bisfluorene dendrimer with biphenyl dendrons. The solid line is a linear fit above threshold.

It is worth mentioning that by using pump pulses from a microchip laser with a shorter duration and a different spot size the lowest recorded threshold was measured to be 4.5 μJ/cm^2 by Scott Richardson and Jean-Charles Ribierre as seen in Figure 5.11.[21] The slope efficiency of the same sample was found to be 8.3 % when including emission from only one side of the DFB laser. These results are directly comparable to those reported for polyfluorene, a benchmark organic semiconductor for blue emission, showing a lasing threshold of 4 μJ/cm^2 and 7.8% slope efficiency.[24]

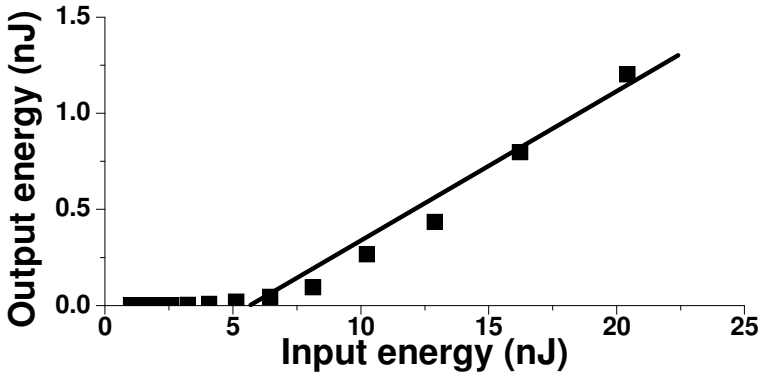

Figure 5.11 Best recorded threshold lasing data from a BP bisfluorene dendrimer excited by a microchip laser .[21]

By varying the DFB grating period, tuning of the dendrimer laser was possible across 10 nm, as seen in Figure 5.12.

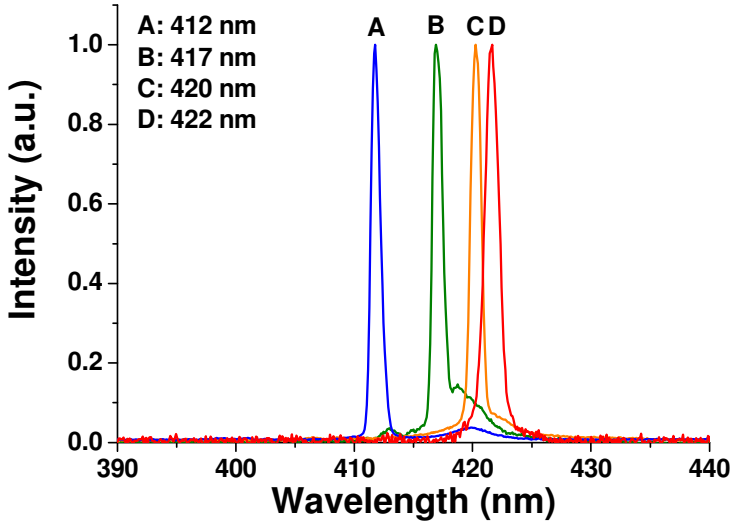

Figure 5.12 Tuning curve of a BP dendrimer DFB laser

5.5. Lasing summary

The key photophysical properties of a family of bisfluorene-cored dendrimers have been studied, including amplified spontaneous emission studies to determine the available optical gain and waveguide losses in thin films. The best dendrimer was then used to make a blue tunable solid-state DFB laser that showed lasing performance similar to polyfluorene, the current benchmark blue-emitting organic semiconductor.

5.6. Two-photon absorption and lasing

These bisfluorene dendrimers show excellent lasing performance and as such have great potential for use in more compact organic semiconductor lasers. They do however require excitation at ultraviolet wavelengths, where pump lasers are still relatively bulky and expensive. A different approach would be to use longer wavelengths to excite the materials via a nonlinear absorption process known as two-photon absorption, whereby two photons of half the energy (twice the wavelength) required to bridge the material's band gap are absorbed simultaneously to excite the molecules to the first emissive state.[25] This pumping scheme builds on the nonlinear optical properties of organic semiconductors and could potentially lead to red laser diodes being used as pump sources, allowing for compact organic laser systems. Two-photon pumped lasing in organic materials has been investigated in depth for small liquid and solid-state dye solutions.[26-29] In organic semiconductors though there is only one previous published example of a solid-state two-photon pumped lasers, based on the ladder polymer MeLPPP, emitting in the green part of the spectrum.[30] Note here that in Chapter 4 of this thesis a two-photon pumped polyfluorene laser is presented, with a publication soon to follow.

A suitable material for this approach needs to combine both good lasing performance as well as a strong two-photon absorption cross-section to enable effective harvesting of the longer-wavelength pump light. As the bisfluorene dendrimers studied here have demonstrated their merits as lasing materials, the question emerged as to their nonlinear optical properties. Previous studies on the bisfluorene core have shown good two-photon absorption properties for optical limiting applications, while the addition of dendrons in our materials can extend the p-electrons delocalisation, a property that is known to enhance two-photon cross-section.[31-34] This study aims to determine the potential of bisfluorene dendrimers as gain media for two-photon lasing through a detailed photophysical analysis and use these results to demonstrate a blue-emitting solid-state two-photon pumped organic laser.

5.6.1. Two-photon absorption and emission studies

The first step in evaluating the performance of the dendrimers under two-photon excitation is to determine the most efficient pump wavelength for light emission. To achieve this, an optical parametric oscillator was used to provide a tunable pump wavelength between 500 and 850 nm in 10 nm steps at energy levels sufficiently high to induce nonlinear absorption effects. The pump beam was incident onto a quartz cuvette containing a 30 mg/ml dendrimer solution in chloroform and the induced fluorescence was collected from the side of the cuvette using a Jobin-Yvon Triax CCD spectrograph with an optical fibre and a collection lens. Photos from this setup showing the observed two-photon induced fluorescence can be seen in Figure 5.13 for two different excitation wavelengths.

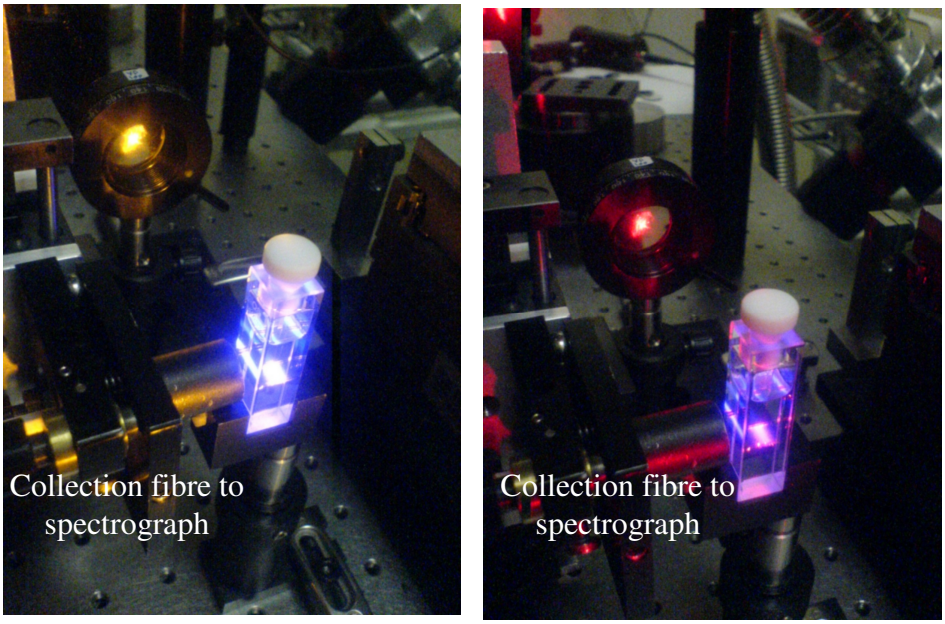

Figure 5.13 Two-photon induced fluorescence in solutions of a bisfluorene-cored dendrimer under nanosecond excitation. Two different pump wavelengths were used (580 nm on the left, 620 nm on the right. Also visible is the collecting optical fibre for the spectrograph.

The resulting data can be seen in Figure 5.14, where fluorescence is plotted as a function of the pump wavelength from the OPO for all three bisfluorene dendrimers studied. The behaviour of the BP and ES dendrimers is very similar, showing a broad peak around 590 nm and no other significant features. The

BPCz dendrimer on the other hand shows a wider peak around 600 nm and a secondary peak at 680 nm. This second peak may be due to the addition of a nitrogen atom between the core and the dendrons. The observed two-photon induced fluorescence spectra can be compared with the linear absorption spectra, also shown in the same figure, giving a direct comparison between the wavelength dependence of the two processes.

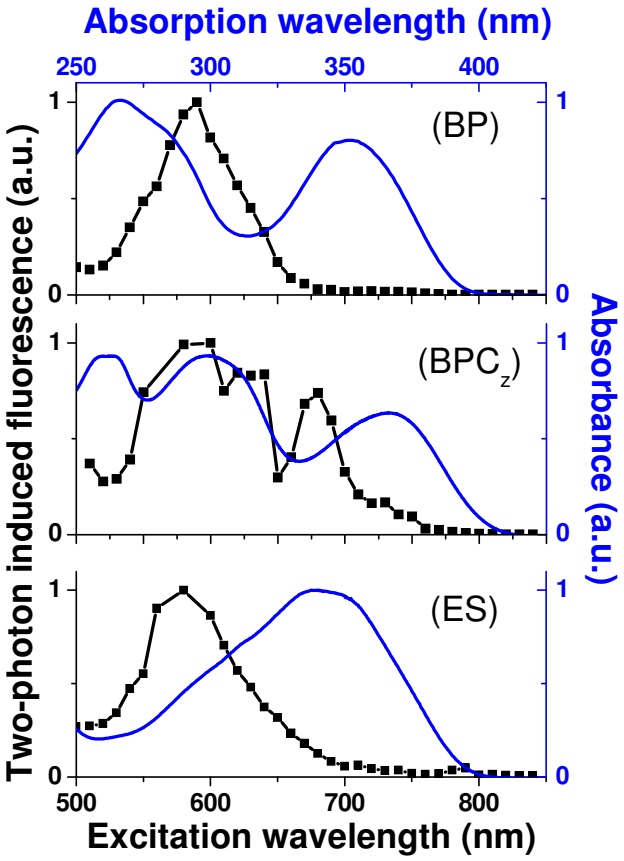

Figure 5.14 Two-photon fluorescence excitation (solid squares) and linear absorption (blue line) spectra of bisfluorene-cored dendrimers in solution under nanosecond excitation.

The shape of the linear absorption is reproduced well in the two-photon fluorescence excitation spectra for each dendrimer. The peaks are blue-shifted in the nonlinear absorption data by approximately 60-80 nm due to the fact that the one-photon transition (1 Ag to 1 Bu) is not spin-allowed for the simultaneous absorption of two photons. The two-photon transition is instead from 1 Ag to m Ag, leading to a slightly higher energy level being accessed by two-photon absorption. This m Ag energy level is 0.6-0.7 eV higher than the 1

Bu state to which the molecules quickly relax and proceed to return back to the relaxed state 1 Ag by emitting light, as seen in Figure 5.15.

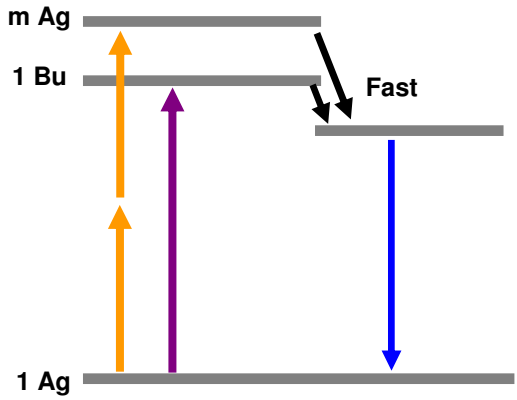

Figure 5.15 Linear (purple arrow) and two-photon (orange arrows) absorption processes in a simple energy level diagram for the bisfluorene dendrimers

In order to confidently assign the observed fluorescence to a two-photon process, measurements of both fluorescence and pump beam transmission through the sample were performed as a function of pump intensity.

For a two-photon absorption process, the fluorescence intensity should be proportional to the square of the pump intensity and when plotted against the square of the pump intensity the resulting graph should be a straight line. Figure 5.16 shows such a graph for all three dendrimers pumped at the peak of their two-photon excitation spectra. The graph clearly verifies the square dependence of the observed fluorescence.

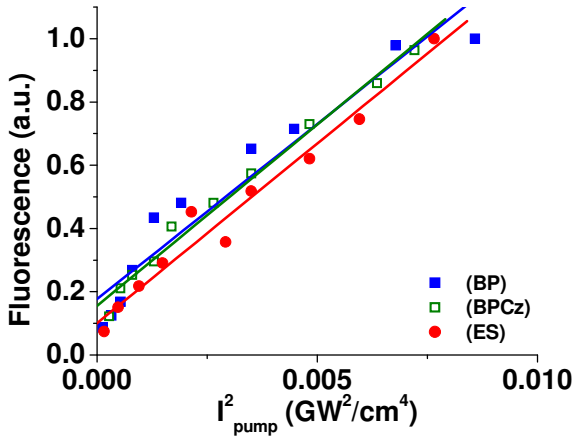

Figure 5.16 Two-photon induced fluorescence as a function of the square of the pump intensity for bisfluorene dendrimers in solution under nanosecond excitation. (BP) and (ES) dendrimers were pumped at 590 nm, while (BPCz) was pumped at 600 nm. The lines correspond to linear fits for the data.

The transmission of the pump beam through the sample for two-photon absorption is also dependant on the pump intensity. More specifically, the inverse of the transmission as a function of the pump intensity can be written as:

$$\frac{1}{T} = 1 + \alpha_2 z I_{pump} \qquad \textbf{5-X}$$

where T is the transmission of the pump beam through the sample, α_2 is the two-photon absorption coefficient and z is the thickness of the sample.[35]

The transmission data can be seen plotted in Figure 5.17 according to the above equation and are in good agreement with the expected two-photon absorption behaviour.

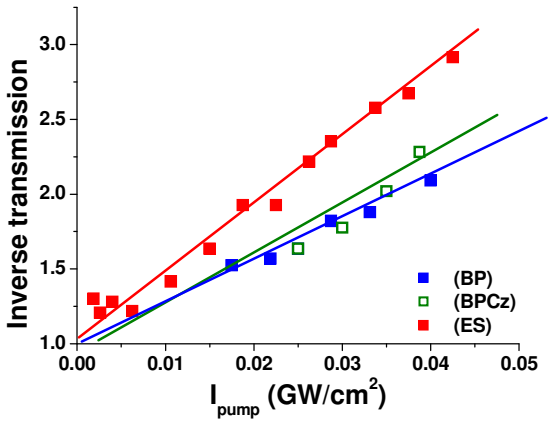

Figure 5.17 Inverse transmission as a function of pump intensity for three bisfluorene-cored dendrimers under nanosecond excitation. The pumping wavelength was 590 nm for the (BP) and (BPCz) dendrimers and 600 nm for the (ES) dendrimer. The lines correspond to linear fits.

For the 1-cm long cuvettes used for these experiments, the slope of the above graph shows the two-photon absorption coefficient of each dendrimer. The resulting values are shown in Table 5.d for the three dendrimers studied. These measurements were performed using both nanosecond and femtosecond pump pulses and correspond to the peak of the two-photon absorption spectrum of each molecule in order to determine the impact of pump pulse duration on nonlinear absorption. The absorption coefficient values for a thin film of the material also are of great interest as it is in the solid state that two-photon lasing will take place. Since absorption coefficients are directly related to the concentration of the material, and by assuming a 1 g/ml concentration for the solid-state, the two-photon absorption coefficient for a thin film of bisfluorene dendrimer is shown to be 33.3 times higher than that measured in solution as seen in Table 5.d.

Dendron type	Solution α_2^{ns} [cm/GW]	Film α_2^{ns} [cm/GW]	Solution α_2^{fs} [cm/GW]	Film α_2^{fs} [cm/GW]
BP	27	899	0.073	2.4
BPCz	35	1166	0.095	3.2
ES	45	1499	0.118	3.9

Table 5.d Two-photon absorption coefficients for 30 mg/ml toluene solutions (measured) and thin films (calculated) of bisfluorene dendrimers.

Note here that the values for nanosecond excitation are on average 370 times higher than the corresponding femtosecond values. This difference has been previously attributed to excited-state absorption and has been discussed in great detail in the previous chapter (Chapter 4).

The two-photon absorption coefficients measured can then be translated into a concentration-independent two-photon absorption cross-section δ using the equation

$$\delta = \frac{hv\alpha_2(M_w)}{N_A\rho} \qquad \textbf{5-XI}$$

where hv is the energy of the pumping photon, M_w is the molecular weight of the molecule, N_A is the Avogadro number and ρ is the density of the system investigated. The unit for two-photon absorption cross-section is 1 GM, defined as

$$1\ GM = 10^{-50} cm^4 \cdot s \cdot photon^{-1} molecule^{-1}$$

An overview of the two-photon absorption coefficients and cross-sections for both nanosecond and femtosecond excitation can be seen in Table 5.e.

Dendron type	α_2^{ns} [cm/GW]	δ^{ns} [GM]	α_2^{fs} [cm/GW]	δ^{fs} [GM]
BP	27	85	0.073	0.30
BPCz	35	120	0.095	0.33
ES	45	148	0.118	0.39

Table 5.e Two-photon absorption coefficient (α_2^{xx}) and cross-section (δ^{xx}) values under nanosecond (ns) and femtosecond (fs) illumination at the peak of the photoexcitation spectrum for each dendrimer.

It is worth noting that the two-photon absorption cross-section of a bare bisfluorene molecule like the core of the dendrimer studied here was measured under nanosecond illumination to be 60 GM.[36] The higher values measured for the dendrimers highlight the effect that the dendrons have on the two-photon absorption properties of these molecules, even though the excited states are mostly confined in the dendrimer cores, as is evident from the similarities in the linear absorption and fluorescence spectra. The addition of the dendrons

enhances the cross-section of all dendrimers for two-photon absorption by further delocalising the p-electrons from the core, a process known to enhance nonlinear absorption without altering the key photophysical properties of the core, a consequence of the modular architecture of dendrimers.

The one- and two-photon studies can be combined to select the best candidate for a two-photon pumped laser. The ideal material should combine high photoluminescence quantum yield with substantial two-photon absorption. Considering this, the bisfluorene-cored dendrimer with biphenyl (BP) dendrons becomes the obvious choice as it combines a film PLQY of 92% with a reasonable two-photon absorption cross-section. This material has also demonstrated excellent one-photon lasing behaviour, with results comparable to those obtained for benchmark blue-emitting organic semiconductors. All the experiments on two-photon pumped lasing were therefore performed using this dendrimer.

5.7. Two-photon pumped lasing experiments

Solid-state lasers were prepared from dendrimer solutions (25 mg/ml in toluene) by spin-coating under various spin speeds between 800 and 150 rpm. The resonator structures used were corrugated silica 1-D and 2-D distributed feedback gratings with periods between 260 and 280 nm and an average depth of 30 nm. The samples were kept in a vacuum chamber in pressures of 10^{-4} mbar to slow down oxidation and photodegradation.

The initial set of experiments was performed using nanosecond pump pulses from an optical parametric oscillator (OPO). The pump wavelength was 590 nm to match the maximum of the two-photon induced fluorescence and was focused using a cylindrical lens to a stripe with dimensions of 170 x 4000 μm in order to give a long interaction length between the excitation field and the material in a direction perpendicular to the 1D grating. Figure 5.18 shows a two-photon pumped bisfluorene laser in operation inside a vacuum chamber when pumped at 590 nm.

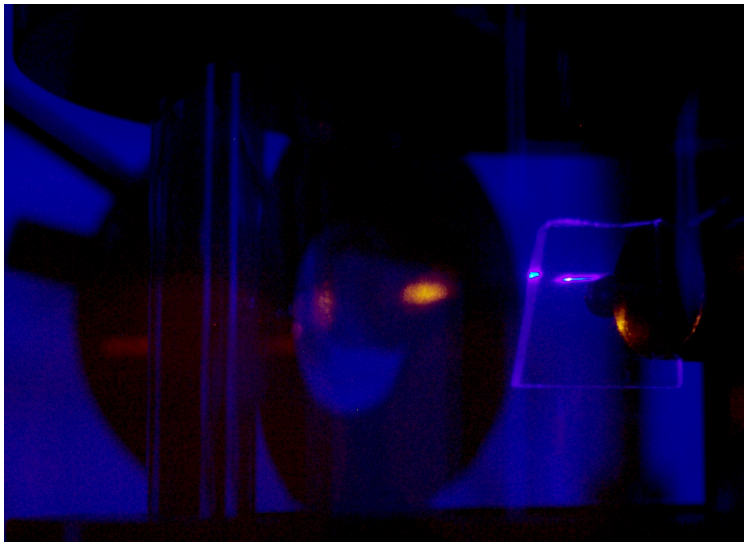

Figure 5.18 A two-photon pumped bisfluorene dendrimer DFB laser (right-hand side of the photograph) under nanosecond excitation. The photo is taken through a blue filter to reduce the intensity of the pump light at 590 nm. The excited region of the film inside the vacuum chamber is visible as a horizontal stripe where the intensity of the emission has saturated the camera.

The lasing spectrum from a bisfluorene DFB laser can be seen in Figure 5.19 plotted against the Bragg-scattered emission peaks that originate in the emission pattern from DFB lasers as discussed in Section 2.4.2 when the fluorescence is collected below lasing threshold.

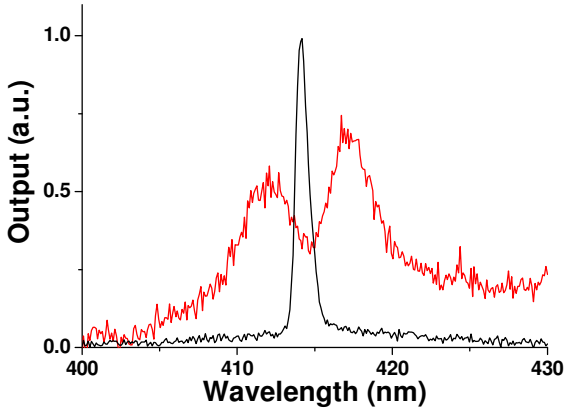

Figure 5.19 Lasing spectrum from a two-photon pumped bisfluorene DFB laser under nanosecond excitation. Also visible are the peaks from the Bragg-scattering of the material's spontaneous emission due to the presence of the grating.

The input-output behaviour of the two-photon pumped BP dendrimer lasers made using different DFB gratings can be seen in Figure 5.20 and folloes the well-established lasing measurement techniques described previously in

Chapter 3 of this thesis. The pump energy was modified using a number of metallic neutral density filters, while the emission intensity was recorded using a CCD spectrograph with a collecting optical fibre.

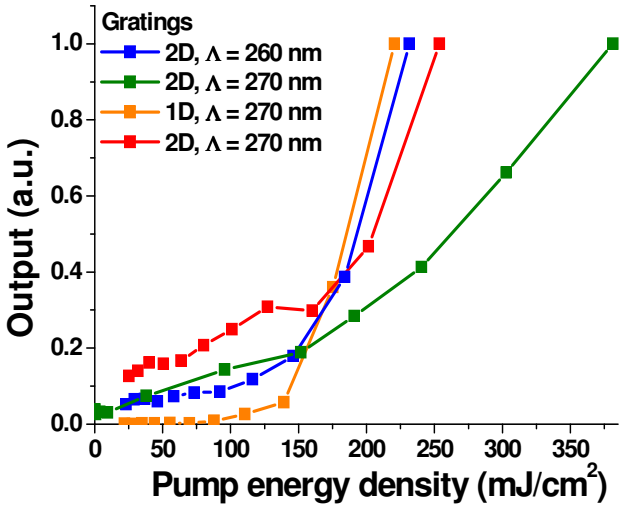

Figure 5.20 Optical output as a function of the pump energy density for a series of BP dendrimer DFB lasers under nanosecond excitation.

The lowest recorded threshold was 140 mJ/cm^2, a value much higher than the one-photon pumped threshold of 16 μJ/cm^2 using the same OPO source. To get a proper estimate of the difference between the two pumping schemes, it is important to consider the very low absorption of the two-photon pump beam in comparison to the very strong linear absorption. The fraction p of the light that is being absorbed by the film is given by

$$p = 1 - e^{-\alpha_2 z I} \qquad \textbf{5-XII}$$

where α_2 is the two-photon absorption coefficient for the film, z is the film thickness and I is the pump intensity. The absorbed lasing threshold intensity can therefore be calculated as

$$I_{thr}^{abs} = pI_{thr} \qquad \textbf{5-XIII}$$

Given a threshold pump intensity of 0.14 GW/cm^2, the absorbed intensity lasing threshold is 0.0875 GW/cm^2 or 350 μJ/cm^2. This value is approximately 22 times higher than the one-photon pumped results, a difference that can be attributed to the additional loss of excitations due to the presence of excited-state absorption.

The lasing output above threshold is expected to have a square dependence on the pump intensity as two pump photons are required for each emitted photon. A graph showing the laser output against the pump energy density in a double-log scale therefore it is expected to show data points following a straight line with a slope of two. Such a graph is shown in Figure 5.21 where the measured slopes of the lasing output are also noted.

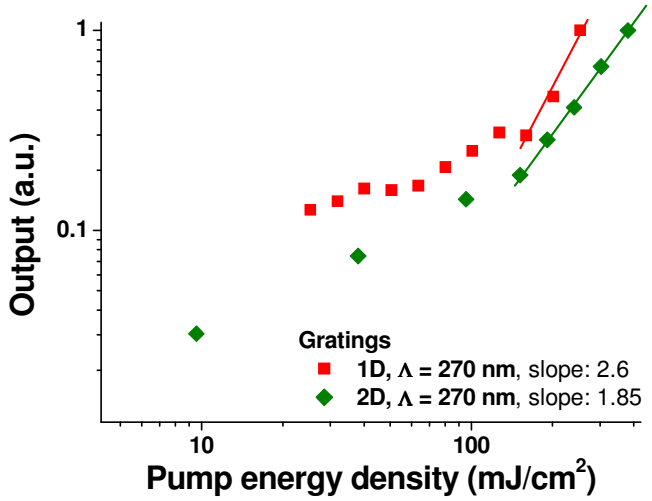

Figure 5.21 Pump energy dependence of the lasing output from two-photon pumped bisfluorene dendrimer DFB lasers under nanosecond excitation.

The observed slopes are close to the expected two-photon behaviour. It must be noted though that other lasers showed much higher slope values of up to 5, for which there is no clear explanation.

To further study the two-photon lasing behaviour observed, different pump wavelengths were used to verify the position and origin of the two-photon pumped lasing. This was to make sure that these results were not the result of some additional excitation such as any residue of the 355 nm laser light from the Nd:YAG laser that pumps the OPO used as the source in these experiments, or even some wavelength produced somewhere in the setup due to the high intensities. Figure 5.22 shows a comparison of the lasing spectrum from a bisfluorene DFB laser when pumped at the one-photon absorption wavelength as well as a few pumping wavelengths along the two-photon photoluminescence excitation peak. This figure demonstrates that the lasing wavelength does not

change for different excitation wavelengths, further proving that the observed phenomenon is indeed lasing from the material.

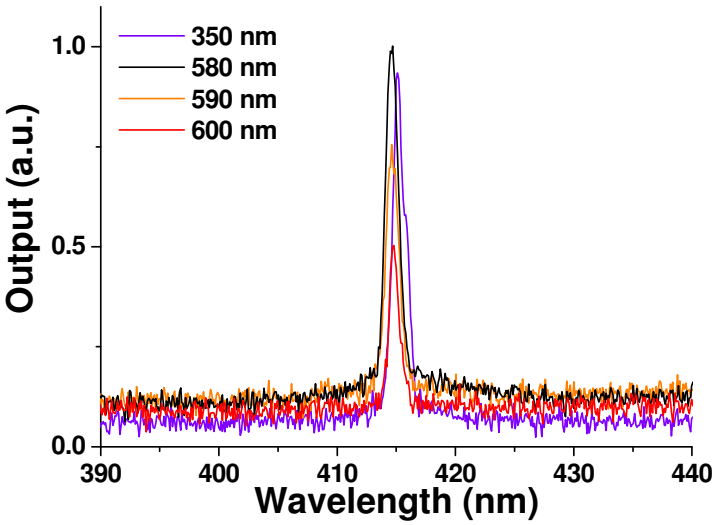

Figure 5.22 Lasing spectrum of a bisfluorene-cored dendrimer DFB laser under nanosecond excitation at different wavelengths.

A lasing spectrum was also taken using a lower resolution grating in the spectrograph to verify that there were no additional ultraviolet wavelength coming from the pump source when the dendrimer laser was pumped with longer wavelengths; indeed there were no evidence for this, as seen in Figure 5.23, verifying that the lasing was indeed the result of two-photon excitation.

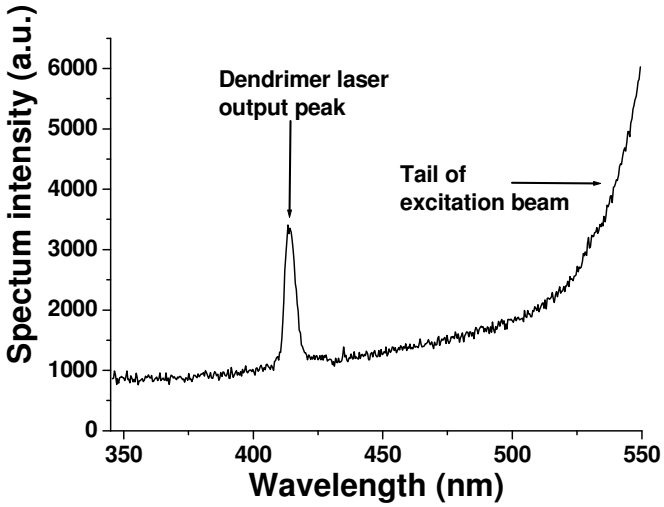

Figure 5.23 Lasing spectrum for a two-photon pumped dendrimer DFB laser acquired using a low resolution spectrograph grating, showing that there is no evidence of ultraviolet pump wavelengths. The rising slope of the graph at the longer wavelengths is the tail of the nanosecond excitation beam at 590 nm.

The lasing emission was tunable by using different DFB grating across 10 nm, as seen in Figure 5.24. This tuning range is exactly the same as for the one-photon excited lasing experiments reported earlier in this chapter, showing that the two-photon excitation of the lasers does not introduce additional limitations in the lasing performance of the material.

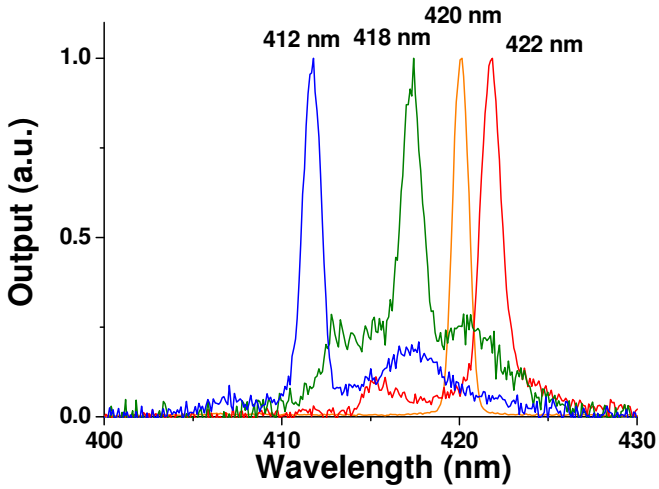

Figure 5.24 Tuning spectrum of nanosecond two-photon pumped bisfluorene dendrimer lasers.

The lasing threshold experiments were repeated using a femtosecond pulse pump source to investigate the impact of excited-state absorption. The resulting lasing threshold was much lower than that achieved under nanosecond excitation as seen in Figure 5.25.

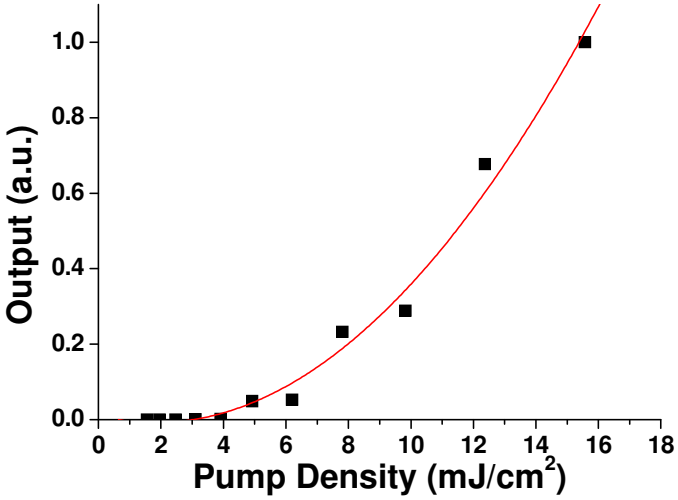

Figure 5.25 Optical output as a function of the pump power density for a bisfluorene two-photon pumped laser under femtosecond excitation. The solid line corresponds to a second-order polynomial fit.

The energy dependence of the lasing output above threshold can be seen in Figure 5.26.

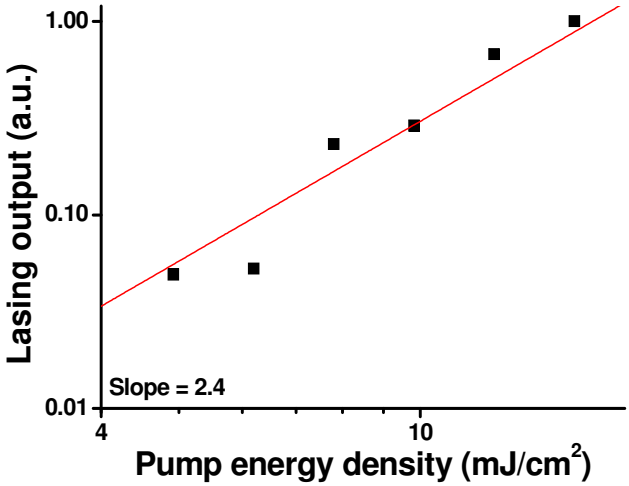

Figure 5.26 Pump energy density dependence of a femtosecond two-photon pumped bisfluorene dendrimer laser plotted on a double-log scale. The solid line corresponds to a linear fit with a slope value of 2.4 ± 0.3

The observed energy dependence matches very well with the theoretical predictions for a two-photon pumped laser. This indicates that any additional loss mechanisms such as excited state absorption have only a small effect on the lasing performance of the material. The femtosecond lasing threshold was measured to be 4.9 mJ/cm^2, whereas the absorbed energy density lasing threshold can be calculated to be 5.2 μJ/cm^2. This compares favourably with the one-photon lasing threshold of 4.5 μJ/cm^2, providing further evidence that, for femtosecond excitation pulses, the additional losses associated with two-photon absorption such as excited-stated absorption are very small. This is only the second published demonstration of solid-state two-photon pumped lasing in organic semiconductors and the only one where lasing is achieved in the deep blue and for both nanosecond and femtosecond excitation. The other published example is based on the ladder-type polymer MeLPPP, but the emission from that laser lies in the green part of the spectrum (498 nm) and lasing was only achieved with femtosecond pulses.[30]

5.8. Summary

A new family of dendrimers was studied in this section with the aim of making one- and two-photon pumped lasers. The dendrimers consisted of a common bisfluorene core and three different types of dendrons attached to them. A complete set of photophysical measurements was performed to characterise the materials' absorption and fluorescence properties as well as to evaluate their potential as laser gain media. Key parameters such as optical gain, waveguide losses and amplified spontaneous emission threshold in thin films were measured and compared across the different dendrimers to select the best candidate for lasing, a bisfluorene dendrimer with biphenyl dendrons that was used to make a tunable blue solid-state laser with lasing performance close to that of polyfluorene, a benchmark material for organic semiconductor lasers.

The same family of materials was then investigated as to their two-photon absorption and subsequent emission properties, as branched organic materials can display large nonlinear absorption cross-sections. The two-photon induced fluorescence was mapped and the absorption coefficients and cross-sections were calculated under both nanosecond and femtosecond excitation, allowing for an estimate of the additional losses present in a nonlinear excitation scheme such as excited-state absorption. The dendrimer with biphenyl dendrons combined excellent one-photon lasing properties with good two-photon absorption behaviour and was therefore selected to make a tunable blue two-photon pumped solid-state DFB laser pumped at 590 nm with both nanosecond and femtosecond pulses. The nanosecond lasing threshold was much higher than the femtosecond threshold, giving an insight to the effects that long pump pulses can have on the performance of a two-photon pumped organic laser. The femtosecond pumped lasing threshold of this laser is comparable to the one-photon pumped threshold once the reduced pump light absorption is taken into consideration, showing that there are very few additional losses that affect lasing. This is one of the very few examples of two-photon pumped lasing in organic semiconductors and the first ever to be reported on dendrimers, highlighting the unique flexibility of organic materials for laser applications.

5.9. References

[1] A. W. Siegman, *Lasers*, University Science Books, Sausalito, California **1986**.

[2] O. Svelto, *Principles of Lasers*, Plenum Press, New York **1982**.

[3] J. F. Holzrichter, A. L. Schawlow, *Ann N Y Acad Sci* **1969**, *168*, 703.

[4] I. D. W. Samuel, G. A. Turnbull, *Materials Today* **2004**, *7*, 28.

[5] A. J. Cadby, P. A. Lane, H. Mellor, S. J. Martin, M. Grell, C. Giebeler, D. D. C. Bradley, M. Wohlgenannt, C. An, Z. V. Vardeny, *Physical Review B* **2000**, *62*, 15604.

[6] M. Leclerc, *J. Polym. Sci. Pol. Chem.* **2001**, *39*, 2867.

[7] J. H. Burroughes, D. D. C. Bradley, A. R. Brown, R. N. Marks, K. Mackay, R. H. Friend, P. L. Burns, A. B. Holmes, *Nature* **1990**, *347*, 539.

[8] H. N. Cho, J. K. Kim, D. Y. Kim, C. Y. Kim, N. W. Song, D. Kim, *Macromolecules* **1999**, *32*, 1476.

[9] A. Donat-Bouillud, I. Levesque, Y. Tao, M. D'Iorio, S. Beaupre, P. Blondin, M. Ranger, J. Bouchard, M. Leclerc, *Chemistry of Materials* **2000**, *12*, 1931.

[10] U. Scherf, S. Riechel, U. Lemmer, R. F. Mahrt, *Current Opinion in Solid State & Materials Science* **2001**, *5*, 143.

[11] R. Gupta, M. Stevenson, A. J. Heeger, *Journal of Applied Physics* **2002**, *92*, 4874.

[12] C. Karnutsch, C. Gyrtner, V. Haug, U. Lemmer, T. Farrell, B. S. Nehls, U. Scherf, J. Wang, T. Weimann, G. Heliotis, C. Pflumm, J. C. deMello, D. D. C. Bradley, *Applied Physics Letters* **2006**, *89*.

[13] C. Rothe, F. Galbrecht, U. Scherf, A. Monkman, *Advanced Materials* **2006**, *18*, 2137.

[14] X. Liu, C. Py, Y. Tao, Y. Li, J. Ding, M. Day, *Applied Physics Letters* **2004**, *84*, 2727.

[15] M. Theander, T. Granlund, D. M. Johanson, A. Ruseckas, V. Sundstrom, M. R. Andersson, O. Inganas, *Advanced Materials* **2001**, *13*, 323.

[16] P. L. Burn, S. C. Lo, I. D. W. Samuel, *Advanced Materials* **2007**, *19*, 1675.

[17] S. C. Lo, N. A. H. Male, J. P. J. Markham, S. W. Magennis, P. L. Burn, O. V. Salata, I. D. W. Samuel, *Advanced Materials* **2002**, *14*, 975.

[18] J. R. Lawrence, G. A. Turnbull, I. D. W. Samuel, G. J. Richards, P. L. Burn, *Optics Letters* **2004**, *29*, 869.

[19] J. R. Lawrence, E. B. Namdas, G. J. Richards, P. L. Burn, I. D. W. Samuel, *Advanced Materials* **2007**, *19*, 3000.

[20] A. Otomo, S. Yokoyama, T. Nakahama, S. Mashiko, *Applied Physics Letters* **2000**, *77*, 3881.

[21] J. C. Ribierre, G. Tsiminis, S. Richardson, G. A. Turnbull, I. D. W. Samuel, *Applied Physics Letters* **2007**, *91*, 081108.

[22] M. D. McGehee, A. J. Heeger, *Advanced Materials* **2000**, *12*, 1655.

[23] S. Yokoyama, A. Otomo, S. Mashiko, *Applied Physics Letters* **2002**, *80*, 7.

[24] G. Heliotis, R. Xia, D. D. C. Bradley, G. A. Turnbull, I. D. W. Samuel, P. Andrew, W. L. Barnes, *Applied Physics Letters* **2003**, *83*, 2118.

[25] K. D. Belfield, S. Yao, M. V. Bondar, in *Photoresponsive Polymers I*, Vol. 213, Springer-Verlag Berlin, Berlin **2008**, 97.

[26] Y. Ren, Q. Fang, W. T. Yu, H. Lei, Y. P. Tian, M. H. Jiang, Q. C. Yang, T. C. W. Mak, *Journal of Materials Chemistry* **2000**, *10*, 2025.

[27] G. Y. Zhou, W. Dong, X. M. Wang, Z. S. Shao, M. H. Jiang, *Optics Communications* **2004**, *241*, 215.

[28] G. Y. Zhou, D. Wang, Y. Ren, Z. S. Shao, M. H. Jiang, *Applied Physics B-Lasers and Optics* **2004**, *79*, 341.

[29] M. Lal, S. Pakatchi, G. S. He, K. S. Kim, P. N. Prasad, *Chemistry of Materials* **1999**, *11*, 3012.

[30] C. Bauer, B. Schnabel, E. B. Kley, U. Scherf, H. Giessen, R. F. Mahrt, *Advanced Materials* **2002**, *14*, 673.

[31] O. Varnavski, X. Z. Yan, O. Mongin, M. Blanchard-Desce, T. Goodson, *Journal of Physical Chemistry C* **2007**, *111*, 149.

[32] O. Varnavski, A. Leanov, L. Liu, J. Takacs, T. Goodson, *Journal of Physical Chemistry B* **2000**, *104*, 179.

[33] M. Samoc, J. P. Morrall, G. T. Dalton, M. P. Cifuentes, M. G. Humphrey, *Angewandte Chemie-International Edition* **2007**, *46*, 731.

[34] M. Albota, D. Beljonne, J. L. Bredas, J. E. Ehrlich, J. Y. Fu, A. A. Heikal, S. E. Hess, T. Kogej, M. D. Levin, S. R. Marder, D. McCord-Maughon, J. W. Perry, H. Rockel, M. Rumi, C. Subramaniam, W. W. Webb, X. L. Wu, C. Xu, *Science* **1998**, *281*, 1653.

[35] R. Schroeder, B. Ullrich, W. Graupner, U. Scherf, *Journal of Physics-Condensed Matter* **2001**, *13*, L313.

[36] Y. Morel, A. Irimia, P. Najechalski, Y. Kervella, O. Stephan, P. L. Baldeck, C. Andraud, *Journal of Chemical Physics* **2001**, *114*, 5391.

6. Lasing in oligofluorene truxenes

In this chapter an oligofluorene truxene, T4, a member of a novel family of materials, is evaluated as a potential gain medium for organic semiconductor lasers. The key photophysical properties of the material are investigated and a blue-emitting distributed feedback solid-state laser is fabricated that shows lasing performance that improves upon the results reported for polyfluorene, the benchmark blue-emitting organic semiconductor gain medium.

The author performed all the photophysical measurements, the ellipsometry and the lasing experiments described in this chapter. Contributions were made by two members of the Organic Semiconductor Optoelectronics group. Yue Wang performed the amplified spontaneous emission measurements and Paul Shaw assisted with the modelling of the ellipsometry data for thin waveguides made from the truxene material.

6.1. Introduction

The search for new light-emitting organic semiconductors continues to explore the different pathways that synthetic chemistry opens up with materials design. The key properties of well-known molecules are fine-tuned to achieve the best possible results while studies of the properties of these materials allow for better understanding of what works best when designing future organic semiconductors.[1]

Fluorene-based materials are a great example of such progress in synthesis and optimisation of organic semiconductors.[2, 3] The interesting properties of polyfluorene, the first in this family of materials, such as highly-efficient light emission, high optical gain, low waveguide losses and good film quality when spun from solution have been the basis of some very interesting materials used in a variety of optoelectronics applications.[4] Materials such as F8BT, F8DP (see Chapter 4 for chemical structures), bisfluorene-cored dendrimers (see Chapter 5) and even a different phase of polyfluorene in thin films called beta

phase have shown that the basic polyfluorene structure can be adapted to optimise results in OLEDs, organic solar cells, optical amplifiers and organic lasers.[1, 5-8]

One of the great challenges in organic semiconductor synthesis is achieving a high level of control over the properties of the material synthesised, something that is more difficult when conjugated polymers are concerned. It is difficult to synthesise long chains consisting of the same number of repeat units and so each polymer chain is slightly different. This has the disadvantage of making purification of the material following initial synthesis relatively difficult. Furthermore, the statistical distribution of the number of conjugated sites along the disordered chains leads to inhomogeneous broadening of the absorption and emission spectra depending on the number of repetition units involved in each chain.[4, 9] Even though this can have certain advantages in separating the absorption and emission bands,[10] the lack of precise control over the properties of the molecules makes predicting and optimising their behaviour more difficult.

In this respect molecules made from a small and controlled number of repetition units, called oligomers, have become attractive as their exact composition and therefore photophysical and electrical properties of each molecule can be accurately determined at the synthesis stage. A number of publications explore both the synthesis and the photophysical characterisation of the different oligomers synthesised, yielding some interesting results in the area of fluorene-based oligomers in particular, such as the red-shift of the absorption and emission bands with increasing number of fluorene units,[9, 11] and the increasing photoluminescence quantum efficiency that larger oligofluorenes have,[12] owning to the larger distances between adjacent molecules. Different geometries are also possible when synthesising oligomers, ranging from short linear fluorene chains to more complicated architectures extending in all three dimensions.[11] One such family of materials, star-shaped oligofluorene truxenes, forms the basis of the work described in this chapter.

6.2. Star-shaped oligofluorene truxenes

The materials studied here are based around a hexahexyltruxene core (T0), an overlap of three fluorene unit as seen in Figure 6.1 and were synthesised in Strathclyde University by Prof Peter Skabara's group. Details about the synthesis of these molecules can be found in reference [12].

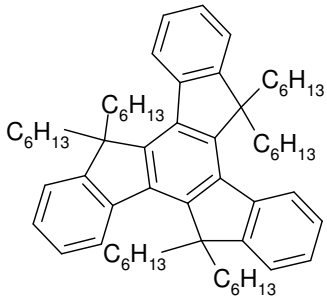

Figure 6.1 The hexahexyltruxene core (T0) that form the basis of the truxene-fluorene oligomers family.

Onto this core, arms consisting of bisfluorene units are attached with varying lengths leading to a family of truxene-fluorene oligomers, starting with the bare core (T0) and adding one (T1), two (T2), three (T3) and four (T4) bisfluorene units (Figure 6.2).

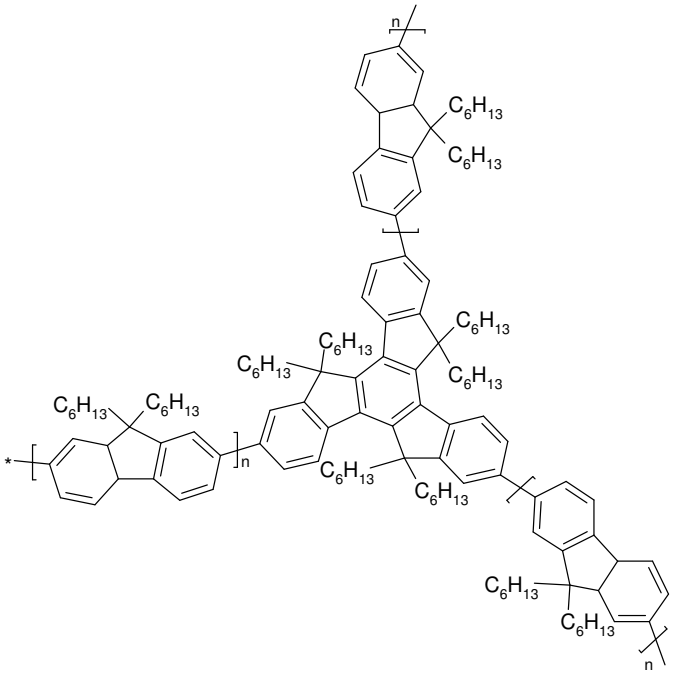

Figure 6.2 Chemical structure of the different oligofluorene truxenes Tn, where n is the number of fluorene units on each arm.

These molecules are large in dimensions, with radii starting from 1.5 nm for T1 and moving to 2.3 nm for T2, 3.1 nm for T3 and 3.9 nm for T4, making T4 one of the largest known star-shaped conjugated systems, though recently even larger systems have been demonstrated.[13]

A collection of data on some key photophysical measurements has been previously published, showing that the photoluminescence quantum yield of the truxene molecules increases as the number of fluorene units in each arm is increased, a change that is accompanied by a red-shift in the absorption and emission spectra.[12] An overview of the absorption (dashed lines) and fluorescence (solid lines) spectra for these truxenes can be seen in Figure 6.3 below:

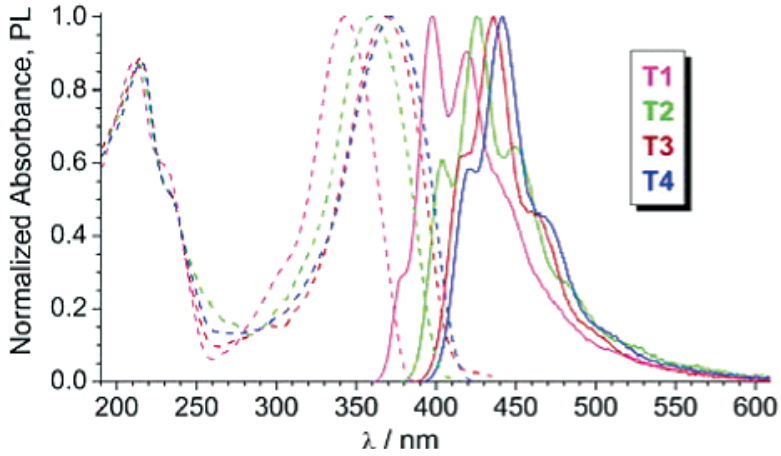

Figure 6.3 Absorption (dashed lines) and fluorescence (solid lines) spectra for the various members of the oligofluorene truxenes family (graph taken from [12]).

In this thesis only the T4 oligofluorene truxene is studied, as this molecule has been previously shown to have a high photoluminescence quantum yield, combined with deep blue emission, as shown in **Table 6.a**.

Material	PL max (nm)	PLQY (%)
T1	373	43
T2	394	51
T3	404	60
T4	408	59

Table 6.a Peak emission wavelength and PLQY values for thin films of truxene materials (taken from [12]).

6.3. Photophysical measurements

The absorption and emission spectra of the T4 truxene can be seen in Figure 6.4 for a thin film (98 nm) on a quartz substrate.

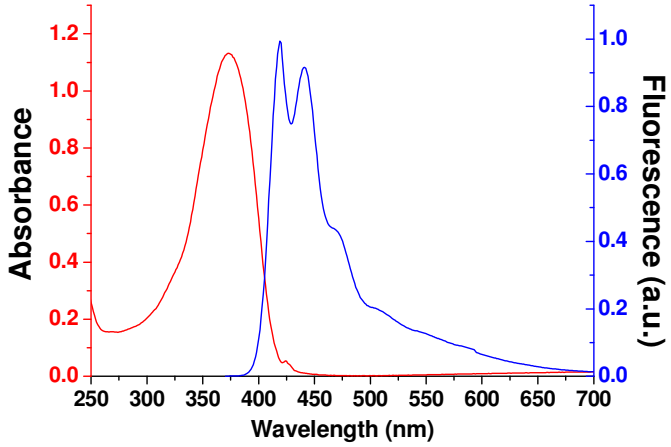

Figure 6.4 Absorption and fluorescence spectra of T4 truxene for a 98 nm thick film.

The absorption peak of T4 is at 373 nm, while the main emission features are found at 419 nm (0-0 transition), 441 nm (0-1 transition), 468 nm (0-2 transition) and 502 nm (0-3 transition). The changes in the relative intensity of the peaks in comparison to the literature spectrum of the emission are due to thin-film effects.

It is interesting to compare this against the absorption and emission of standard polyfluorene that consists of the same repetition units but with a statistically distributed number of units per polymer chain. The corresponding absorption and emission spectra for a polyfluorene film of comparable thickness can be seen in Figure 6.5.

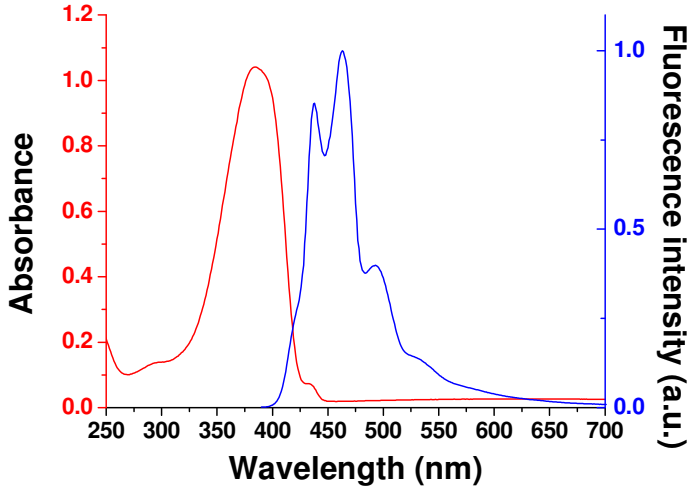

Figure 6.5 Absorption and fluorescence spectra of a polyfluorene film (film thickness 96 nm).

Even though the main features in the above spectra are similar, the wavelengths at which the different features appear are longer than for T4. The absorption maximum of polyfluorene is at 385 nm, 12 nm red-shifted in comparison to the T4 molecule, while the emission peaks are further red-shifted at 438 nm (0-0 transition), 463 nm (0-1 transition), 493 nm (0-2 transition) and 526 nm (0-3 transition). The red-shift for each peak is increasing for loner wavelengths, starting at 19 nm for the first peak and progressing to 22 nm for the second, 25 nm for the third and 28 nm for the final peak. These differences are the result of the longer number of fluorene units in the polymer chains that tend to further delocalise the π-electrons and thus lower the energy gap of the material.[9]
Photoluminescence quantum yield (PLQY) measurements were performed to evaluate the efficiency of light emission from the material. A number of thin films were spin-coated from a T4 truxene solution in toluene on quartz discs and were excited by a HeCd laser at 325 nm. The PLQY values recorded varied between 66 and 80% depending on the sample preparation and measurement errors (typically 10%), with an average value of 73% that matches the value measured for polyfluorene.

As the optical pumping power is increased, a narrowing of the emission spectrum occurs and amplified spontaneous emission can be observed coming

from the film as seen in Figure 6.6, where the fluorescence spectrum is overlaid with the ASE peak.

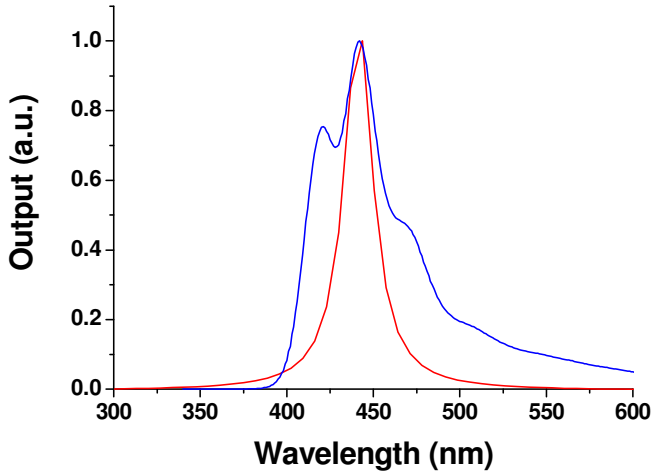

Figure 6.6 Fluorescence (blue line) and amplified spontaneous emission (red line) from a thin film of T4 oligofluorene truxene.

As is common in organic semiconductors, the ASE peak overlaps with the 0-1 energy transition of the material. This is a good indication of the wavelength region where lasing is expected in the material, with the lowest thresholds expected when lasing occurs at the peak wavelength of ASE.[14]

Optical gain and waveguide loss measurements were performed by Yue Wang by using the ASE variable stripe technique.[10] A comparison with polyfluorene can be seen in Table 6.b, where the polyfluorene data is taken from reference [15].

	Gain (cm^{-1})	Losses (cm^{-1})	ASE threshold ($\mu J/cm^2$)
T4 truxene	19	2.3	15
Polyfluorene	74	3.5	29

Table 6.b Optical gain, waveguide losses and ASE threshold comparison between the T4 oligofluorene truxene and polyfluorene.

The maximum optical gain available from T4 is lower than that of polyfluorene but the amplified spontaneous emission threshold is also lower as a consequence of the lower waveguide losses that the T4 films demonstrate.

6.4. Optical characterisation of films

Ellipsometry was used to determine the optical constants for T4 oligofluorene truxene films. Six samples were prepared on silicon wafer substrates by spin-coating from a toluene solution (25 mg/ml) at different speeds, resulting in different film thicknesses. By fitting the ellipsometry data across all samples, values for refractive index and extinction coefficients can be extracted across different wavelengths, as shown in Figure 6.7.

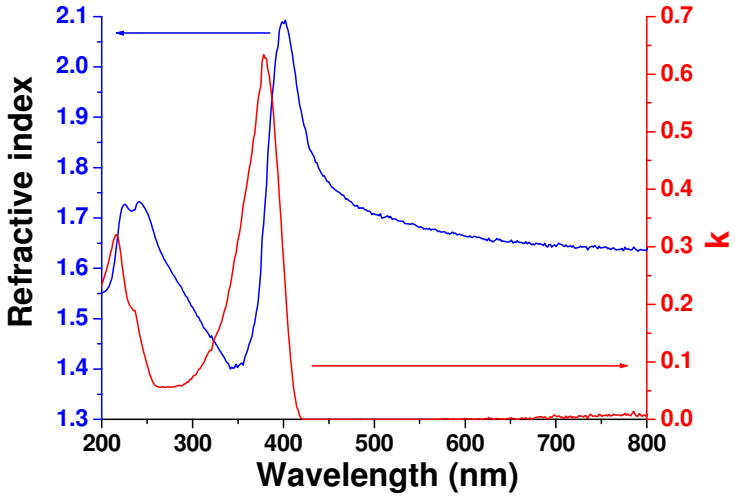

Figure 6.7 Refractive index and extinction coefficients of a thin film of T4 oligofluorene truxene as calculated through ellipsometry measurements.

These measurements are useful as they aid the design of distributed feedback lasers, where the wavelength for which optical feedback occurs is directly related to the effective refractive index of the waveguide by $m\,\lambda_{lasing}=2\,n_{eff}\Lambda$, as described in Section 2.4.2. During the fitting of the ellipsometry data used to extract the above parameters it emerged that T4 oligofluorene truxene films are isotropic, meaning that there is no clear preference in the orientation of the molecules in the film.[16] Most conjugated polymers have been found to be birefringent, owning to the fact that the long polymer chains assume specific orientations within the bulk of the film, usually lying in the plane of the film, meaning that differently polarised light experiences a slightly different environment depending on the direction in which it is travelling through the film.[17, 18] These results highlight how isotropically-orientated organic

molecules in a thin film lead to high quality waveguides that demonstrate low optical losses .[19]

6.5. Distributed feedback lasers

The T4 truxene was used to fabricate distributed-feedback lasers by spin-coating thin films on a corrugated silica substrate with a grating period of 280 nm. As the energy of the pump is increased, waveguided fluorescence from the material is scattered out of the surface of the film by the grating structure, leading to the appearance of Bragg-scattered peaks at wavelengths defined by

$$\lambda_{Bragg} = 2n_{eff}\Lambda / m \qquad \textbf{6-I}$$

where n_{eff} is the effective refractive index of the waveguide at that wavelength, Λ is the period of the grating and m is the order of diffraction (2 for surface-emitting DFB lasers like the ones fabricated here). When the pump energy is further increased, the lasing peak emerges between the two Bragg-peaks as seen in Figure 6.8 and proceeds to dominate the emission from the laser at higher pump intensities.

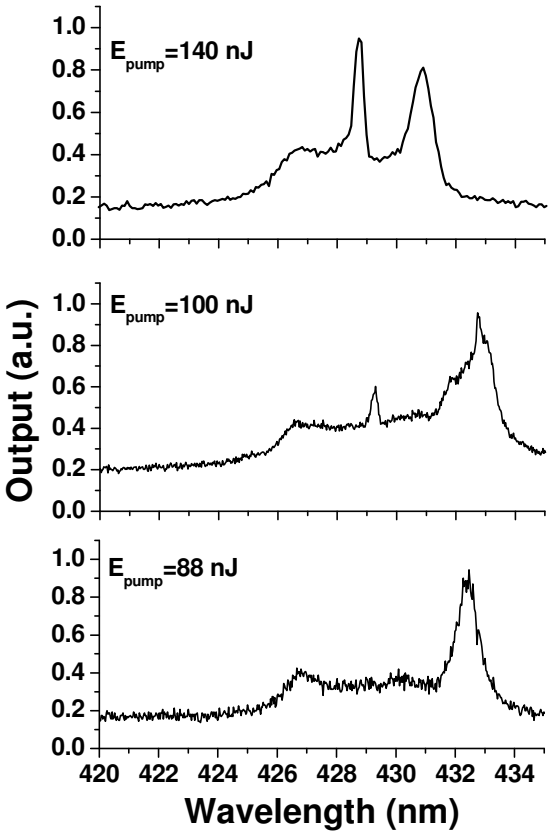

Figure 6.8 Evolution of emission spectrum from a T4 oligofluorene truxene DFB laser near lasing threshold. The pump energy increases from the bottom up in these graphs from 88 nJ to 100 nj for the middle figure and up to 140 nJ for the top graph.

The output intensity of the light emitted by these structures also changes once lasing threshold is achieved, as lasing causes the output to increase at a faster pace than normal fluorescence.[20] This results in the characteristic "kink" in the input-output curve of organic semiconductor lasers, as seen in Figure 6.9.

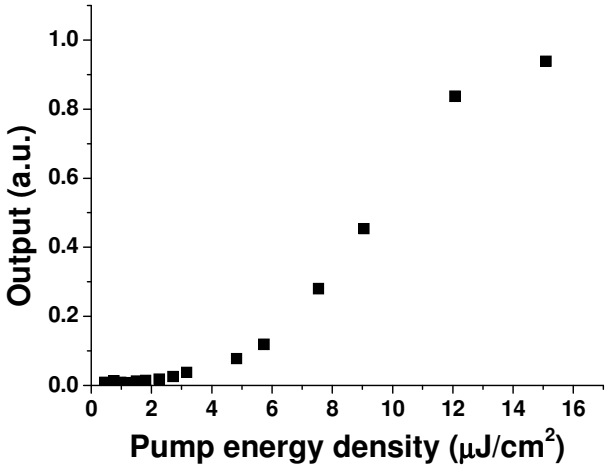

Figure 6.9 Input-output curve for a T4 oligofluorene truxene distributed feedback laser emitting at 435 nm.

The lowest recorded threshold was 5.7 μJ/cm^2 for lasing at 435 nm, which is somewhat higher than the value of 4 μJ/cm^2 reported for polyfluorene. [14] This can be explained if we consider that the lasing emission for T4 at 435 nm is offset from the peak of the ASE at 442 nm, leading to higher lasing thresholds. This can be seen in where the lasing wavelength at 430 nm is offset by more than 10 nm from the ASE peak where a lot of the light is still being emitted.

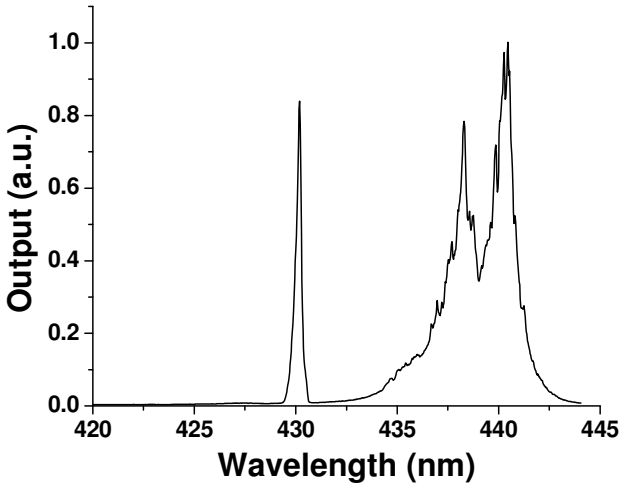

Figure 6.10 Lasing peak (430 nm) at a wavelength much shorter than the ASE emission (440 nm). Note that the splitting of the ASE peak is due to Bragg-scattering from the DFB grating.

The emission pattern of this Bragg-scattered ASE is clearly visible as a set of two arcs emitted vertically from the surface of the grating when excited with a

UV laser, as seen in Figure 6.11. Note that the emitted arcs of light diverge much more than what is typically expected from a DFB laser due to the range of wavelengths included within them and the lack of spatial coherence.

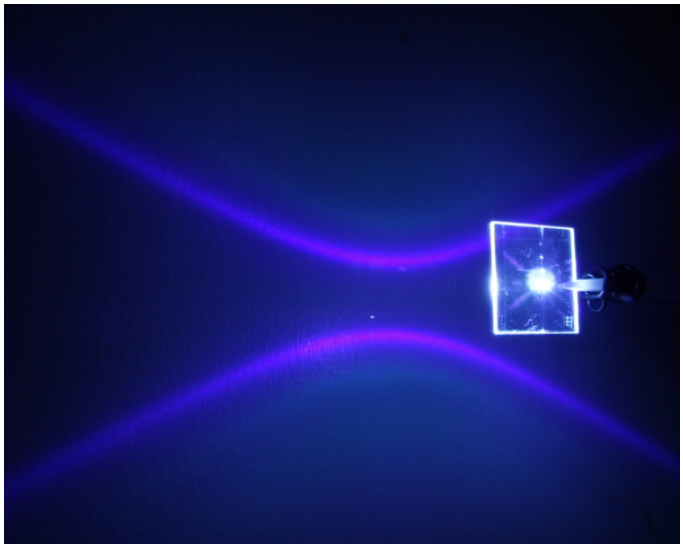

Figure 6.11 Bragg-scattered amplified spontaneous emission from a film of T4 oligofluorene truxene on a one-dimensional corrugated silica substrate.

Changing the film thickness between 145 to 190 nm by altering the spin speed allows for a range of lasing wavelengths from the same material, as seen in Figure 6.4.

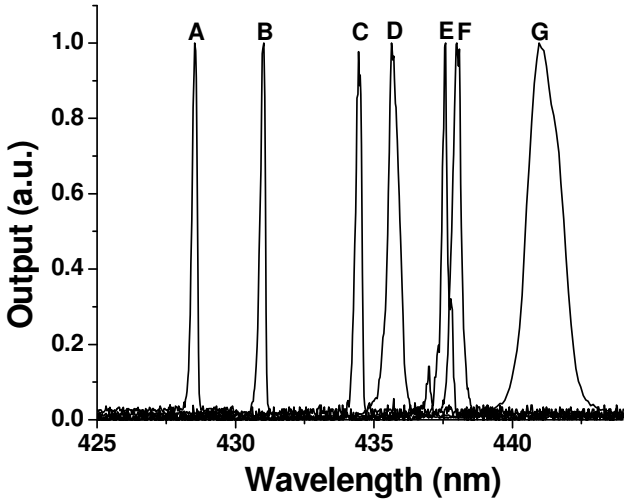

Figure 6.12 Emission wavelengths from T4 truxene DFB lasers (A: 428.5 nm, B: 431 nm, C: 434.5 nm, D: 435.6 nm, E: 437.6 nm, F: 438 nm, G: 441 nm). Curve G was collected using a different spectrograph at a lower resolution than the rest of the peaks.

Recent experiments performed by Yue Wang on the same material using slightly longer-period gratings (301 nm) have shown that the lowest lasing threshold in T4 was 2.7 μJ/cm^2 (270 W/cm^2) for lasing at 446 nm, one of the lowest lasing thresholds reported in organic lasers.[21] The tuning range was also expanded to 453 nm, giving a total tuning range for T4 DFB lasers of 25 nm. A careful optimisation of the structures and the fabrication of the laser devices should aim for an organic film that is as thin as possible to only support one lasing mode that would take up all the available gain and thus have the lowest lasing threshold combined with a grating period that is suitable for matching the Bragg-supported lasing wavelength to the peak of the ASE spectrum of the material.

6.5.1. Laser devices lifetime

The lifetime of organic semiconductor lasers is an important aspect of a materials' lasing performance, as photo oxidation can lead to degradation of the material and a drop in the laser output, a damaged that is irreversible. The T4 truxene is a new material with many similarities to polyfluorene, therefore it makes sense to compare its device lifetime to a similar device based on PFO.

Devices were fabricated by spin-coating from toluene solutions (30 mg/ml) onto a corrugated silica substrate with a grating period of 270 nm. The third harmonic (355 nm) of a Nd:YVO_4 laser with a pulse duration of 10 ns and a repetition rate of 1 kHz was used for optically pumping both the T4 and PFO-based DFB lasers and was focused using a cylindrical lens to a spot size of 1300 x 75 μm. The samples were placed inside a vacuum chamber (pressure 10^{-3} mbar) to slow down photodegradation. Note that these are not the ideal conditions for an absolute lifetime measurement as the vacuum is not very high, but the objective was to compare the two materials under identical conditions rather than optimise the lifetime of the devices.

The lasing spectra for the two lasers made can be seen in Figure 6.13. The T4 truxene output wavelength matches the ASE peak of the material very well,

while the polyfluorene laser emits at a shorter wavelength (ASE for polyfluorene is approximately 460 nm).

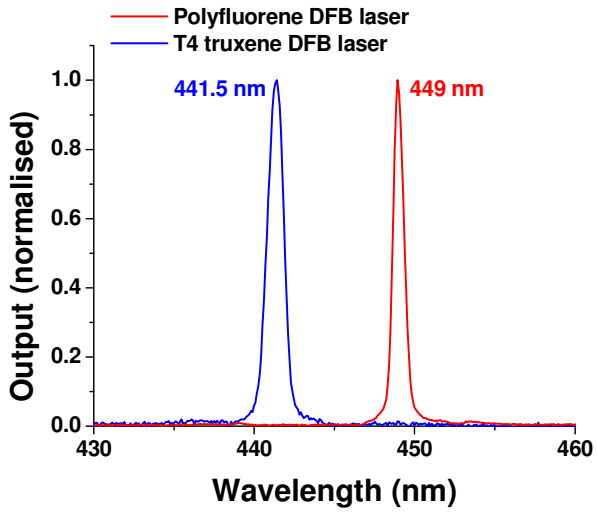

Figure 6.13 Output wavelength for two DFB lasers, one based on polyfluorene and the other on T4 truxene.

The energy-dependant output for both lasers can be seen in Figure 6.14 plotted against the pump energy. The threshold of these two lasers are very close, 158 nJ/pulse for the truxene laser and 199 nJ/pulse for the PFO laser.

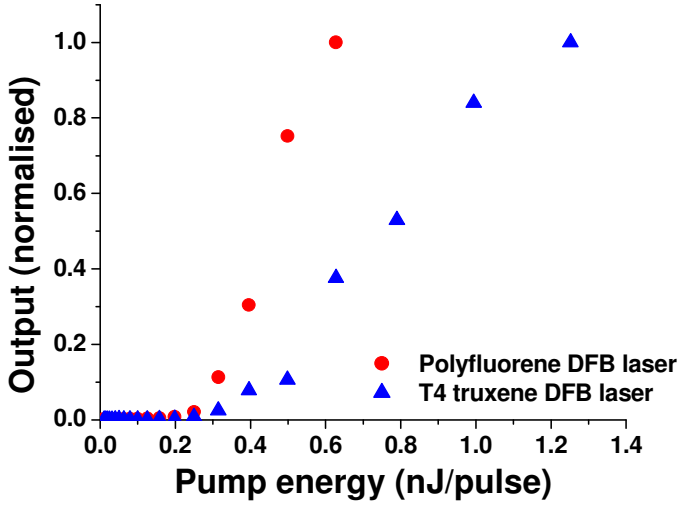

Figure 6.14 Optical output as a function of the pump pulse energy for a polyfluorene and a T4 truxene laser.

The two lasers were then pumped for an extended period of time at 2.5 times their respective thresholds and their optical output was measured at regular intervals to monitor the performance of the material. A comparison between the

two materials can be seen in Figure 6.15, where the lasing output is plotted against the number of pump pulses on a linear scale.

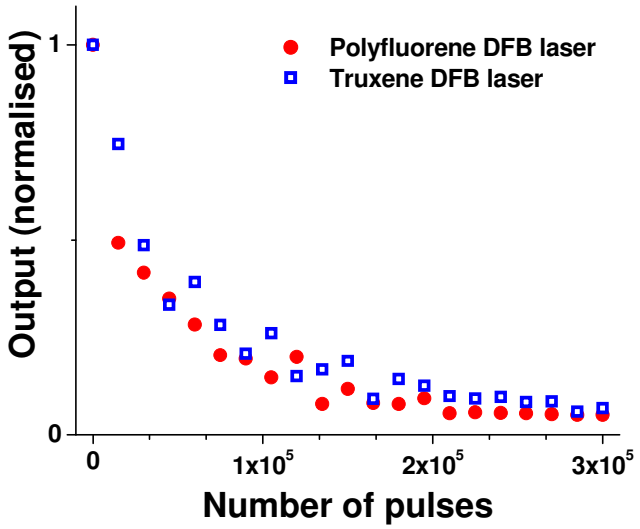

Figure 6.15 Output from two DFB lasers based on polyfluorene and T4 truxene as a function of the number of pump pulses. The initial intensity has been normalised for both lasers to account for the differences in collection efficiency and output power.

The difference becomes clearer if we compare the output of the laser when it is firstly pumped with that half way through the measurement after 150,000 pump pulses, as seen in Figure 6.16.

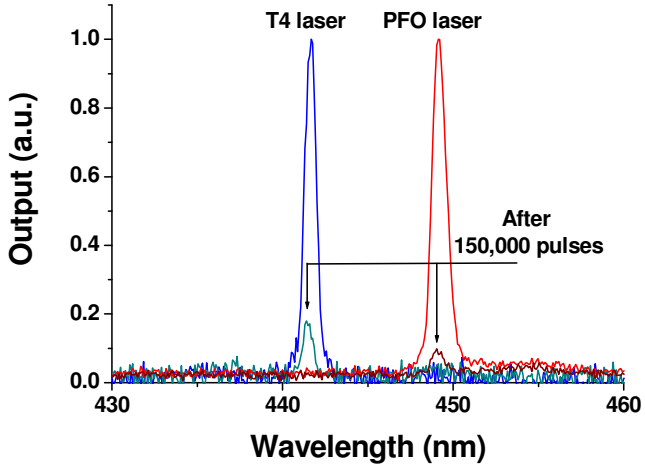

Figure 6.16 Evolution of lasing output from a polyfluorene and a T4 truxene DFB laser as a function of the number of pump pulses.

There is a small advantage for the T4 truxene laser, though perhaps the mismatch of the lasing wavelength to the peak of the ASE for polyfluorene could account for the slightly shorter lifetime of the device. It's safe to say then

that both materials have comparable performance under lasing conditions and that the T4 truxene studied here compares favourably against the well-established PFO in all crucial aspects for use as gain medium in solid-state lasers.

These measurements do not represent the best possible results for the lifetime of organic lasers and should only be used to compare the behaviour of two different materials under similar conditions. DFB lasers based on red-emitting polyfluorene derivatives have shown lifetimes of more than 2 million pulses under high vacuum [22], while similar protection can be achieved by encapsulation of the active layer by an inert medium. In a MEH-PPV DFB laser for example, the lifetime of the device when the polymer film was encapsulated using a commercially available epoxy was increased by a factor of 2,500x in comparison to a non-encapsulated device to reach more than 1.5 million pulses.[23]

6.6. Summary

The oligofluorene truxene family is of great interest for lasing applications as it combines the very desirable blue emission with a high level of molecular control and ease of chemical design. In this chapter the photophysical, optical and lasing properties of an oligofluorene truxene molecule have been studied in the interest of using this material as a gain medium for organic semiconductor lasers. [21]

The photophysical characterisation of the T4 oligofluorene truxene investigated here are in line with the good properties that most fluorene-based organic semiconductors have in common. The combination of reasonable optical gain with very low waveguide optical losses leads to a low threshold for the appearance of amplified spontaneous emission, a precursor of lasing. The lasing performance of this material improves upon the already excellent performance of standard polyfluorene, one of the benchmark blue-emitting organic semiconductors used in lasers, with lower lasing threshold and comparable tuning range, while the device lifetime under the same conditions is also similar.

These results demonstrate that the T4 truxene is an excellent lasing material and highlight the improvements possible on already successful organic semiconductors with the aid of synthetic chemistry and detailed understanding of the key properties that define an efficient organic semiconductor laser gain medium.

6.7. References

[1] I. D. W. Samuel, G. A. Turnbull, *Chem. Rev.* **2007**, *107*, 1272.

[2] A. J. Cadby, P. A. Lane, H. Mellor, S. J. Martin, M. Grell, C. Giebeler, D. D. C. Bradley, M. Wohlgenannt, C. An, Z. V. Vardeny, *Physical Review B* **2000**, *62*, 15604.

[3] M. Leclerc, *J. Polym. Sci. Pol. Chem.* **2001**, *39*, 2867.

[4] U. Scherf, E. J. W. List, *Advanced Materials* **2002**, *14*, 477.

[5] R. D. Xia, G. Heliotis, Y. B. Hou, D. D. C. Bradley, *Organic Electronics* **2003**, *4*, 165.

[6] H. Nakanotani, N. Matsumoto, H. Uchiuzou, M. Nishiyama, M. Yahiro, C. Adachi, *Optical Materials* **2007**, *30*, 630.

[7] J. C. Ribierre, G. Tsiminis, S. Richardson, G. A. Turnbull, I. D. W. Samuel, *Applied Physics Letters* **2007**, *91*.

[8] K. G. Jespersen, W. J. D. Beenken, Y. Zaushitsyn, A. Yartsev, M. Andersson, T. Pullerits, V. Sundstrom, *Journal of Chemical Physics* **2004**, *121*, 12613.

[9] D. Wasserberg, S. P. Dudek, S. C. J. Meskers, R. A. J. Janssen, *Chemical Physics Letters* **2005**, *411*, 273.

[10] M. D. McGehee, A. J. Heeger, *Advanced Materials* **2000**, *12*, 1655.

[11] X. H. Zhou, J. C. Yan, J. Pei, *Org. Lett.* **2003**, *5*, 3543.

[12] A. L. Kanibolotsky, R. Berridge, P. J. Skabara, I. F. Perepichka, D. D. C. Bradley, M. Koeberg, *Journal of the American Chemical Society* **2004**, *126*, 13695.

[13] W. Y. Lai, R. D. Xia, Q. Y. He, P. A. Levermore, W. Huang, D. D. C. Bradley, *Advanced Materials* **2009**, *21*, 355.

[14] G. Heliotis, R. D. Xia, G. A. Turnbull, P. Andrew, W. L. Barnes, I. D. W. Samuel, D. D. C. Bradley, *Advanced Functional Materials* **2004**, *14*, 91.

[15] G. Heliotis, D. D. C. Bradley, G. A. Turnbull, I. D. W. Samuel, *Applied Physics Letters* **2002**, *81*, 415.

[16] G. H. M. Campoy-Quiles, R. Xia, M. Ariu, M. Pintani, P. Etchegoin, D. D. C. Bradley,, *Advanced Functional Materials* **2005**, *15*, 925.

[17] D. Yokoyama, M. Moriwake, C. Adachi, *Journal of Applied Physics* **2008**, *103*, 13.

[18] J. M. Winfield, C. L. Donley, J. S. Kim, *Journal of Applied Physics* **2007**, *102*, 7.

[19] H. Azuma, T. Kobayashi, Y. Shim, N. Mamedov, H. Naito, *Organic Electronics* **2007**, *8*, 184.

[20] N. Tessler, *Advanced Materials* **1999**, *11*, 363.

[21] G. Tsiminis, Y. Wang, P. E. Shaw, A. L. Kanibolotsky, I. F. Perepichka, M. D. Dawson, P. J. Skabara, G. A. Turnbull, I. D. W. Samuel, *Applied Physics Letters* **2009**, *94*, 3.

[22] G. Heliotis, R. Xia, D. D. C. Bradley, G. A. Turnbull, I. D. W. Samuel, P. Andrew, W. L. Barnes, *Journal of Applied Physics* **2004**, *96*, 6959.

[23] S. Richardson, O. P. M. Gaudin, G. A. Turnbull, I. D. W. Samuel, *Applied Physics Letters* **2007**, *91*, 3.

7. A diode-pumped polymer laser

In this chapter a diode-pumped polymer laser is demonstrated, pumped by an inorganic GaN laser diode. The polymer used, MEH-PPV, has a low absorption at the emission wavelength of the dye, therefore it is blended with a Coumarin laser dye that absorbs most of the diode light and transfers the energy over to the polymer. This efficient host-guest blend is combined with a distributed Bragg reflector cavity that show low losses at the lasing wavelength and allows for the material to achieve population inversion when excited by the laser diode. This is the first example of an organic laser gain medium where a dye is used for light harvesting and one of the very few examples of a diode-pumped polymer laser.

The author has performed all the measurements relating to the characterisation of the gain medium and has contributed to the lasing measurements. The resonator design and fabrication, as well as the lasing experiments were performed by Andreas Vasdekis.

7.1. Introduction

One of the main challenges for organic semiconductor lasers is the miniaturisation of the pump source which will allow them to be easily implemented in practical laser systems and compete with their inorganic counterparts [1]. In time, it is quite possible that the pumping of organic lasers will be done electrically, as is already the case for inorganic semiconductor lasers; in the meantime though the objective is to improve on the optical pumping sources required.

The first organic lasers had to be pumped by large regenerative amplifiers, but the progress in materials and resonator research have allowed for a great downsizing of optical pump sources [2, 3]. The current compact all-solid-state pump sources for organic lasers are monolithic microchip lasers, a category of matchbox-sized devices based around neodymium crystals that are robust and

reasonably sized. These systems are wide-spread in laboratory environments and have significantly reduced the bulk of pump sources for organic lasers. [4, 5] A microchip laser is based around an infrared laser diode pumping a neodymium crystal (such as ND:YAG or ND:YVO_4) producing stimulated emission that lies in the infrared (1064 nm typically) [6, 7]. As organic semiconductors are visible emitters, additional components are required to produce suitable pump wavelengths in the visible or ultraviolet part of the spectrum. Frequency doubling, a nonlinear optical process, is used to produce green light at 532 nm and requires the presence of a suitable nonlinear crystal such as KTP or LBO, while frequency tripling produces ultraviolet light at 355 nm. The two nonlinear conversion steps make pumping red and blue emitting materials possible but at the cost of increased complexity and price and decreased overall efficiency of the laser.

Inorganic laser diodes emerge as a potential candidate to replace microchip lasers. They offer compact dimensions, excellent power efficiency and reasonable costs, while the ability to directly control their emission intensities through their current source allows for easy control of the whole laser system. So far though laser diodes operating at suitable wavelengths for providing energy to organic semiconductors have been lacking in output power, as the most efficient laser diodes are found in the near-infrared (NIR) and infrared (IR) parts of the spectrum, the emission regime of GaAs-based semiconductors and additional processes are involved in changing the emission wavelength, introducing further losses of optical power.

This changed with the emergence of GaN light-emitting diodes and laser diodes (Figure 7.1) emitting in the blue part of the visible spectrum [8-11]. Their development has been rapid and has already reached considerable maturity, as evident by the abundance of blue GaN diodes in consumer electronics such as Blue-ray players for home entertainment.

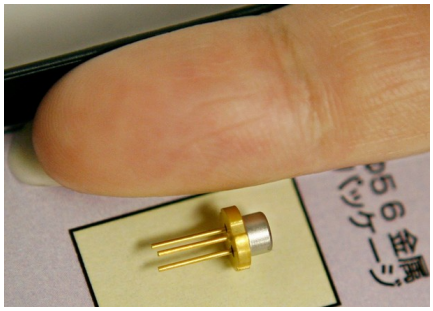

Figure 7.1 A GaN violet-emitting laser diode (AFP/Getty Images)

Blue laser emission from a solid-state device is quite attractive for a number of other applications such as optical spectroscopy, laser printing and projection displays to name but a few [12, 13]. The availability of high-power versions of these laser diodes also means that they could be of use for optically pumping organic semiconductor lasers offering a very compact optical pump source.

The low optical output of GaN laser diodes however remains a restricting factor in using them as pump sources for organic lasers, meaning that for such a pump scheme to be successful the diode should be combined with organic lasers demonstrating very low threshold powers as a result of careful resonator design and very efficient materials. Most work has revolved around fluorene-based materials whose absorption spectrum overlaps with the short emission wavelengths of InGaN laser diodes combined with distributed feedback (DFB) grating for optical feedback [14, 15]. In this thesis a different approach was chosen whereby a GaN laser diode (670 pJ maximum pulse energy, 1ns pulse duration) was combined with the red-emitting polymer poly(2-methoxy-5-(2'-ethyl-hexyloxy)-p-phenylenevinylene (MEH-PPV) as the gain medium and a distributed Bragg-reflector (DBR) cavity as the resonator structure. [16]

7.2. Gain medium

The absorption and emission spectrum of MEH-PPV can be seen in Figure 7.2 for a thin film (100nm) on a quartz disc.

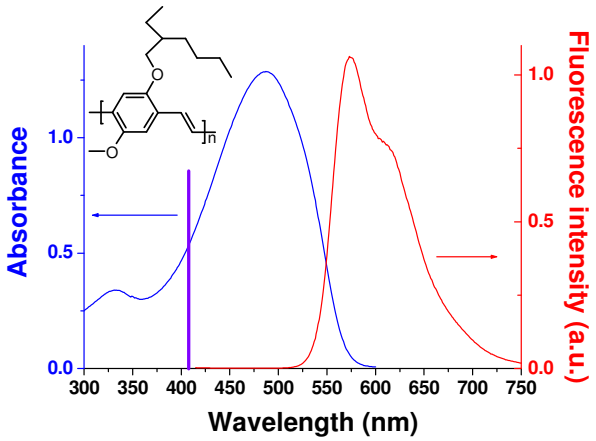

Figure 7.2 Absorption and emission spectrum of MEH-PPV (100 nm thin film). The violet line shows the emission wavelength from a GaN laser diode. The inset shows the chemical structure of the molecule.

The emission wavelength of the GaN laser diode used in these experiments is 409 nm, as that was the most powerful such diode available with pulse energy of 0.67 nJ, pulse duration of 1 ns and repetition rate 10kHz. The absorption of MEH-PPV however at 409 nm is very low, a fact that will lead to higher lasing thresholds under GaN excitation.

Similar problems where the material's absorption of the excitation light is not high enough can be dealt with by separating the roles of absorption and emission and assign them to different materials. One of the materials (donor) has a suitable absorption that allows for efficient harvesting of the laser diode light and that energy can then be transferred to the second material (acceptor) for subsequent emission. This process can be so efficient as to allow the acceptor material to reach population inversion. Examples of such donor-acceptor schemes have been demonstrated using laser dyes and polymer blends, showing an enhancement of the operational characteristics of organic lasers [17-20].

7.2.1. Förster energy transfer

One of the processes by which energy transfer is carried out with minimal losses (and applies for the materials and conditions found in polymers) is

known as Förster energy transfer, a dipolar non-radiative excitation transfer process [21]. It is the dominant energy transfer mechanism when the intermolecular distances within the material exceed the sum of the van der Waals radii [46]. A transfer rate constant $k_{D \to A}$ can be defined, given by

$$k_{D \to A} = \frac{K^2 \cdot J \cdot 8.8x10^{-28} mol}{n^4 \cdot \tau_0 \cdot r^6} \qquad \textbf{7-I}$$

where K is an orientation factor, n the refractive index of the medium, τ_0 the radiative lifetime of the donor, r the distance (cm) between donor (D) and acceptor (A), and J the spectral overlap (in coherent units $cm^6 mol^{-1}$) between the absorption spectrum of the acceptor and the fluorescence spectrum of the donor.

From the above equation, assuming that the intermolecular distances and the radiative lifetime of the donor are suitable for Förster energy transfer, the key factor is the overlap between the fluorescence and the absorption spectra of the donor and the acceptor respectively. This means that, in order for two materials to work well together, the photoluminescence spectrum of the donor material must overlap with the absorption spectrum of the acceptor, otherwise the energy transfer will not be efficient.

7.3. Photophysical measurements

Based on the above energy transfer process, suitable donor materials are required that combined both a strong absorption of the laser diode light and a large overlap of their emission spectrum with the absorption spectrum of MEH-PPV. To this end two laser dyes were chosen from the Coumarin family, namely Coumarin 153 and Coumarin 102 (Lambda Physik), the chemical structures of which can be seen in Figure 7.3 along with their absorption spectra and the laser diode emission.

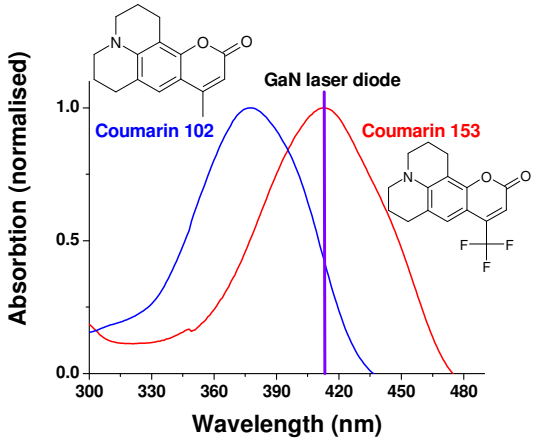

Figure 7.3 Absorption spectra of the two laser dyes (Coumarin 102 in blue, Coumarin 153 in red) used as energy donors, along with their chemical structures. Also visible is the emission of a GaN laser diode as 409 nm.

A problem with creating a blend of materials that perform different roles lies with trying to optimise all important aspects of the composite material at the same time. In the case of the donor-acceptor scheme discussed here, the amount of dye required to harvest a large part of the GaN pump light has to be balanced against the lasing performance of MEH-PPV. In addition, blends of organic materials have been known to phase-separate, leading to isolated areas within the film that contain mostly one kind of material rather than a uniform blend. The ratio between the dye and the polymer concentrations was therefore varied in order to achieve the best balance between energy transfer efficiency and optical gain. The dye concentration was varied between 2.5, 5 and 7.5 mg/ml while the concentration of the polymer remained fixed at 5 mg/ml, giving blends where the ratio of concentrations was 1:2, 1:1 and 2:1 respectively.

7.3.1. Absorption measurements

The first step was to verify that the dye was active within the blend and that energy transfer was taking place. Absorption measurements were performed on thin films spin-coated from the different blend solutions and the recorded spectra can be seen in Figure 7.4.

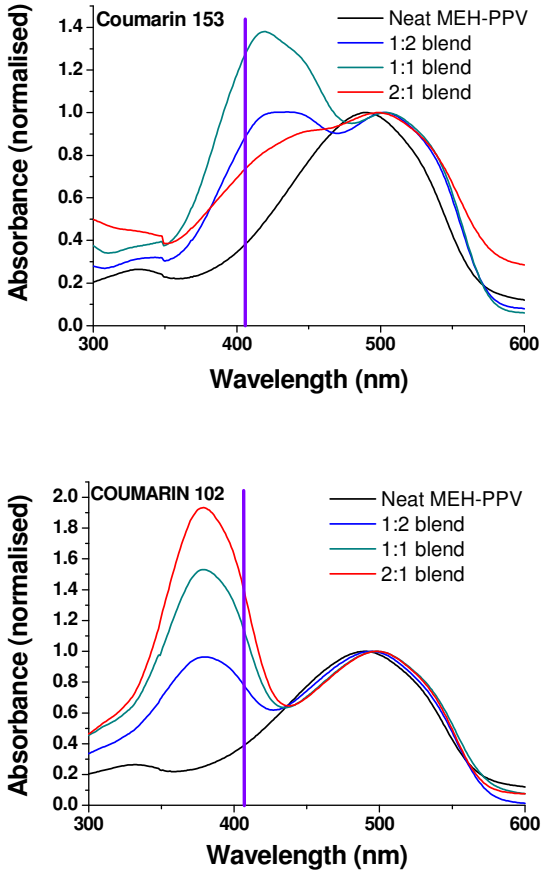

Figure 7.4 Absorption spectra for laser dye – polymer blends. The violet line corresponds to the GaN laser diode emission.

The effect of the dye in the blend in terms of absorption increase at 409 nm can be expressed as an enhancement factor, showing how many times the absorption of the blend at that wavelength has increased in comparison to a neat film of MEH-PPV as seen in Table 7.a.

	Enhancement factor	
	Coumarin 153	Coumarin 102
Neat MEH-PPV	1.0	1.0
1:2 blend	2.3	1.9
1:1 blend	3.3	2.7
2:1 blend	1.9	3.3

Table 7.a Enhancement of dye – polymer blend absorption at 409 nm for different blends tested.

From the above table it is clear that both types of dyes enhance the absorption of the polymer at the desired wavelength by up to 3.3 times, although that occurs for different blend ratios for each dye. In the case of Coumarin 153 it is interesting to notice that the enhancement factor for the blend with the highest dye concentration drops, indicating some problem in the energy transfer mechanism. This will be discussed in more detail later on in this chapter (section 7.3.4).

7.3.2. Photoluminescence measurements

The emission of the two laser dyes is plotted in Figure 7.5 along with the absorption spectrum of MEH-PPV. The large overlap between the dye emission and the polymer absorption contributes to efficient energy transfer.

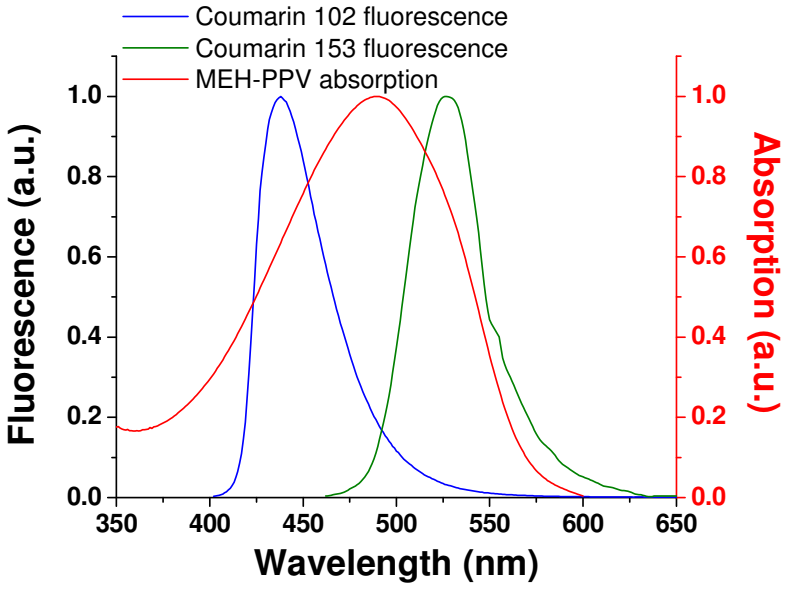

Figure 7.5 Fluorescence of the two Coumarin dyes used in this study (in solution), along with the absorption spectrum of MEH-PPV.

The dye – polymer blends under consideration should ideally exhibit as little of the dye emission as possible. If the dye is showing photoluminescence then part of the energy it absorbs at 409 nm is not transferred to the polymer, meaning that the overall donor – acceptor scheme is inefficient. The photoluminescence of the samples prepared can be seen in Figure 7.6 for excitation at 409 nm.

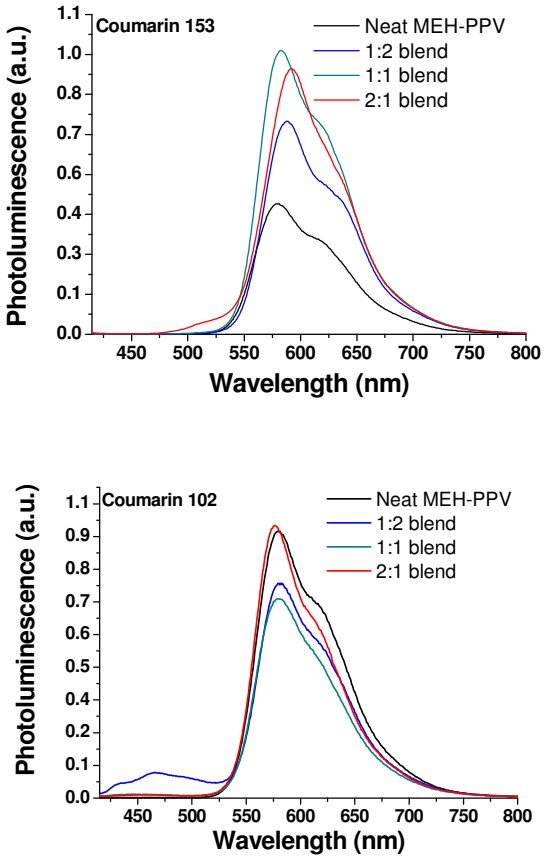

Figure 7.6 Steady-state photoluminescence spectra of dye–polymer blends excited at 409 nm.

There are very little traces of dye emission in most samples, indicating that the energy-transfer process is very efficient. The only exception is the 1:2 blend of Coumarin 102, but even in this case an amount of dye equal to 2/3rds of the polymer shows emission more than 10 times lower than the polymer.

7.3.3. Photoluminescence quantum yield measurements

The best way to evaluate the efficiency of the prepared blends is to examine what effect the dye has on the photoluminescence quantum yield (PLQY) value of MEH-PPV. When the polymer molecules are closely packed in a film some of the energy they absorb does not contribute to light emission but is instead lost due to intermolecular interactions. The addition of a laser dye could separate the molecules further apart than in the neat film and thus increase the

PLQY even when the blend is excited at a wavelength where only the polymer absorbs light.

Furthermore, in such concentrated dye films there is a possibility that the radiative and non-radiative decay processes compete with the energy transfer. As very little dye emission was observed under steady-state fluorescence measurements, it appears that energy transfer takes place. However, it is also possible that the non-radiative decay is stronger than the energy transfer, leading to very little dye emission combined with poor energy transfer to the polymer molecules. The PLQY measurements help in determining which of these two rates is faster by looking for changes in the light emission efficiency.

PLQY measurements were performed at two different wavelengths to verify these hypotheses. One excitation wavelength was 514 nm, on the long side of the polymer's absorption where neither laser dye absorbs any light, while measurements at 407 nm were also perform to investigate the behaviour of the blends when the dye molecules were excited. These measurements are summarised in Figure 7.7 for both laser dyes.

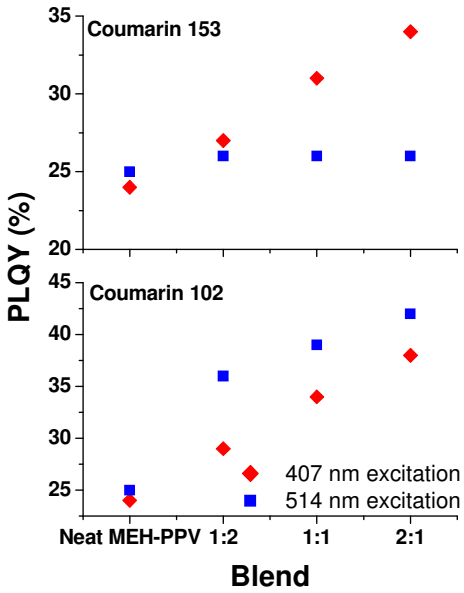

Figure 7.7 PLQY values for different dye – polymer blends at two different excitation wavelengths.

In the case of the 514 nm excitation, Coumarin 153 does not appear to have any significant effect on the performance of the material, while the addition of Coumarin 102 increases the PLQY of a neat MEH-PPV film from 24% to 42%, a factor of 1.7 times higher, indicating that the dye acts as an isolator for polymer chains in the film. When the excitation was at 407 nm, the addition of either dye increases the PLQY of the blend with Coumarin 102 showing a larger improvement than Coumarin 153 for equal concentrations. This means that both types of laser dye achieve some degree of energy transfer to MEH-PPV.

From these measurements it is possible to calculate the actual energy transfer efficiency. If *p* is the percentage of light absorbed by either polymer or laser dye (as denoted by the subscripts), then the PLQY of the blend for 407 nm excitation is a result of the contribution of the individual PLQY values of the dye and polymer molecules and can be written as

$$PLQY_{blend}^{407} = \frac{PL_{blend}}{p_{polymer} + p_{dye}} = \frac{p_{dye}^{407} \cdot PLQY_{dye} + p_{polymer}^{407} \cdot PLQY_{polymer}}{p_{polymer} + p_{dye}} \quad \textbf{7-II}$$

Since in these samples the dye molecules are dispersed in a polymer matrix and therefore do not display the usual photoluminescence quenching associated with neat laser dye films, the PLQY of the dye molecules in the system can be estimated to be the PLQY of the blend when exciting the polymer multiplied by the transfer efficiency, *n*

$$PLQY_{dye} = n \cdot PLQY_{polymer}^{514} = n \cdot PLQY_{blend}^{514} \quad \textbf{7-III}$$

where the PLQY values of the polymer and the blend are the same for 514 nm excitation as the dye molecules do not absorb at this wavelength.
Substituting in equation 7-II, the PLQY of the blend when excited at 407 nm becomes

$$PLQY_{blend}^{407} = \frac{n \cdot p_{dye}^{407} \cdot PLQY_{blend}^{514} + p_{polymer}^{407} \cdot PLQY_{blend}^{514}}{p_{polymer}^{407} + p_{dye}^{407}} =$$

7-IV

$$= PLQY_{blend}^{514} \cdot \frac{n \cdot p_{dye}^{407} + p_{polymer}^{407}}{p_{polymer}^{407} + p_{dye}^{407}} = PLQY_{blend}^{514} \cdot \frac{1 + n\frac{p_{dye}^{407}}{p_{polymer}^{407}}}{1 + \frac{p_{dye}^{407}}{p_{polymer}^{407}}} \Rightarrow$$

$$n = [\frac{PLQY_{blend}^{407}}{PLQY_{blend}^{514}} \cdot (1 + \frac{p_{dye}^{407}}{p_{polymer}^{407}}) - 1] \cdot \frac{p_{polymer}^{407}}{p_{dye}^{407}} \quad \textbf{7-V}$$

Substituting the corresponding values from the absorption and PLQY measurements for the various blends, we can extract the energy transfer efficiency of each blend, as shown in Table 7.b.

This approach works well for Coumarin 102 but it leads to invalid results for Coumarin 153. This is due to the fact that adding Coumarin 153 to MEH-PPV does not offer any improvement in the PLQY for 514 nm excitation, an indication that some aspect of the material's properties was not as expected. This could be due to phase-separation between the laser dye and the polymer, leading to isolated areas of Coumarin 153 that only exchange energy at the interface with the MEH-PPV domains rather than throughout the bulk of the blend, as is the assumption for the calculations presented above.

	Energy transfer efficiency	
	Coumarin 153	Coumarin 102
1:2 blend	1.08	0.55
1:1 blend	1.47	0.75
2:1 blend	1.64	0.82

Table 7.b Energy transfer efficiency of dye-polymer blends for excitation at 407 nm. Note the incorrect (larger than 1) values for Coumarin 153.

7.4. Film quality

As numerous films of both dye-polymer blends were made, it became apparent that the films containing Coumarin 153 were suffering from morphological degradation. Even though the films looked smooth and featureless when first made, within a few minutes there were visible changes in the uniformity of their surface. Some examples of this can be seen in Figure 7.8, where the surface of films made from the two laser dyes can be seen under an optical microscope (optical magnification of 5x).

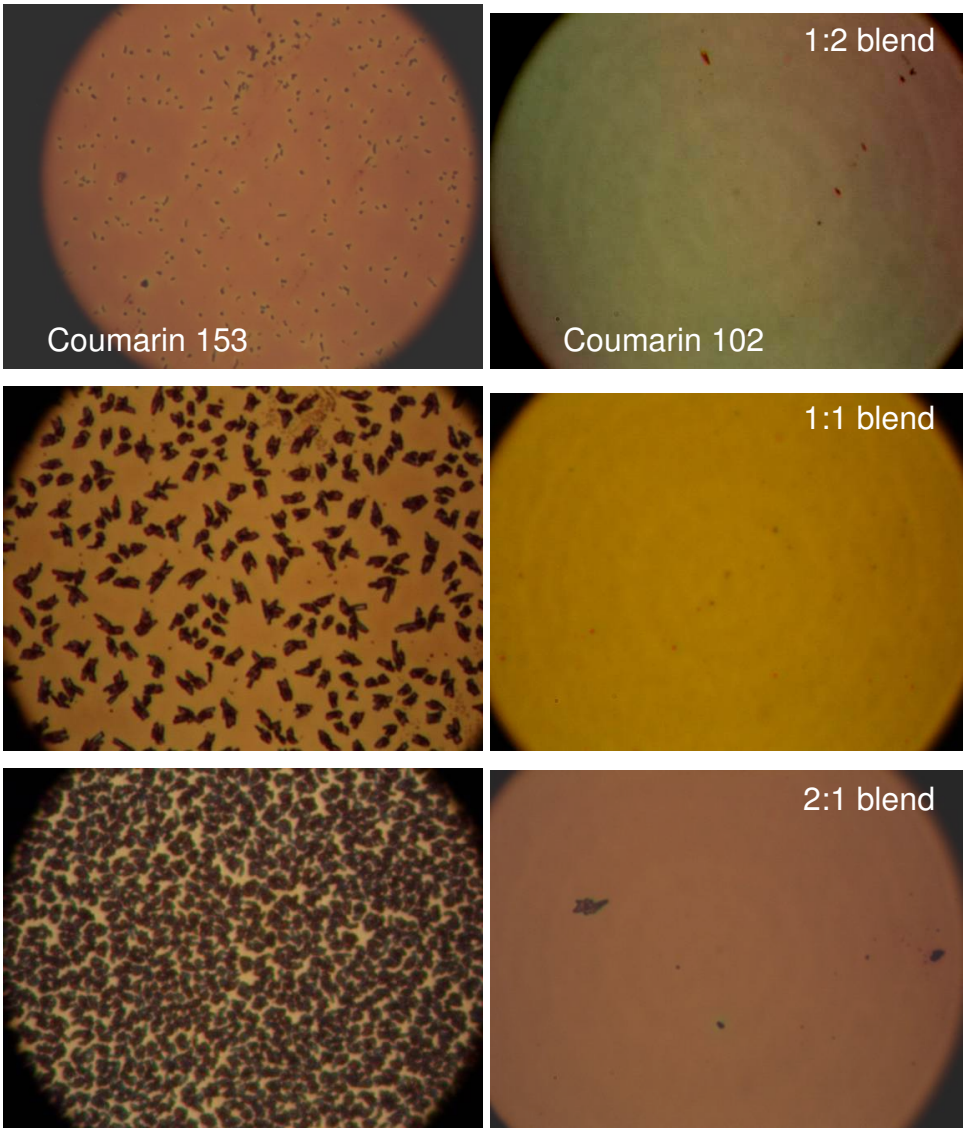

Figure 7.8 Images of the surface of films made from blends of laser dyes and MEH-PPV. On the left is Coumarin 153 blends, on the right Coumarin 102.

It is obvious from these photos that the samples made using Coumarin 153 display strong phase separation, whereby the two materials in the blend form

their own separate domains in the bulk of the film [22, 23]. This means that the two materials are less likely to interact, leading to significantly impaired energy transfer efficiency as the significant amount of pump light absorbed occurs in dye-rich clusters within the film that don't energy-transfer to MEH-PPV. This problem becomes more severe as the amount of laser dye added to the blend increases. In contrast, the samples made from the Coumarin 102 blends display no such problems as can be seen from the very homogenous image they presented under the optical microscope. Given that the only difference between the two dye molecules is the addition of a 3-F unit, it is likely that this group is responsible for the phase separation between Coumarin 153 and MEH-PPV and should probably be avoided in the future for similar blends. The choice was thus made to focus all further efforts on Coumarin 102 as the donor material from this point onwards.

7.5. Amplified spontaneous emission experiments

When MEH-PPV is excited at high intensities, amplified spontaneous emission (ASE) occurs as the light emitted by the material is preferentially amplified over a narrow range of wavelengths where the optical gain is stronger, leading to narrowing of the emission spectrum. [24]. The ASE spectrum of MEH-PPV has a peak at 630 nm and is shown in Figure 7.9, along with the emission spectrum for lower excitation power.

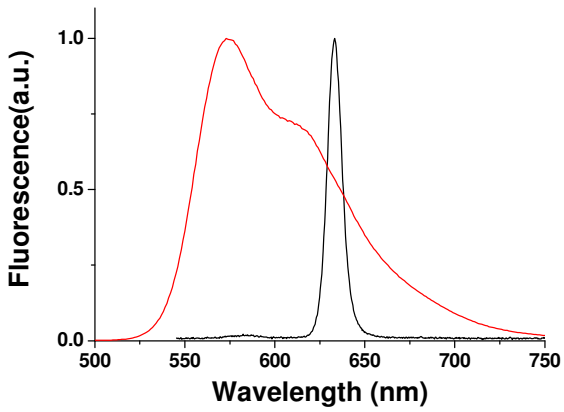

Figure 7.9 Amplified spontaneous emission and fluorescence (red line) spectra from a thin film of MEH-PPV.

ASE is a precursor to lasing and is therefore a good indication of the performance of a material as a laser gain medium regardless of resonator. Amplified spontaneous emission measurements were performed at two different pumping wavelengths, one at 410 near the emission wavelength of a GaN laser diode where the laser dye absorbs most of the light and one at 532 nm, where the absorption of the dye is minimal and the polymer absorbs the pump light directly. The results can be seen plotted in Figure 7.10, where the ASE threshold measured is plotted for the different dye-polymer blends for the two different pump wavelengths.

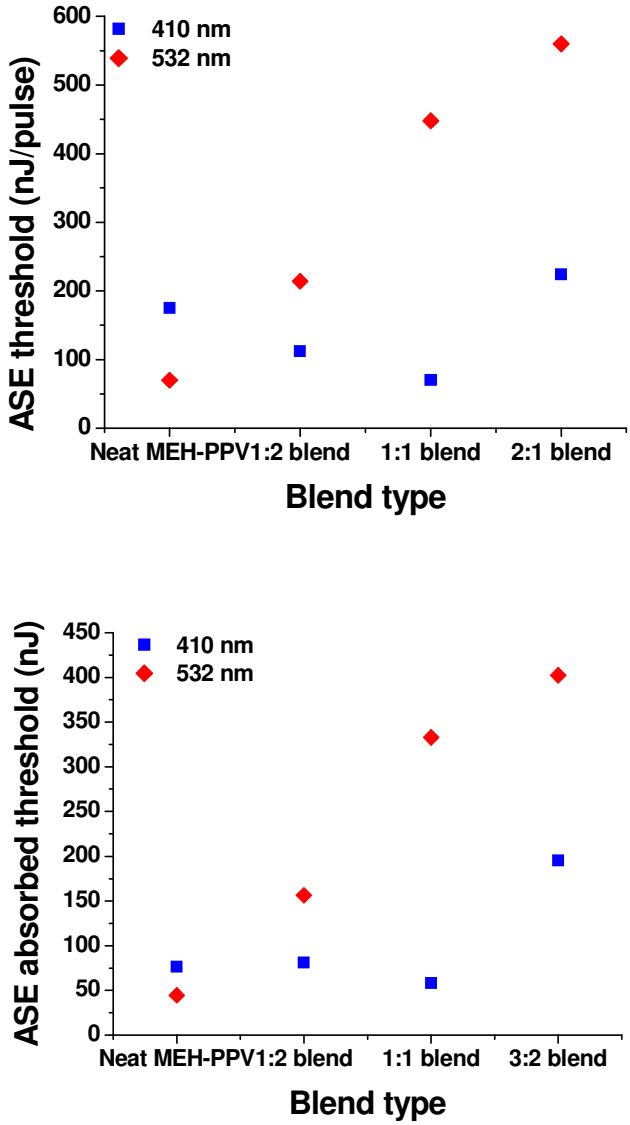

Figure 7.10 ASE thresholds (incident and absorbed energy) for different dye-polymer blends.

The first thing to notice in the above graph is the higher ASE threshold value for a neat MEH-PPV film at 410 nm than at 532 nm. This is because only a small part of the incident pump light at 410 nm is absorbed by the polymer, highlighting the need for a donor-acceptor scheme if the MEH-PPV laser is to be pumped at that wavelength.

The addition of the laser dye has a pronounced effect on the observed ASE threshold. For excitation at 410 nm, the ASE threshold is lowered with the addition of laser dye until it reaches a minimum for the 1:1 blend where the material's performance becomes equivalent to the neat polymer excited at the maximum of its absorption. The addition of more dye does not improve the performance of the material as the measured ASE threshold starts increasing, as the balance between energy transfer and optical gain is disturbed, possibly due to an increase of the scattering losses within the film.

For the 532 nm data, the addition of laser dye has a detrimental effect on the ASE threshold as it is greatly increased in comparison to the neat polymer film. This can be understood by considering that, for the same volume of material required to create a film on a glass substrate, the addition of a large amount of dye means that there will be less of the polymer material present, leading to reduced pump light absorption through the volume of the film. It could also be due to the fact that the larger amount of laser dye in the blend is causing more scattering as the light is waveguided through the film, meaning that the optical losses are increased.

From the above studies it becomes clear that the blend containing equal amounts of the laser dye Coumarin 102 and MEH-PPV is the best candidate for the proposed energy transfer-based polymer laser. The combination of increased absorption and reduced ASE threshold makes this combination the best candidate for a laser pumped by a GaN laser diode.

7.6. Lasing experiments

To evaluate the potential for a laser-diode pumped organic semiconductor laser a GaN laser diode was used, emitting 1 ns long pulses at 409 nm with an energy of 670 pJ per pulse, at a repetition rate of 10 kHz. The output of the laser diode was focused using a spherical lens to a spot measuring 76 x 66 μm onto the surface of the sample. The resonator structures used were fabricated by Andreas Vasdekis, who also performed the bulk of the lasing measurements [25].

7.6.1. Laser resonator

Making a successful laser system requires as low a lasing threshold as possible to account for the limited output power of GaN laser diodes. Achieving lasing under low pump powers requires not only a material with the right properties but also a feedback structure that displays low lasing thresholds. The optimal resonator should display low-loss feedback at the required lasing wavelength along with efficient light extraction, a balance which is not always straightforward.

In these experiments a distributed Bragg reflector (DBR) cavity was used [26, 27]. This type of cavity consists of two 40 x 100 μm^2 Bragg-reflection mirrors where the grating period of 408 nm was chosen for surface-emitted output coupling and an amplification region width of 20 μm. The second order of Bragg reflection occurs in the plane of the film and creates a standing wave between the two Bragg reflectors that then work as the mirrors in a typical Fabry-Perot lasing cavity. The first order of diffraction at the Bragg reflectors is then responsible for extracting the light perpendicular to the mirrors, leading to a laser cavity with optical feedback in the plane of the structure and out-of-plane light extraction. A 120 nm film from a dye-polymer blend solution was spin coated on top of the substrate leading to device architecture like the one shown in Figure 7.11.

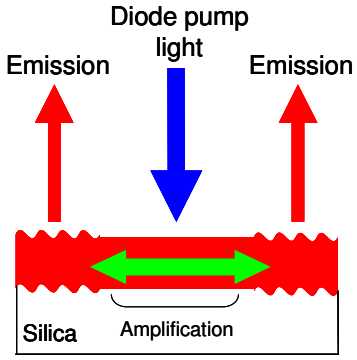

Figure 7.11 A polymer laser based on a distributed Bragg reflector (DBR) cavity.

7.6.2. Lasing performance

When the diode light is incident on the laser structure, the emission spectrum is characteristic of a DBR laser showing a number of features at 624 nm, 625.7 nm, 628.2 nm and 630.4 nm (see Figure 7.12). The shortest and longest modes originate in the Bragg scattered modes emitted within the Bragg mirrors, as the pump beam is larger than the amplification region of the DBR laser. The intermediate peaks at 625.7 nm and 628.2 nm originate in the different longitudinal modes present within the cavity.

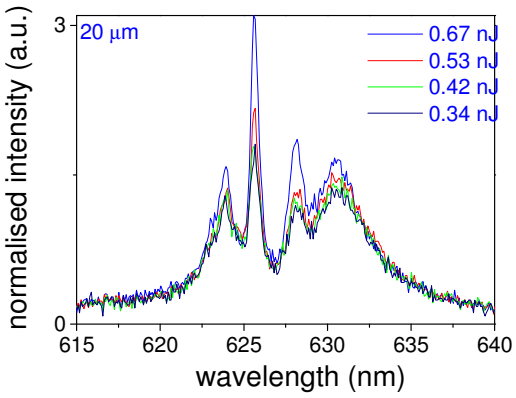

Figure 7.12 Emission spectrum from a dye-polymer DBR laser at different pumping energies. [25]

As the pumping energy is increased, the features in the emission spectrum all increase linearly in intensity. Above 0.42 nJ though, the peak at 625.7 nm increases faster than the other features, indicating the nonlinearity associated with stimulated emission near the threshold of a laser. At the same time, the

intensity of the background emission becomes “pinned” at a certain level as the available optical gain is taken up by lasing. This can be clearly seen in Figure 7.13 where the intensity of both the 625.7 nm lasing peak and the emission at 624 nm are plotted as a function of pump energy. As the lasing peaks graph changes slope and increases at a faster rate above 420 pJ, the spontaneous emission flattens out due to the onset of lasing at 625.7 nm. Similar performance was observed for a range of cavity lengths, but the 20 μm cavity reported here had the lowest lasing threshold.

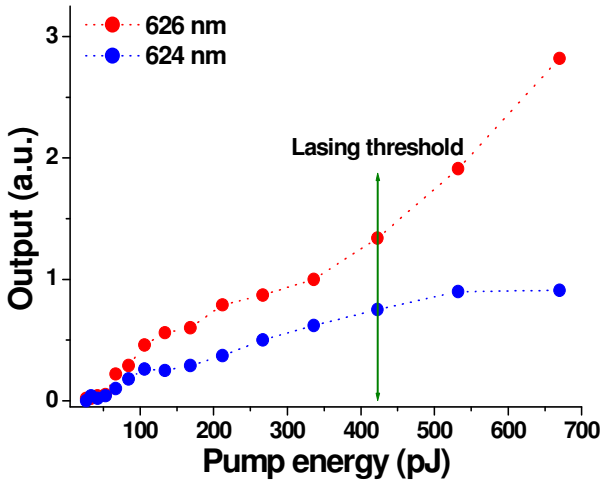

Figure 7.13 Energy dependence of lasing (626 nm) and spontaneous emission (624 nm) peaks from a DBR laser based on a laser dye - MEH-PPV blend.

Due to the limited energy available from the GaN laser diode however the polymer laser could only be pumped up to 1.5 times above threshold, meaning that the laser peak changes only by a modest amount. When comparing the spectra below and above threshold though, a clear change in the shape due to lasing can still be seen (Figure 7.14).

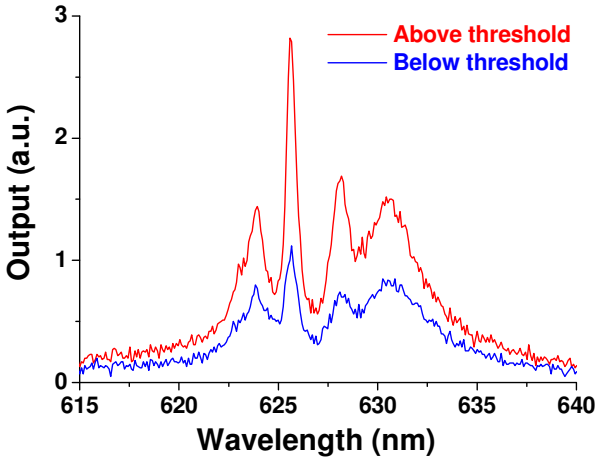

Figure 7.14 Output spectra for a DBR laser based on a dye-polymer energy transfer blend below and above threshold.

When the pump energy is further increased by pumping with a microchip laser, the laser emission dominates completely, as seen in Figure 7.15.

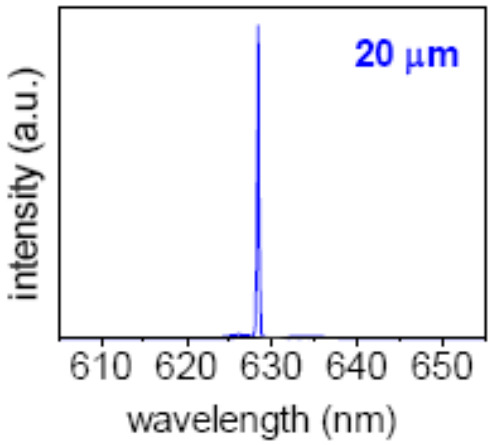

Figure 7.15 Lasing spectrum for a DBR laser based on a laser dye-MEH-PPV blend excited by a microchip laser. [25]

7.7. Summary

In conclusion, a laser-diode pumped solid state polymer laser was demonstrated. The key components of this achievement are the acceptor-donor blend constituting of a Coumarin laser dye and the polymer MEH-PPV that allowed for efficient harvesting of the laser dye light, as well as a DBR resonator with exceptionally low lasing threshold. The combination of materials research and resonator design holds the key for advancements towards compact organic laser systems. This is the first example of a donor-acceptor blend where the dye harvests the excitation light and the polymer is responsible for lasing.

As this thesis was being written, this is one of a very small number of laser diode pumped organic lasers.[14] The other published example concentrates around custom-synthesised fluorene-based materials that have inherently better lasing thresholds and are perhaps a better match to the emission wavelengths available from GaN laser diodes.[28] This research though uses commercially available materials to deliver results that are comparable to the literature, especially in terms of being able to pump these lasers high enough above threshold.

Further progress has been made since this research was published. The basic principle of low lasing threshold materials and suitable resonators demonstrated here been further developed and has led to the recent demonstration by this group of a LED-pumped polymer laser, [29] helping to pave the way for more compact and practical organic lasers for implementation in applications where their unique properties will make them stand out against their inorganic counterparts.

7.8. References

[1] I. D. W. Samuel, G. A. Turnbull, *Chem. Rev.* **2007**, *107*, 1272.

[2] I. D. W. Samuel, G. A. Turnbull, *Materials Today* **2004**, *7*, 28.

[3] N. Tessler, *Advanced Materials* **1999**, *11*, 363.

[4] T. Voss, D. Scheel, W. Schade, *Applied Physics B-Lasers and Optics* **2001**, *73*, 105.

[5] G. A. Turnbull, P. Andrew, W. L. Barnes, I. D. W. Samuel, *Applied Physics Letters* **2003**, *82*, 313.

[6] J. J. Zayhowski, A. Mooradian, *Optics Letters* **1989**, *14*, 24.

[7] C. J. Norrie, B. D. Sinclair, N. Gallaher, M. H. Dunn, W. Sibbett, *Electron. Lett.* **1989**, *25*, 1115.

[8] I. Akasaki, H. Amano, S. Sota, H. Sakai, T. Tanaka, M. Koike, *Jpn. J. Appl. Phys. Part 2 - Lett.* **1995**, *34*, 1517.

[9] S. Nakamura, M. Senoh, S. Nagahama, N. Iwasa, T. Yamada, T. Matsushita, H. Kiyoku, Y. Sugimoto, *Jpn. J. Appl. Phys. Part 2 - Lett.* **1996**, *35*, L217.

[10] I. Akasaki, S. Sota, H. Sakai, T. Tanaka, M. Koike, H. Amano, *Electron. Lett.* **1996**, *32*, 1105.

[11] G. Fasol, *Science* **1996**, *272*, 1751.

[12] M. Kneissl, L. T. Romano, C. G. Van de Walle, J. E. Northrup, W. S. Wong, W. Treat, M. Teepe, N. Miyashita, N. M. Johnson, I. I. Ipap, "Advances in blue laser diode development for high resolution printing", presented at *International Workshop on Nitride Semiconductors (IWN 2000)*, Nagoya, Japan, Sep 24-27, **2000**.

[13] T. Strite, *Laser Focus World* **1998**, *34*, 15.

[14] T. Riedl, T. Rabe, H. H. Johannes, W. Kowalsky, J. Wang, T. Weimann, P. Hinze, B. Nehls, T. Farrell, U. Scherf, *Applied Physics Letters* **2006**, *88*, 3.

[15] C. Karnutsch, C. Gyrtner, V. Haug, U. Lemmer, T. Farrell, B. S. Nehls, U. Scherf, J. Wang, T. Weimann, G. Heliotis, C. Pflumm, J. C. deMello, D. D. C. Bradley, *Applied Physics Letters* **2006**, *89*.

[16] A. E. Vasdekis, G. Tsiminis, J. C. Ribierre, L. O'Faolain, T. F. Krauss, G. A. Turnbull, I. D. W. Samuel, *Optics Express* **2006**, *14*, 9211.

[17] V. Bulovic, V. G. Kozlov, V. B. Khalfin, S. R. Forrest, *Science* **1998**, *279*, 553.

[18] A. K. Sheridan, A. R. Buckley, A. M. Fox, A. Bacher, D. D. C. Bradley, I. D. W. Samuel, *Journal of Applied Physics* **2002**, *92*, 6367.

[19] R. Gupta, M. Stevenson, A. Dogariu, M. D. McGehee, J. Y. Park, V. Srdanov, A. J. Heeger, H. Wang, *Applied Physics Letters* **1998**, *73*, 3492.

[20] F. Marchioni, R. Chiechi, S. Patil, F. Wudl, Y. Chen, J. Shinar, *Applied Physics Letters* **2006**, *89*, 3.

[21] Th. Förster, *Annalen der Physik* **1948**, *437*, 55.

[22] S. Reich, Y. Cohen, *J. Polym. Sci. Pt. B-Polym. Phys.* **1981**, *19*, 1255.

[23] S. H. Wu, *Polym. Eng. Sci.* **1987**, *27*, 335.

[24] M. D. McGehee, M. A. Diaz-Garcia, F. Hide, R. Gupta, E. K. Miller, D. Moses, A. J. Heeger, *Applied Physics Letters* **1998**, *72*, 1536.

[25] A. E. Vasdekis, *PhD Thesis, University of St Andrews* **2007**.

[26] N. Suganuma, A. Seki, Y. Tanaka, M. Ichikawa, T. Koyama, Y. Taniguchi, *J. Photopolym Sci. Technol.* **2002**, *15*, 273.

[27] T. Baba, T. Hamano, F. Koyama, K. Iga, *Ieee Journal of Quantum Electronics* **1991**, *27*, 1347.

[28] C. Karnutsch, C. Pflumm, G. Heliotis, J. C. Demello, D. D. C. Bradley, J. Wang, T. Weimann, V. Haug, C. Gartner, U. Lemmer, *Applied Physics Letters* **2007**, *90*, 3.

[29] Y. Yang, G. A. Turnbull, I. D. W. Samuel, *Applied Physics Letters* **2008**, *92*, 163306.

8. Conclusions

Organic semiconductor lasers have made great progress since their early demonstrations and have opened up a new applications field for organic semiconductors. The novel laser resonators that became possible as a result of the unique processing properties of organic semiconductors certainly have played an important role in establishing and enhancing these lasers but it is the materials themselves that have been the driving force in the development of organic lasers.[1]

Research in new materials and new methods of using organic semiconductors for lasing is an ongoing process based on the combination of synthetic chemistry and photophysical measurements. The molecules synthesised in a chemistry lab are evaluated in a number of ways for their performance as laser gain media and the results are fed back to the people synthesising them to guide the development of improved materials. This process has lead to solution-processable organic materials with very high values of photoluminescence quantum yield and optical gain, low waveguide losses and the ability to spin coat high-quality thin films, leading to compact, low lasing threshold lasers pumped by inorganic LEDs.[2]

This thesis has dealt with some of the methods followed to evaluate organic semiconductors as optical gain media for solid-state surface-emitting lasers. It has also demonstrated a number of organic semiconductor lasers based on a range of both commercial and custom-synthesised molecules and explored some of the different pumping schemes available to achieve lasing.

The first experimental chapter (chapter 4) explored an alternative optical pumping method for polyfluorene lasers based on two-photon absorption, a nonlinear process in which two photons of half the energy (twice the wavelength) of the material's bandgap are absorbed simultaneously. Two-photon absorption has the advantage that the excitation wavelength moves away for the high-energy UV photons that can speed up photodegradation. The two-

photon absorption properties of polyfluorene were investigated across a wide range of pump pulse wavelengths, energies and durations, making this a comprehensive study of the nonlinear properties of polyfluorene. This information was then used to demonstrate the first blue-emitting two-photon pumped polymer laser that was excited at 640 nm and had an absorbed energy density threshold of 1.3 mJ/cm^2.[3] This nonlinear approach to optical excitation could eventually allow the use of red laser diodes that are cheaper than their UV counterparts for optically pumped organic lasers.

The next chapter studied a new family of conjugated dendrimers that share a bisfluorene core. The key photophysical properties that are important for lasing of these molecules were investigated, highlighting some of the attractive properties of organic semiconductors such as high optical gain, low waveguide losses and large photoluminescence quantum yield in the solid state. The availability of a family of materials sharing the same fluorescence core was also used to relate the lasing threshold to the photoluminescence quantum yield. to The material with the highest gain was used to make a tunable deep-blue dendrimer laser based on distributed feedback resonators. The lowest lasing threshold recorded was 4.5 $\mu J/cm^2$, while the slope efficiency was also very high at 8.3% when including surface emission from only one side of the DFB laser.[4]

Two-photon absorption in these same bisfluorene dendrimers was also studied, as branched organic molecules are expected to have higher nonlinear absorption coefficients. This allowed the demonstration of the first two-photon pumped dendrimer laser.[5] This had an absorbed energy density lasing threshold of 5.2 $\mu J/cm^2$ that is directly comparable to the one-photon pumped threshold mentioned above.

It is interesting at this point to compare the two-photon absorption and two-photon pumped lasing properties of polyfluorene and the bisfluorene dendrimers. The basic unit is the same for both materials and therefore some similarities are expected, as is also evident from their linear absorption and emission spectra. The resulting comparison can be seen in Table 8.a, where all

the values refer to solutions of the same concentration excited at the peak of the two-photon absorption spectrum of each material using identical setups as described previously in chapter 4 and 5.

Material	PFO	Bisfluorene (BP)	Bisfluorene (BPCz)	Bisfluorene (ES)
α_2^{ns} (cm/GW)	6.9	27	35	45
α_2^{fs} (cm/GW)	0.040	0.073	0.095	0.118
δ^{ns} (GM)	$9.6x10^4$	85	120	148
δ^{fs} (GM)	557	0.3	0.33	0.39
Lasing threshold ($mJcm^{-2}$)	42	4.9	-	-
Absorbed lasing threshold ($mJcm^{-2}$)	1.3	0.005	-	-

Table 8.a Overview of the two-photon absorption properties of polyfluorene and the bisfluorene-cored dendrimers studied in this thesis.

The much larger size of the polyfluorene chromophore gives rise to much larger two-photon absorption cross-section δ for both nanosecond and femtosecond illumination. This increase in apparent absorption does not however lead to increased stimulated emission, as the lasing threshold for a two-photon pumped polyfluorene laser is approximately 10 times higher than the bisfluorene dendrimer laser. The advantage of the polyfluorene laser though lies in the fact that it is commercially available, whereas the bisfluorene dendrimers were custom-synthesised.

Chapter 7 described the process of making a distributed feedback laser based on an oligofluorene truxene, a material consisting of a specific number of fluorene units that are joined together to create a star-shaped molecule.[6] The truxene material showed an exceptionally low (for a solution processable material) waveguide loss coefficient of 2.3 cm^{-1} that allowed the demonstration of a distributed feedback truxene laser with a very low lasing threshold of 270 W/cm^2, [7] placing the truxene into the small category of materials that could potentially be pumped by an inorganic LED. Since the basic unit of the truxene molecule is also fluorene, it is interesting to compare the key photophysical properties between polyfluorene, the oligofluorene truxene and the bisfluorene dendrimers, as well as their lasing performance. This comparison is summarised in Table 8.b where all the materials where optically excited at the peak of their absorption spectra and the measurements were carried out using the variable

stripe technique for the gain and loss values and similar setups for the lasing studies.

Material	Polyfluorene	Bisfluorene dendrimer	Truxene (T4)
Optical gain (cm^{-1})	74	51	19
Waveguide losses (cm^{-1})	3.5	4.0	2.3
Film PLQY (%)	73	92	73
ASE threshold (μJcm^{-2})	29	16	16
Lasing threshold ($kWcm^{-2}$)	4.0	1.13	0.27

Table 8.b Comparison of the key parameters for lasing for the fluorene-based organic semiconductors studied here. Values for polyfluorene taken from [8].

These results show the advantages that can be achieved by the progress in material synthesis. The bisfluorene dendrimer had a lasing threshold that is almost one quarter of the polyfluorene threshold, while the truxene molecule showed a further reduction in the lasing threshold of almost 20 times in comparison to polyfluorene, in part due to the lower optical losses of the truxene films.

The final experimental chapter reported the optimisation of the gain medium for a diode-pumped organic laser. The offset between the excitation wavelength of a GaN laser diode and the light-emitting polymer MEH-PPV was compensated by blending the polymer with a Coumarin laser dye that absorbed the pump light and then transferred it to MEH-PPV by Förster energy transfer. This is the first time light has been harvested by a dye and transferred to a polymer in a semiconducting laser gain medium and, in combination with a low-loss distributed Bragg reflector resonator lead to one of the very few examples of diode-pumped organic lasers.[9]

The progress of organic semiconductor lasers has been as rapid as it has been exciting, with new materials synthesised based on better understanding of the key properties that improve the lasing performance. Organic lasers are now reaching a stage of maturity as a technology based on the combination of optical and photophysical properties with the ease of processing that organic semiconductors demonstrate. Further research can only bring more improvements that will help plastic lasers move from the lab environment to the

wider world of practical applications such as optical spectroscopy, chemical [10] and bio sensing [11] and point-of-care medical diagnostics, ultimately making a contribution to improving the world around us.

8.1. References

[1] I. D. W. Samuel, G. A. Turnbull, *Chem. Rev.* **2007**, *107*, 1272.

[2] Y. Yang, G. A. Turnbull, I. D. W. Samuel, *Applied Physics Letters* **2008**, *92*, 163306.

[3] G. Tsiminis, A. Ruseckas, I. D. W. Samuel, G. A. Turnbull, *Submitted to Applied Physics Letters*.

[4] J. C. Ribierre, G. Tsiminis, S. Richardson, G. A. Turnbull, I. D. W. Samuel, *Applied Physics Letters* **2007**, *91*.

[5] G. Tsiminis, J. C. Ribierre, A. Ruseckas, H. S. Barcena, G. J. Richards, G. A. Turnbull, P. L. Burn, I. D. W. Samuel, *Advanced Materials* **2008**, *20*, 1940.

[6] A. L. Kanibolotsky, R. Berridge, P. J. Skabara, I. F. Perepichka, D. D. C. Bradley, M. Koeberg, *Journal of the American Chemical Society* **2004**, *126*, 13695.

[7] G. Tsiminis, Y. Wang, P. E. Shaw, A. L. Kanibolotsky, I. F. Perepichka, P. J. Skabara, G. A. Turnbull, I. D. W. Samuel, *Submitted to Applied Physics Letters*.

[8] G. Heliotis, D. D. C. Bradley, G. A. Turnbull, I. D. W. Samuel, *Applied Physics Letters* **2002**, *81*, 415.

[9] A. E. Vasdekis, G. Tsiminis, J. C. Ribierre, L. O'Faolain, T. F. Krauss, G. A. Turnbull, I. D. W. Samuel, *Optics Express* **2006**, *14*, 9211.

[10] A. Rose, Z. Zhu, C. F. Madigan, T. M. Swager, V. Bulovic, *Nature* **2005**, *434*, 876.

[11] D. Schneider, T. Rabe, T. Riedl, T. Dobbertin, M. Kroger, E. Becker, H. H. Johannes, W. Kowalsky, T. Weimann, J. Wang, P. Hinze, A. Gerhard, P. Stossel, H. Vestweber, *Advanced Materials* **2005**, *17*, 31.

9. Appendix: Publications arising from this work

9.1. Publications in scientific journals

G. Tsiminis, Y. Wang, A. L. Kanibolotsky, I. F. Perepichka, P. J. Skabara, I. D. W. Samuel, G. A. Turnbull, *Low-threshold organic laser based on an oligofluorene truxene with low optical losses.* Applied Physics Letters **2009**, 94, 24, 243304

G. Tsiminis, A. Ruseckas, I. D. W. Samuel, G. A. Turnbull*, A two-photon pumped polyfluorene laser*. Applied Physics Letters **2009**, 94, 25, 253304.

G. Tsiminis, J. C. Ribierre, A. Ruseckas, H. S. Barcena, G. J. Richards, G. A. Turnbull, P. L. Burn, I. D. W. Samuel, *Two-photon absorption and lasing in first-generation bisfluorene dendrimers.* Advanced Materials **2008**, *20*, 1940.

J. C. Ribierre, G. Tsiminis, S. Richardson, G. A. Turnbull, I. D. W. Samuel, *Amplified spontaneous emission and lasing properties of bisfluorene-cored dendrimers.* Applied Physics Letters **2007**, *91*.

A. E. Vasdekis, G. Tsiminis, J. C. Ribierre, L. O'Faolain, T. F. Krauss, G. A. Turnbull, I. D. W. Samuel, *Diode pumped distributed Bragg reflector lasers based on a dye-to-polymer energy transfer blend.* Optics Express **2006**, *14*, 9211.

9.2. Conference proceedings

I. D. W. Samuel, A. E. Vasdekis, G. Tsiminis, G. A. Turnbull, "Shrinking polymer lasers - art. no. 671304", presented at *Conference on Nanophotonics and Macrophotonics for Space Environments*, San Diego, CA, Aug 27-28, **2007**.

G. A. Turnbull, A. E. Vasdekis, G. Tsiminis, I. D. W. Samuel, "Diode pumped polymer lasers - art. no. 66550W", presented at *Conference on Organic Light Emitting Materials and Devices XI*, San Diego, CA, Aug 26-29, **2007**.